Quantum dynamics and thermalization for out-of-equilibrium ϕ^4 theory

S. Juchem, W. Cassing, and C. Greiner
Institut für Theoretische Physik, Universität Giessen, D-35392 Giessen, Germany
(Received 29 July 2003; published 30 January 2004)

The quantum time evolution of ϕ^4-field theory for a spatially homogeneous system in 2+1 space-time dimensions is investigated numerically for out-of-equilibrium initial conditions on the basis of the Kadanoff-Baym equations including the tadpole and sunset self-energies. Whereas the tadpole self-energy yields a dynamical mass, the sunset self-energy is responsible for dissipation and an equilibration of the system. In particular we address the dynamics of the spectral (''off-shell'') distributions of the excited quantum modes and the different phases in the approach to equilibrium described by Kubo-Martin-Schwinger relations for thermal equilibrium states. The investigation explicitly demonstrates that the only translation invariant solutions representing the stationary fixed points of the coupled equation of motions are those of full thermal equilibrium. They agree with those extracted from the time integration of the Kadanoff-Baym equations for $t\rightarrow\infty$. Furthermore, a detailed comparison of the full quantum dynamics to more approximate and simple schemes such as that of a standard kinetic (on-shell) Boltzmann equation is performed. Our analysis shows that the consistent inclusion of the dynamical spectral function has a significant impact on relaxation phenomena. The different time scales that are involved in the dynamical quantum evolution towards a complete thermalized state are discussed in detail. We find that far off-shell $1\leftrightarrow 3$ processes are responsible for chemical equilibration, which is missed in the Boltzmann limit. Finally, we briefly address the case of (bare) massless fields. For sufficiently large couplings λ we observe the onset of Bose condensation, where our scheme within symmetric ϕ^4 theory breaks down.

DOI: 10.1103/PhysRevD.69.025006 PACS number(s): 05.70.Ln, 05.60.−k, 11.10.Wx, 24.10.Cn

I. INTRODUCTION

Nonequilibrium many-body theory or quantum field theory has become a major topic of research for describing transport processes in nuclear physics, cosmological particle physics and condensed matter physics. The multidisciplinary aspect arises due to a common interest in understanding the various relaxation phenomena of quantum dissipative systems. Recent progress in cosmological observations has also intensified the research on quantum fields out of equilibrium. Some important questions in high-energy nuclear or particle physics at the highest energy densities are as follows. (i) How do nonequilibrium systems in extreme environments evolve? (ii) How do they eventually thermalize? (iii) How do phase transitions occur in real-time with possibly nonequilibrium remnants? (iv) How do such systems evolve for unprecedented short and nonadiabatic time scales?

The very early history of the Universe provides scenarios, in which nonequilibrium effects might have played an important role, such as in the (post-) inflationary epoque (see, e.g., Refs. [1–3]), for the understanding of baryogenesis (see, e.g., Ref. [1]) and also for the general phenomena of cosmological decoherence (see, e.g., Ref. [4]). In modern nuclear physics the understanding of the dynamics of heavy-ion collisions at various bombarding energies has always been a major motivation for research on nonequilibrium quantum many-body physics and relativistic quantum field theories, since the initial state of a collision resembles an extreme nonequilibrium situation while the final state might even exhibit a certain degree of thermalization. Indeed, at the presently highest energy heavy-ion collider experiments at the BNL Relativistic Heavy Ion Collider (RHIC), where one expects to create experimentally a transient deconfined state of matter denoted as the quark-gluon plasma (QGP) [5], there are experimental indications—such as the build up of collective flow—for an early thermalization accompanied with the build up of a very large pressure. Furthermore, the phenomenon of disoriented chiral condensates (DCCs) during the chiral phase transition has lead to a considerable progress for our understanding of nonequilibrium phase transitions at short time scales over the last decade (see, e.g., Refs. [6–8]). All these examples demonstrate that one needs an *ab initio* understanding of the dynamics of out-of-equilibrium quantum field theory.

The powerful method of the ''Schwinger-Keldysh'' [9–12] or ''closed-time-path'' (CTP) (nonequilibrium) real-time Green functions has been shown to provide an appropriate basis for the formulation of the special and complex problems in the various areas of nonequilibrium quantum many-body physics. Within this framework one can derive and find valid approximations—depending, of course, on the problem under consideration—by preserving overall consistency relations. Originally, the resulting causal Dyson-Schwinger equation of motion for the one-particle Green function (or two-point function), i.e., the Kadanoff-Baym (KB) equations [13], has served as a basis for deriving various transport phenomena and generalized transport equations. These equations might be considered as an ensemble average over the initial density matrix $\rho^{(i)}(t_0)\equiv|i\rangle\rho^{(i)}_{ij}\langle j|$ characterizing the preparation of the initial state of the system, which can be far out of equilibrium. For review articles on the Kadanoff-Baym equations in the various areas of nonequilibrium quantum physics we refer the reader to Refs. [14–19]. We note in passing, that also the ''influence functional formalism'' has been shown to be directly related to the KB equations [20]. Such a relation allows us to address

inherent stochastic aspects of the latter and also to provide a rather intuitive interpretation of the various self-energy parts that enter the KB equations. The presence of (quantum) noise and dissipation—related by a fluctuation-dissipation theorem—guarantees that the modes or particles of an open system become thermally populated on average in the long-time limit if coupled to an environmental heat bath [20].

Furthermore, kinetic transport theory is a convenient tool to study many-body nonequilibrium systems, nonrelativistic or relativistic. Kinetic equations, which do play the central role in more or less all practical simulations, can be derived by means of appropriate KB equations within suitable approximations. Hence, a major impetus in the past has been to derive semiclassical Boltzmann-like transport equations within the standard quasiparticle approximation [21–23]. Additionally, off-shell extensions by means of a gradient expansion in the space-time inhomogeneities—as already introduced by Kadanoff and Baym [13]—have been formulated for: a relativistic electron-photon plasma [24], transport of electrons in a metal with external electrical field [25], transport of nucleons at intermediate heavy-ion reactions [26], transport of particles in ϕ^4 theory [18,27], transport of electrons in semiconductors [19,28], transport of partons or fields in high-energy heavy-ion reactions [29–32], or a trapped Bose system described by effective Hartree-Fock-Bogolyubov kinetic equations [33]. We recall that on the formal level of the KB equations the various forms assumed for the self-energy have to fulfill consistency relations in order to preserve symmetries of the fundamental Lagrangian [13,34,35]. This also allows for a unified treatment of stable and unstable (resonance) particles. We will shortly come back to this last development.

In nonequilibrium quantum field theory typically the nonperturbative description of (second-order) phase transitions has been in the foreground of interest by means of mean-field (Hartree) descriptions [2,7,36–39], with applications for the evolution of disoriented chiral condensates or the decay of the (oscillating) inflaton in the early reheating era. ''Effective'' mean-field dissipation (and decoherence)—solving the so-called ''back-reaction'' problem—was incorporated by particle production through order parameters explicitly varying in time. However, it had been soon realized that such a dissipation mechanism, i.e., transferring collective energy from the time-dependent order parameter to particle degrees of freedom, cannot lead to true dissipation and thermalization. Such a conclusion has already been known for quite some time within the effective description of heavy-ion collisions at low energy. Full time-dependent Hartree or Hartree-Fock descriptions [40] were insufficient to describe the reactions with increasing collision energy; additional Boltzmann-like collision terms had to be incorporated in order to provide a more adequate description of the collision processes.

The incorporation of true collisions has also been formulated for the various quantum field theories [18,41–44]. In any case, the understanding and the influence of dissipation with the chance for true thermalization—by incorporating collisions—has become a major focus of recent investigations. The resulting equations of motion always resemble the KB equations; in their general form [beyond the mean-field or Hartree(-Fock) approximation] they do break time invariance and thus lead to irreversibility. This macroscopic irreversibility arises from the truncations of the full theory to obtain the self-energy operators in a specific limit. As an example, we mention the truncation of the (exact) Martin-Schwinger hierarchy in the derivation of the collisional operator in Ref. [26] or the truncation of the (exact) BBGKY hierarchy in terms of n-point functions [26,45–51].

In principle, the nonequilibrium quantum dynamics is nonperturbative in nature. Unphysical singularities only appear in a limited truncation scheme, e.g., ill-defined pinch singularities [52], which arise at higher order in a perturbative expansion in out-of-equilibrium quantum field theory, are regularized by a consistent nonperturbative description (of Schwinger-Dyson type) of the nonequilibrium evolution, since the resummed propagators obtain a finite width [53]. Such a regularization is also observed by other resummation schemes such as the dynamical renormalization group technique developed recently [43].

Although the analogy of KB-type equations to a Boltzmann-like process is quite obvious, this analogy is far from trivial. The full quantum formulation contains much more information than a semiclassical (generally) on-shell Boltzmann equation. The dynamics of the spectral (i.e., ''off-shell'') information is fully incorporated in quantum dynamics while it is missing in the Boltzmann limit. A full answer to the question of quantum equilibration can thus only be obtained by a detailed numerical solution of the quantum description itself. This is the basic aim of our present study.

Before pointing out the scope of the present paper, we briefly address previous works that have investigated numerically approximate or full solutions of KB-type equations. A seminal work was carried out by Danielewicz [54], who for the first time investigated the full KB equations for a spatially homogeneous system with a deformed Fermi sphere in momentum space for the initial distribution of occupied momentum states in order to model the initial condition of a heavy-ion collision in the nonrelativistic domain. In comparison to a standard on-shell semiclassical Boltzmann equation the full quantum Boltzmann equation showed quantitative differences, i.e., a larger collective relaxation time for complete equilibration of the momentum distribution $f(\mathbf{p},t)$. This ''slowing down'' of the quantum dynamics was attributed to quantum interference and off-shell effects. Similar quantum modifications in the equilibration and momentum relaxation have been found in Ref. [21] and for a relativistic situation in Ref. [55]. Particular emphasis was put in this study [55,56] on nonlocal aspects (in time) of the collision process and thus the potential significance of memory effects on the nuclear dynamics. Full and more detailed solutions of nonrelativistic KB equations were performed by Köhler [57,58] with special emphasis on the build up of initial many-body correlations on short time scales. Moreover, the role of memory effects has been clearly shown experimentally by femtosecond laser spectroscopy in semiconductors [59] in the relaxation of excitons. Solutions of quantum transport equations for semiconductors [19,60]—to explore relaxation phenomena on short time and distance scales—

have also become a very active field of research.

During the last years the description of nonequilibrium real-time dynamics within the two-particle irreducible (2PI) effective action formalism has regained strong interest. First numerical studies in this context for the time evolution of relativistic quantum fields have been carried out for ϕ^4 theory in $1+1$ dimensions within the three-loop approximation of the effective action [61]. The method has also been applied to the homogeneous $O(N)$ model performing a systematic expansion in $1/N$ [62] or within the bare vertex approximation [63]. All these calculations exhibit thermalization since true scattering processes are included, i.e., beyond leading order. Thus the treatment within the 2PI effective action remedies the shortcomings of one-particle irreducible effective action approaches, that fail to show thermalization and do not reach the appropriate long-time limit [7,64]. The investigations have been extended to the symmetry broken phase where the bare vertex approximation resums a larger series than contained in the 2PI-$1/N$ expansion at next-to-leading order [65–67]. Furthermore, first extraploratory studies have been performed for the $O(N)$ model in $3+1$ dimensions also including a finite expectation value for the scalar field [68]. Very recently, a study in $3+1$ dimensions [69]—treating spherical symmetric distributions of momentum excitations for a coupled fermion-boson Yukawa-type system—has shown equilibration and thermalization in the fermionic as well as bosonic momentum occupation at the same temperature. Still, a detailed and quantitative interpretation of the time scales found was not given.

While the aforementioned studies restrict to homogeneous systems in space, there is a further branch dealing with general inhomogeneous settings. The dynamical behavior of relativistic scalar self-interacting field theories in $1+1$ space-time dimensions is investigated within the Hartree and classical approximation in the symmetric or broken phase [70–73]. Since true collisions are absent at the Hartree level no thermalization is observed [70]. Only when additional ensemble averaging is invoked are there hints for quantum equilibration at intermediate times and classical equilibration at large times [71,72]. The simulations have also been performed for initial configurations relevant for heavy-ion collisions [74] as well as in the presence of semiclassical field configurations that lead to bound states such as topological defects [75] and phase interfaces [76].

As already stressed, in the present study we will focus in particular on the full quantum dynamics of the spectral (i.e., ''off-shell'') information contained in the nonequilibrium single-particle spectral function. A discussion of this issue was previously given in Ref. [77] by Aarts and Berges. Here we want to show by using the spectral representation how complete thermalization of all single-particle quantum fluctuations will be achieved. In addition, the quantum dynamics of the spectral function is also a lively issue in the microscopic modeling of hadronic resonances with a broad mass distribution. This is of particular relevance for simulations of heavy-ion reactions [78–85], where, e.g., the Δ resonance or the ρ meson already show a large decay width in vacuum. The ρ vector meson is an especially promising hadronic particle for showing possible in-medium modifications in hot and compressed nuclear matter (see, e.g., Refs. [85,86]), since the leptonic decay products are of only weakly interacting electromagnetic nature. Indeed, the CERES experiment [87] at the SPS at CERN has found a significant enhancement of lepton pairs for invariant masses below the pole of the ρ meson, giving evidence for such modifications. Hence, a consistent formulation for the transport of extremely short-lived particles beyond the standard quasiparticle approximation is needed. On the one side, purely formal developments exist starting from a first-order gradient expansion of the underlying KB equations [78,80,84], while on the other side, first practical realizations for various questions have already emerged [79,81–83,88]. The general idea is to obtain a description for the propagation of the off-shell mass squared $M^2-M_0^2$. A fully *ab initio* investigation, however, without any further approximations, does not exist so far.

Our work is organized as follows. In Sec. II we will present the relevant equations for the nonequilibrium dynamics in case of ϕ^4 theory, i.e., briefly derive the Kadanoff-Baym equations of interest. Section III is devoted to the first numerical studies on equilibration phenomena and separation of time scales employing different initial configurations. The actual numerical algorithm used is described in Appendix A as well as the renormalization by counterterms in Appendix B in order to achieve ultraviolet convergent results. The individual phases of the quantum evolution are analyzed in more detail in Sec. IV, i.e., the initial build-up of correlations, the time evolution of the spectral functions and the approach to chemical equilibrium. Furthermore, it is shown that the solutions of the Kadanoff-Baym equations for $t \to \infty$ yield the proper off-shell thermal state, i.e., the Green functions fulfill the Kubo-Martin-Schwinger (KMS) relation in the long-time limit. Section V concentrates on approximate dynamical schemes, in particular, the well-known Boltzmann limit. The solutions of the latter limit as well as from a simple relaxation approximation will be confronted with the numerical results from the Kadanoff-Baym equations. We close this work in Sec. VI with a summary of our findings and a brief presentation of the results for massless Bose fields. Appendix C discusses the most general choices for the initial conditions of the Kadanoff-Baym equations. Furthermore, in Appendix D we present an efficient method for the calculation of the self-consistent resummed spectral function in thermal equilibrium for the present field theory, while Appendix E addresses the stationary solution of the Boltzmann limit.

II. NONEQUILIBRIUM DYNAMICS FOR ϕ^4 THEORY

The scalar ϕ^4 theory is an example for a fully relativistic field theory of interacting scalar particles that allows us to test theoretical approximations [48–50,61,77] without coming to the problems of gauge-invariant truncation schemes [51]. Its Lagrangian density is given by $[x=(t,\mathbf{x})]$

$$\mathcal{L}(x)=\frac{1}{2}\partial_\mu\phi(x)\partial^\mu\phi(x)-\frac{1}{2}m^2\phi^2(x)-\frac{\lambda}{4!}\phi^4(x), \tag{2.1}$$

where m denotes the "bare" mass and λ is the coupling constant determining the interaction strength of the scalar fields.

A. The Kadanoff-Baym equations

As mentioned in the Introduction, a natural starting point for nonequilibrium theory is provided by the closed-time-path (CTP) method. Here all quantities are given on a special real-time contour with the time argument running from $-\infty$ to ∞ on the chronological branch $(+)$ and returning from ∞ to $-\infty$ on the antichronological branch $(-)$. In the cases of systems prepared at time t_0 this value is (instead of $-\infty$) the start and end point of the real-time contour. In particular the path-ordered Green functions are defined as

$$\begin{aligned} G(x,y) &= \langle T^p\{\phi(x)\phi(y)\}\rangle \\ &= \Theta_p(x_0-y_0)\langle\phi(x)\phi(y)\rangle \\ &\quad + \Theta_p(y_0-x_0)\langle\phi(y)\phi(x)\rangle, \end{aligned} \tag{2.2}$$

where the operator T^p orders the field operators according to the position of their arguments on the real-time path as accomplished by the path step-functions Θ_p. The expectation value in Eq. (2.2) is taken with respect to some given density matrix ρ_0, which is constant in time, while the operators in the Heisenberg picture contain the whole information of the time dependence of the nonequilibrium system.

Self-consistent equations of motion for these Green functions can be obtained with help of the two-particle irreducible (2PI) effective action $\Gamma[G]$. It is given by the Legendre transform of the generating functional of the connected Green functions W as

$$\Gamma[G] = \Gamma^0 + \frac{i}{2}[\ln(1-\odot_p G_0 \odot_p \Sigma) + \odot_p G \odot_p \Sigma] + \Phi[G] \tag{2.3}$$

in the case of vanishing vacuum expectation value $\langle 0|\phi(x)|0\rangle = 0$ [34]. In Eq. (2.3) Γ^0 depends only on free Green functions G_0 and is treated as a constant with respect to variation, while the symbols $\odot_p$ represent convolution integrals over the closed-time-path with the contour specified above. The functional Φ is the sum of all closed 2PI diagrams built up by full propagators G; it determines the self-energies by functional variation as

$$\Sigma(x,y) = 2i\frac{\delta\Phi}{\delta G(y,x)}. \tag{2.4}$$

From the effective action (2.3) the equations of motion for the Green function are obtained by the stationarity condition

$$\frac{\delta\Gamma}{\delta G} = 0 \tag{2.5}$$

giving the Dyson-Schwinger equation for the full path-ordered Green function as

$$G(x,y)^{-1} = G_0(x,y)^{-1} - \Sigma(x,y). \tag{2.6}$$

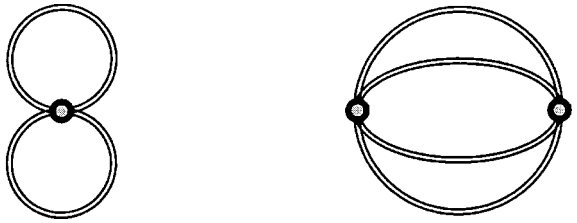

FIG. 1. Contributions to the Φ functional for the Kadanoff-Baym equation: two-loop contribution (LHS) giving the tadpole self-energy and three-loop contribution (RHS) generating the sunset self-energy. The Φ-functional is built up by full Green functions (double lines) while open dots symbolize the integration over the internal coordinates.

In our present calculation we take into account contributions up to the three-loop order for the Φ functional (see Fig. 1), which reads explicitly

$$i\Phi = \frac{i\lambda}{8}\int_p d^{d+1}x G(x,x)^2 - \frac{\lambda^2}{48}\int_p d^{d+1}x \int_p d^{d+1}y\, G(x,y)^4, \tag{2.7}$$

where d denotes the spatial dimension of the problem ($d=2$ in the case considered below).

This approximation corresponds to a weak coupling expansion such that we consider contributions up to the second superficial order in the coupling constant λ (see Fig. 2). For the superficial coupling constant order we count the explicit coupling factors λ associated with the visible vertices. The hidden dependence on the coupling strength—which is implicitly incorporated in the self-consistent Green functions that build up the Φ-functional and the self-energies—is ignored on that level. For our present purpose this approximation is sufficient since we include the leading mean-field effects as well as the leading order scattering processes that pave the way to thermalization.

For the actual calculation it is advantageous to change to a single-time representation for the Green functions and self-energies defined on the closed-time-path. In line with the position of the coordinates on the contour there exist four different two-point functions

$$\begin{aligned} iG^c(x,y) &= iG^{++}(x,y) = \langle T^c\{\phi(x)\phi(y)\}\rangle, \\ iG^<(x,y) &= iG^{+-}(x,y) = \langle\{\phi(y)\phi(x)\}\rangle, \\ iG^>(x,y) &= iG^{-+}(x,y) = \langle\{\phi(x)\phi(y)\}\rangle, \end{aligned} \tag{2.8}$$

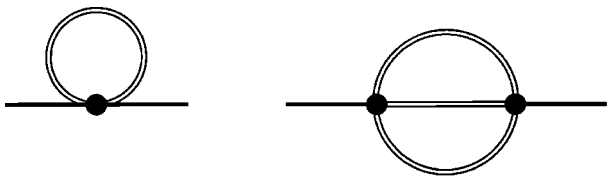

FIG. 2. Self-energies of the Kadanoff-Baym equation: tadpole self-energy (LHS) and sunset self-energy (RHS). Since the lines represent full Green functions the self-energies are self-consistent (see text) with the external coordinates indicated by full dots.

$$iG^a(x,y) = iG^{--}(x,y) = \langle T^a\{\phi(x)\phi(y)\}\rangle.$$

Here $T^c(T^a)$ represent the (anti-)time-ordering operators in case of both arguments lying on the (anti)chronological branch of the real-time contour. These four functions are not independent of each other. In particular the noncontinuous functions G^c and G^a are built up by the Wightman functions $G^>$ and $G^<$ and the usual Θ functions in the time coordinates. Since for the real bosonic theory (2.1) the relation $G^>(x,y) = G^<(y,x)$ (2.8) holds, the knowledge of the Green functions $G^<(x,y)$ for all x,y characterizes the system completely. Nevertheless, we will give the equations for $G^<$ and $G^>$ explicitly since this is the familiar representation for general field theories [27].

By using the stationarity condition for the action (2.5) and resolving the time structure of the path ordered quantities in the Dyson-Schwinger equation (2.6) we obtain the Kadanoff-Baym equations for the time evolution of the Wightman functions [27,61]

$$\begin{aligned}
&-[\partial_\mu^x \partial_x^\mu + m^2] G^{\gtrless}(x,y) \\
&\quad = \Sigma^\delta(x) G^{\gtrless}(x,y) \\
&\qquad + \int_{t_0}^{x_0} dz_0 \int d^d z\, [\Sigma^>(x,z) - \Sigma^<(x,z)] G^{\gtrless}(z,y) \\
&\qquad - \int_{t_0}^{y_0} dz_0 \int d^d z\, \Sigma^{\gtrless}(x,z)[G^>(z,y) - G^<(z,y)], \\
&-[\partial_\mu^y \partial_y^\mu + m^2] G^{\gtrless}(x,y) \\
&\quad = \Sigma^\delta(y) G^{\gtrless}(x,y) \\
&\qquad + \int_{t_0}^{x_0} dz_0 \int d^d z\, [G^>(x,z) - G^<(x,z)] \Sigma^{\gtrless}(z,y) \\
&\qquad - \int_{t_0}^{y_0} dz_0 \int d^d z\, G^{\gtrless}(x,z)[\Sigma^>(z,y) - \Sigma^<(z,y)].
\end{aligned} \tag{2.9}$$

Here the path-ordered self-energy has been divided into a local contribution Σ^δ and a nonlocal one, which can be expressed—analogously to the Green functions (2.2)—by a sum over path Θ functions. The self-energy entering the Dyson-Schwinger equation (2.6) is thus written as

$$\begin{aligned}
\Sigma(x,y) = \Sigma^\delta(x)\delta_p^{(d+1)}(x-y) + \Theta_p(x_0-y_0)\Sigma^>(x,y) \\
+ \Theta_p(y_0-x_0)\Sigma^<(x,y).
\end{aligned} \tag{2.10}$$

Within the three-loop approximation for the 2PI effective action [i.e., the Φ-functional (2.7)] we get two different self-energies: In leading order of the coupling constant only the local tadpole diagram (LHS of Fig. 2) contributes and leads to the generation of an effective mass for the field quanta. This self-energy (in coordinate space) is given by

$$\Sigma^\delta(x) = \frac{\lambda}{2} iG^<(x,x). \tag{2.11}$$

In next order in the coupling constant (i.e., λ^2) the nonlocal sunset self-energy (RHS of Fig. 2) enters the time evolution as

$$\begin{aligned}
\Sigma^{\gtrless}(x,y) &= -\frac{\lambda^2}{6} G^{\gtrless}(x,y) G^{\gtrless}(x,y) G^{\lessgtr}(y,x) \\
&= -\frac{\lambda^2}{6} [G^{\gtrless}(x,y)]^3.
\end{aligned} \tag{2.12}$$

Thus the Kadanoff-Baym equation (2.9) in our case includes the influence of a mean-field on the particle propagation—generated by the tadpole diagram—as well as scattering processes as inherent in the sunset diagram.

The Kadanoff-Baym equation (2.9) describes the full quantum nonequilibrium time evolution on the two-point level for a system prepared at an initial time t_0, i.e., when higher order correlations are discarded. The causal structure of this initial value problem is obvious since the time integrations are performed over the past up to the actual time x_0 (or y_0, respectively) and do not extend to the future.

Furthermore, also linear combinations of the Green functions in single time representation are of interest. The retarded Green function G^R and the advanced Green function G^A are given as

$$\begin{aligned}
G^R(x,y) &= \Theta(x_0-y_0)[G^>(x,y) - G^<(x,y)] \\
&= \Theta(x_0-y_0)\langle[\phi(x),\phi(y)]_-\rangle,
\end{aligned} \tag{2.13}$$

$$\begin{aligned}
G^A(x,y) &= -\Theta(y_0-x_0)[G^>(x,y) - G^<(x,y)] \\
&= -\Theta(y_0-x_0)\langle[\phi(x),\phi(y)]_-\rangle.
\end{aligned} \tag{2.14}$$

These Green functions contain exclusively spectral, but no statistical information of the system. Their time evolution is given by

$$\begin{aligned}
&-[\partial_\mu^x \partial_x^\mu + m^2 + \Sigma^\delta(x)] G^{R/A}(x,y) \\
&\quad = \delta^{(d+1)}(x-y) + \int d^{d+1} z\; \Sigma^{R/A}(x,z) G^{R/A}(z,y),
\end{aligned} \tag{2.15}$$

where the retarded and advanced self-energies Σ^R, Σ^A are defined via $\Sigma^>$, $\Sigma^<$ similar to the Green functions (2.13) and (2.14). Thus the retarded (advanced) Green functions are determined by retarded (advanced) quantities, only.

B. Homogeneous systems in space

In the following we will restrict to homogeneous systems in space. In order to obtain a numerical solution the Kadanoff-Baym equation (2.9) is transformed to momentum space:

$$\partial_{t_1}^2 G^<(\mathbf{p},t_1,t_2)$$
$$= -[\mathbf{p}^2 + m^2 + \overline{\Sigma}^{\delta}(t_1)]G^<(\mathbf{p},t_1,t_2)$$
$$- \int_{t_0}^{t_1} dt' [\Sigma^>(\mathbf{p},t_1,t') - \Sigma^<(\mathbf{p},t_1,t')]G^<(\mathbf{p},t',t_2)$$
$$+ \int_{t_0}^{t_2} dt' \Sigma^<(\mathbf{p},t_1,t')[G^>(\mathbf{p},t',t_2) - G^<(\mathbf{p},t',t_2)]$$
$$= -[\mathbf{p}^2 + m^2 + \overline{\Sigma}^{\delta}(t_1)]G^<(\mathbf{p},t_1,t_2) + I_1^<(\mathbf{p},t_1,t_2), \tag{2.16}$$

where we have summarized both memory integrals into the function $I_1^<$. The equation of motion in the second time direction t_2 is given analogously.

In two-time and momentum space $(\mathbf{p},t,t')$ representation the self-energies in Eq. (2.16) read

$$\overline{\Sigma}^{\delta}(t) = \frac{\lambda}{2}\int \frac{d^d p}{(2\pi)^d} iG^<(\mathbf{p},t,t),$$

$$\Sigma^{\gtrless}(\mathbf{p},t,t') = -\frac{\lambda^2}{6}\int \frac{d^d q}{(2\pi)^d}\int \frac{d^d r}{(2\pi)^d} G^{\gtrless}(\mathbf{q},t,t')$$
$$\times G^{\gtrless}(\mathbf{r},t,t')G^{\gtrless}(\mathbf{p}-\mathbf{q}-\mathbf{r},t,t'). \tag{2.17}$$

For the numerical solution of the Kadanoff-Baym equations (2.16) we have developed a flexible and accurate algorithm, which is described in more detail in Appendix A. Furthermore, a straightforward integration of the Kadanoff-Baym equations (2.16) in time does not lead to meaningful results since in 2+1 space-time dimensions both self-energies (2.17), (2.18) are ultraviolet divergent. We note that due to the finite mass m adopted in Eq. (2.1) no problems arise from the infrared momentum regime. The ultraviolet regime, however, has to be renormalized by introducing proper counterterms. The details of the renormalization scheme are given in Appendix B as well as a numerical proof for the convergence in the ultraviolet regime.

III. FIRST NUMERICAL STUDIES ON EQUILIBRATION

In the following sections we will use the renormalized mass $m=1$, which implies that times are given in units of the inverse mass or $t\cdot m$ is dimensionless. Accordingly, the coupling λ in Eq. (2.1) is given in units of the mass m such that λ/m is dimensionless, too.

As already observed in the (1+1)-dimensional case [62] the mean-field term, generated by the tadpole diagram, does not lead to an equilibration of arbitrary initial momentum distributions since it only modifies the propagation of the particles by the generation of an effective mass. Our calculations lead to the same findings and thus we skip an explicit presentation of the actual results. Accordingly, thermalization in 2+1 dimensions requires the inclusion of the collisional self-energies as generated by the sunset diagram. All calculations to be shown in the following consequently involve both self-energies.

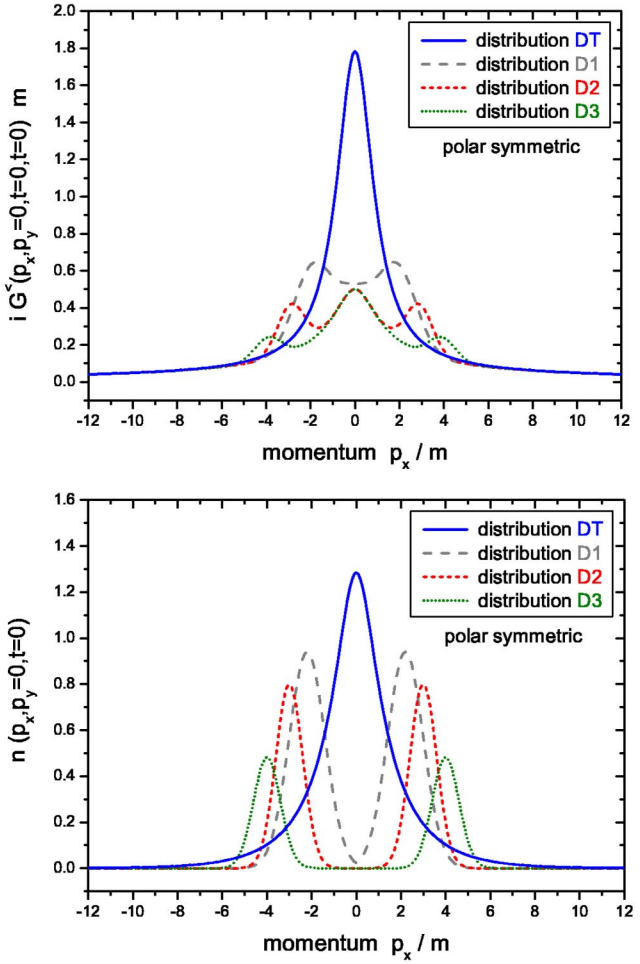

FIG. 3. Initial Green functions $iG^<(|\mathbf{p}|,t=0,t=0)$ (upper part) and corresponding initial distribution functions $n(|\mathbf{p}|,t=0)$ (lower part) for the distributions D1, D2, D3, and DT in momentum space (for a cut of the polar symmetric distribution in the p_x direction for $p_y=0$).

A. Initial conditions

In order to investigate equilibration phenomena on the basis of the Kadanoff-Baym equations for our (2+1)-dimensional problem, we first have to specify the initial conditions for the time integration. This is a problem of its own and discussed in more detail in Appendix C. For our present study we consider four different initial distributions that are all characterized by the same energy density (see Sec. IV A for an explicit representation). Consequently, for large times $(t\to\infty)$ all initial value problems should lead to the same equilibrium final state. The initial equal-time Green functions $G^<(\mathbf{p},t=0,t=0)$ adopted are displayed in Fig. 3 (upper part) as a function of the momentum p_x (for $p_y=0$). We concentrate here on polar symmetric configurations due to

the large numerical expense for this investigation.[1] Since the equal-time Green functions $G^<(\mathbf{p},t,t) \equiv G^<_{\phi\phi}(\mathbf{p},t,t)$ are purely imaginary, we show only the real part of $iG^<$ in Fig. 3. Furthermore, the corresponding initial distribution functions in the occupation density $n(\mathbf{p},t=0)$, related to $iG^<(\mathbf{p},t=0,t=0)$ via

$$2\omega_{\mathbf{p}} iG^<_{\phi\phi}(\mathbf{p},t=0,t=0) = n(\mathbf{p},t=0) + n(-\mathbf{p},t=0) + 1, \tag{3.1}$$

are shown in Fig. 3 in the lower part. For an explicit representation of the other Green functions $G^<_{\phi\pi}$, $G^<_{\pi\phi}$, and $G^<_{\pi\pi}$ (see Appendix A) at initial time t_0 we refer to the discussion of the general initial conditions in Appendix C. While the initial distributions D1, D2, D3 have the shape of (polar symmetric) ''tsunami'' waves [39] with maxima at different momenta in p_x, the initial distribution DT corresponds to a free Bose gas at a given initial temperature $T_0 \approx 1.736m$ that is fixed by the initial energy density. According to Eq. (3.1) the difference between the Green functions and the distribution functions is basically given by the vacuum contribution, which has its maximum at small momenta. Thus even for the distributions D1, D2, D3 the corresponding Green functions are nonvanishing for $|\mathbf{p}| \approx 0$.

Since we consider a finite volume $V=a^2$ we work in a basis of momentum modes characterized by the number of nodes in each direction. The number of momentum modes is typically in the order of 40; we checked that all our results are stable with respect to an increasing number of basis states and do not comment on this issue any more, since this is a strictly necessary condition for our analysis. For times $t<0$ we consider the systems to be noninteracting and switch on the interaction ($\sim\lambda$) for $t=0$ to explore the quantum dynamics of the interacting system for $t>0$. We directly step on with the actual numerical results.

B. Equilibration in momentum space

The time evolution of various (selected) momentum modes of the equal-time Green function for the different initial states D1, D2, D3, and DT is shown in Fig. 4, where the dimensionless time $t\cdot m$ is displayed on a logarithmic scale. We observe that starting from very different initial conditions—as introduced in Fig. 3—the single momentum modes converge to the same respective numbers for large times as characteristic for a system in equilibrium. As noted above, the initial energy density is the same for all distributions and energy conservation is fulfilled strictly in the time integration of the Kadanoff-Baym equations. The different momentum modes in Fig. 4 typically show a three-phase structure. For small times ($t\cdot m<10$) one finds damped oscillations that can be identified with a typical switching on effect at $t=0$, where the system is excited by a sudden increase of the coupling constant to $\lambda/m=18$. Here dephasing and relaxation of the initial conditions happen on a time

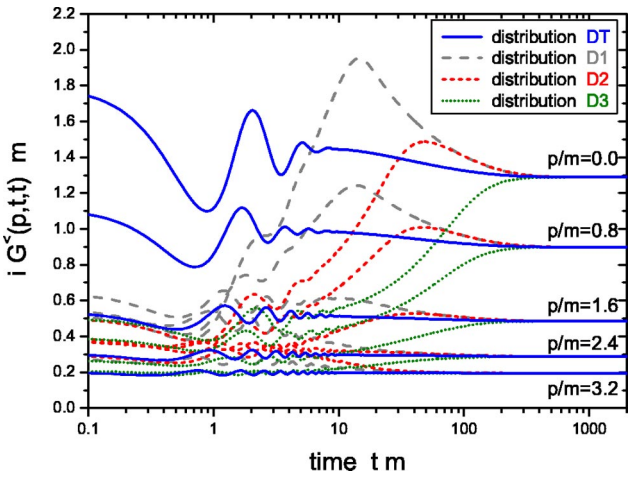

FIG. 4. Time evolution of selected momentum modes of the equal-time Green function $|\mathbf{p}|/m =$ 0.0, 0.8, 1.6, 2.4, 3.2 (from top to bottom) for four different initial configurations D1, D2, D3, and DT (characterized by the different line types) with the same energy density. For the rather strong coupling constant $\lambda/m=18$ the initial oscillations—from switching on the interaction at $t=0$—are damped rapidly and disappear for $t\cdot m>10$. Finally, all momentum modes assume the same respective equilibrium value for long times ($t\cdot m>500$) independent of the initial state.

scale of the inverse damping rate (see Appendix C). We note in passing that one might also start with an effective initial mass m^* including the self-consistent tadpole contribution [62], however, our numerical solutions showed no significant difference for the equilibration process such that we discard an explicit representation. The damping of the initial oscillations depends on the coupling strength λ/m and is more pronounced for strongly coupled systems.

For ''intermediate'' time scales ($10<t\cdot m<500$) one observes a strong change of all momentum modes in the direction of the final stationary state. We address this phase to ''kinetic'' equilibration and point out, that—depending on the initial conditions and the coupling strength—the momentum modes can temporarily even exceed their respective equilibrium value. This can be seen explicitly for the lowest momentum modes ($|\mathbf{p}|/m=0.0,\ 0.8$) of the distribution D1 (long dashed lines) in Fig. 4, which possesses initially maxima at small momentum. Thus the time evolution towards the final equilibrium value is—after an initial phase with damped oscillations—not necessarily monotonic. For different initial conditions this behavior may be weakened significantly as seen for example in case of the initial distribution D2 (short dashed lines) in Fig. 4. Coincidentally, both calculations D1 and D2 show approximately the same equal-time Green function values for times $t\cdot m>80$. Note, that for the initial distribution D3 (dotted lines) the nonmonotonic behavior is not seen any more.

In general, we observe that only initial distributions (of the well type) show this feature during their time evolution, if the maximum is located at sufficiently small momenta. Initial configurations such as the distribution DT (solid lines)—where the system initially is given by a free gas of particles at a temperature T_0—do not show this property. We

[1]In Sec. V we will also present calculations for nonsymmetric systems.

also remark that this ''overshooting''—as in the particular case of D1—is *not* observed in a simulation with a kinetic Boltzmann equation (see Appendix E). Hence this highly nonlinear effect must be attributed to quantal off-shell and memory effects not included in the standard Boltzmann limit. Although the DT distribution is not the equilibrium state of the interacting theory, the actual numbers are much closer to the equilibrium state of the interacting system than the initial distributions D1, D2, and D3. Therefore, the evolution for DT proceeds less violently. We point out that in contrast to the calculations performed for ϕ^4 theory in 1+1 space-time dimensions [62] we find no power law behavior for intermediate time scales.

The third phase, i.e., the late time evolution ($tm > 300$) is characterized by a smooth approach of the single momentum modes to their respective equilibrium values. As we will see in Sec. IV D this phase is adequately characterized by chemical equilibration processes. The three phases addressed in context with Fig. 4 will be investigated and analyzed in more detail in the following section.

IV. THE DIFFERENT PHASES OF QUANTUM EQUILIBRATION

A. Build up of initial correlations

The time evolution of the interacting system within the standard Kadanoff-Baym equations is characterized by the build up of early correlations. This can be seen from Fig. 5 where all contributions to the energy density [34] are displayed separately as a function of time with the initial value

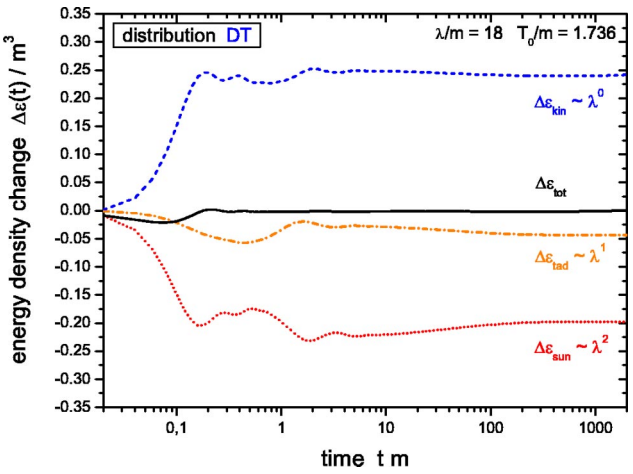

FIG. 5. Change of the different contributions to the total energy density in time. The sunset energy density $\varepsilon_{\rm sun}$ decreases rapidly in time; this contribution is approximately compensated by an increase of the kinetic energy density $\varepsilon_{\rm kin}$. Together with the smaller tadpole contribution $\varepsilon_{\rm tad}$ the total energy density $\varepsilon_{\rm tot}$ is conserved.

at $t_0=0$ subtracted. The kinetic energy density $\varepsilon_{\rm kin}$ is represented by all parts of $\varepsilon_{\rm tot}$ that are independent of the coupling constant ($\propto\lambda^0$). All terms proportional to λ^1 are summarized by the tadpole energy density $\varepsilon_{\rm tad}$ including the actual tadpole term as well as the corresponding tadpole mass counterterm (see Appendix B). The contributions from the sunset diagram ($\propto\lambda^2$)—again given by the correlation integral as well as by the sunset mass counterterm (see Appendix B)—are represented by the sunset energy density $\varepsilon_{\rm sun}$:

$$\varepsilon_{\rm tot}(t)=\varepsilon_{\rm kin}(t)+\varepsilon_{\rm tad}(t)+\varepsilon_{\rm sun}(t),$$

$$\varepsilon_{\rm kin}(t)=\frac{1}{2}\int\frac{d^dp}{(2\pi)^d}(\mathbf{p}^2+m^2)iG^<_{\phi\phi}(\mathbf{p},t,t)+\frac{1}{2}\int\frac{d^dp}{(2\pi)^d}iG^<_{\pi\pi}(\mathbf{p},t,t),$$

$$\varepsilon_{\rm tad}(t)=\frac{1}{4}\int\frac{d^dp}{(2\pi)^d}\bar{\Sigma}_{\rm tad}(t)iG^<_{\phi\phi}(\mathbf{p},t,t)+\frac{1}{2}\int\frac{d^dp}{(2\pi)^d}\delta m^2_{\rm tad}\,iG^<_{\phi\phi}(\mathbf{p},t,t),$$

$$\varepsilon_{\rm sun}(t)=\underbrace{-\frac{1}{4}\int\frac{d^dp}{(2\pi)^d}iI^<_1(\mathbf{p},t,t)}_{\varepsilon_{\rm cor}(t)}+\frac{1}{2}\int\frac{d^dp}{(2\pi)^d}\delta m^2_{\rm sun}\,iG^<_{\phi\phi}(\mathbf{p},t,t). \tag{4.1}$$

The calculation in Fig. 5 has been performed for the initial distribution DT (which represents a free gas of Bose particles at temperature $T_0\approx 1.736m$) with a coupling constant of $\lambda/m=18$. This state is stationary in the well-known Boltzmann limit (see Sec. V), but it is not for the Kadanoff-Baym equation. In the full quantum calculation the system evolves from an uncorrelated initial state and the correlation energy density $\varepsilon_{\rm sun}$ decreases rapidly with time. The decrease of the correlation energy $\varepsilon_{\rm sun}$ which is—with the exception of the sunset mass counterterm contribution—initially zero is ap-

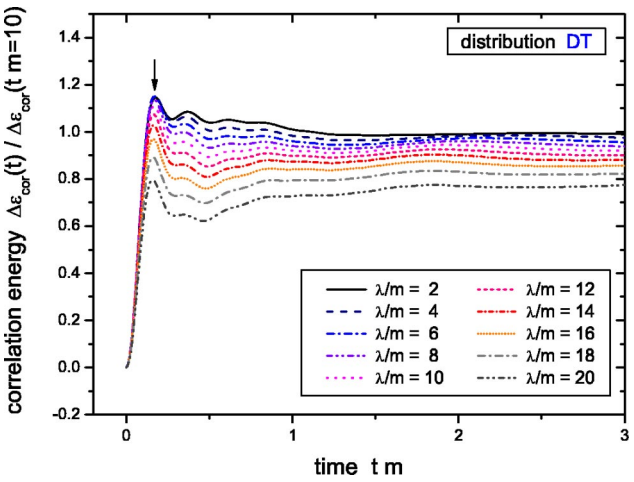

FIG. 6. Normalized change of the correlation energy density $\varepsilon_{\mathrm{cor}}$ for various coupling constants $\lambda/m=2-20$ in steps of 2 for the same initial distribution DT. The normalization has been performed with respect to the asymptotic correlation strength (for $t\cdot m>10$). The systems correlate approximately independent from the coupling strength after $\tau_{\mathrm{cor}}\cdot m\approx 0.16$.

proximately compensated by an increase of the kinetic energy density $\varepsilon_{\mathrm{kin}}$. Since the kinetic energy increases in the initial phase, the final temperature T_f is slightly higher than the initial ''temperature'' T_0. The remaining difference is compensated by the tadpole energy density $\varepsilon_{\mathrm{tad}}$ such that the total energy density is conserved.

While the sunset energy density and the kinetic energy density always show a time evolution comparable to Fig. 5, the change of the tadpole energy density depends on the initial configuration and may be positive as well. Since the self-energies are obtained within a Φ-derivable scheme the fundamental conservation laws, such as, e.g., energy conservation, are respected to all orders in the coupling constant. When neglecting the $\propto\lambda^2$ sunset contributions and starting with a nonstatic initial state of identical energy density one observes the same compensating behavior between the kinetic and the tadpole terms.

From Fig. 5 one finds that the system correlates in a very short time ($t\cdot m<1$) in comparison to the time for complete equilibration. The time to build up the correlations τ_{cor} is rather independent of the interaction strength as seen from Fig. 6, where calculations with the same initial state DT are compared for several coupling constants $\lambda/m=2-20$ in steps of 2. For all couplings λ/m the change of the correlation energy density here has been normalized to the asymptotic correlation strength ($t\cdot m>10$). Figure 6 shows that the correlation time τ_{cor} (which we define by the position of the first maximum) is approximately the same for all coupling constants. Within our definition the correlation time is $\tau_{\mathrm{cor}}\cdot m\approx 0.16$ for all couplings λ. This result is in line with the KB studies of nonrelativistic nuclear matter problems, where the same independence from the coupling strength has been observed for the correlation time [58]. A similar result has, furthermore, been obtained within the correlation dynamical approach of Ref. [46]. Thus quantum systems apparently correlate on time scales that are very short compared to ''kinetic'' or ''chemical'' equilibration time scales.

The question now arises how such short time scales come about. We recall, that equations of motion containing memory integrals, such as the Kadanoff-Baym equations, are the inevitable result of a reduction of multiparticle dynamics to the one-body level which induces phase correlations into the history of the system [89,90]. This is similar to the situation encountered in the derivation of the standard Boltzmann equation, which only holds if one can separate between two time scales $\tau_{\mathrm{cor}}\ll\tau_{\mathrm{rel}}$ (relaxation time scale), distinguishing between rapidly changing (''irrelevant'') observables and smoothly behaving (''relevant'') observables. Indeed, it had been shown for a nucleonic system [56] that such a finite memory in the collision process may have a profound influence on thermalization for medium-energy nuclear reactions. In any case, a finite correlation time is generated by first a constructive and then destructive interference of the various scattering channels building up for times going more and more in the past. For a fermionic system typical memory kernels for the collision integral are given in Refs. [55–57]. The structure of such memory kernels is governed by the off-shell behavior and the phase-space average of the two-particle scattering amplitude, i.e.,

$$\tau_{\mathrm{mem}}\sim\frac{\hbar}{\langle\Delta E\rangle}. \tag{4.2}$$

Of present concern is now the formation of the correlation energy and not the memory kernels of the collisional integrals, although they are closely related. The explicit correlation part of $\varepsilon_{\mathrm{sun}}$ contains the momentum integral over the function $I_1^<(\mathbf{p},t,t)$, which itself is given by a memory integral over time as stated in Eq. (A4) in Appendix A. From the explicit expression one notices that $I_1^<(\mathbf{p},t=0,t=0)\equiv 0$ and for small times builds up coherently by the various ''scattering'' contributions. For a fermionic system describing cold nuclear matter, similar expressions for the collisional energy density have been found and analyzed in detail by Köhler and Morawetz [58]. It has been found that the time to build up correlation energy by collisions from an initially uncorrelated system is given by $\tau_{\mathrm{cor}}\approx 2\hbar/E_F$, where E_F denotes the Fermi energy. The memory integrals of $I_1^<$—or those entering the quantal transport equations—can also contain classical contributions. For a dilute and equilibrated Maxwell-Boltzmann gas of nonrelativistic particles at finite temperature T and assuming a static, Gaussian interaction potential $V(r)=V_0\exp(-r^2/r_0^2)$, the various kernels can be worked out analytically [15,58,90]. The correlation time is then given by

$$\tau_{\mathrm{cor}}\approx\sqrt{r_0^2 m/T+(\hbar/T)^2}. \tag{4.3}$$

The first part reflects the intuitive expectation, i.e., the time a classical particle passes through the range of a potential; the second part reflects the average temporal extent associated with the time-energy uncertainty relation induced by the characteristic (off-shell) energy scale in a typical collision. For our present situation, i.e., a relativistic bosonic theory interacting via a four-point coupling, the temperature defines

the only scale. Hence, $\tau_{\rm cor}\approx\hbar/T$, which is a pure quantal effect. This estimate is in agreement with our numerical findings.

B. Time evolution of the spectral function

Within the Kadanoff-Baym calculations the full quantum information of the two-point functions is retained. Consequently, one has access to the spectral properties of the nonequilibrium system during its time evolution. A similar study has been carried out for 1+1 dimensions in Ref. [77]. The spectral function $A(x,y)$ for the present settings is given by

$$A(x,y)=\langle[\phi(x),\phi(y)]_-\rangle=i[G^>(x,y)-G^<(x,y)]. \tag{4.4}$$

From our dynamical calculations the spectral function in Wigner space for each system time $t=(t_1+t_2)/2$ is obtained via Fourier transformation with respect to the relative time coordinate $\Delta t=t_1-t_2$:

$$A(\mathbf{p},p_0,t)=\int_{-\infty}^{\infty}d\Delta t\,\exp(i\Delta t p_0)\times A(\mathbf{p},t_1=t+\Delta t/2,t_2=t-\Delta t/2). \tag{4.5}$$

We note that a damping of the function $A(\mathbf{p},t_1,t_2)$ in relative time Δt corresponds to a finite width Γ of the spectral function in Wigner space. This width in turn can be interpreted as the inverse life time of the interacting scalar particle. We recall, that the spectral function—for all times t and for all momenta $\mathbf{p}$—obeys the normalization

$$\int_{-\infty}^{\infty}\frac{dp_0}{2\pi}p_0A(\mathbf{p},p_0,t)=1,\quad\forall\mathbf{p},t, \tag{4.6}$$

which is nothing but a reformulation of the equal-time commutation relation.

In Fig. 7 we display the time evolution of the spectral function for the initial distributions D1, D2, D3, and DT for two different momentum modes $|\mathbf{p}|/m=0.0$ and $|\mathbf{p}|/m=2.0$. Since the spectral functions are antisymmetric in energy for the momentum symmetric configurations considered, i.e., $A(\mathbf{p},-p_0,t)=-A(\mathbf{p},p_0,t)$, we only show the positive energy part. For our initial value problem in two-times and momentum space the Fourier transformation (4.5) is restricted for system times t to an interval $\Delta t\in[-2t,2t]$. Thus in the very early phase the spectral function assumes a finite width already due to the limited support of the Fourier transform in the time interval and a Wigner representation is not very meaningful. We, therefore, present the spectral functions for various system times t starting from $t\cdot m=15$ up to $t\cdot m=480$.

For the free thermal initialization DT the evolution of the spectral function is very smooth and comparable to the smooth evolution of the equal-time Green function as discussed in Sec. III. In this case the spectral function is already close to the equilibrium shape at small times being initially only slightly broader than for late times. The maximum of the spectral function (for all momenta) is higher than the (bare) on-shell value and nearly keeps its position during the whole time evolution. This results from a positive tadpole mass shift, which is only partly compensated by a downward shift originating from the sunset diagram.

The time evolution for the initial distributions D1, D2, and D3 has a richer structure. For the distribution D1 the spectral function is broad for small system times (see the line for $t\cdot m=15$) and becomes a little sharper in the course of the time evolution (as presented for the momentum mode $|\mathbf{p}|/m=0.0$ as well as for $|\mathbf{p}|/m=2.0$). In line with the decrease in width the height of the spectral function is increasing [as demanded by the normalization property (4.6)]. This is indicated by the small arrow close to the peak position. Furthermore, the maximum of the spectral function (which is approximately the on-shell energy) is shifted slightly upwards for the zero mode and shifted downwards for the mode with higher momentum being always higher than the vacuum on-shell value.

For the initial distribution D3 we find the opposite behavior. Here the spectral function is quite narrow for early times and increases its width during the time evolution as observed for both momentum modes. Especially in the case of $|\mathbf{p}|/m=2.0$ the width for early times is so small that the spectral function shows oscillations originating from the finite range of the Fourier transformation from relative time to energy. Although we have already increased the system time for the first curve to $t\cdot m=21$ (for $t\cdot m=15$ the oscillations are much stronger) the spectral function is not fully resolved, i.e., it is not sufficiently damped in relative time Δt in the interval available for the Fourier transform. For later times the oscillations vanish and the spectral function tends to the common equilibrium shape.

The time evolution of the spectral function for the initial distribution D2 is in between the last two cases. Here the spectral function develops (at intermediate times) a slightly higher width than in the beginning before it is approaching the narrower static shape again. The corresponding evolution of the maximum is again indicated by the (bent) arrow. Finally, all spectral functions show the (same) equilibrium form represented by the solid gray line.

As already observed in Sec. III for the equal-time Green functions, we emphazise, that there is no unique time evolution for the nonequilibrium systems. In fact, the evolution of the system during the equilibration process depends on the initial conditions. Our findings are slightly different from the conclusions drawn in Ref. [77] stating that the Wigner transformed spectral function is slowly varying, which might be due to the lower dimension. Still the time dependence of the spectral function is moderate enough, such that one might also work with some time averaged or even the equilibrium spectral function. In order to investigate this issue in more quantitative detail, we concentrate on the maxima and widths of the spectral functions in the following.

Since the solution of the Kadanoff-Baym equation provides the full spectral information for all system times the evolution of the on-shell energies can be studied as well as

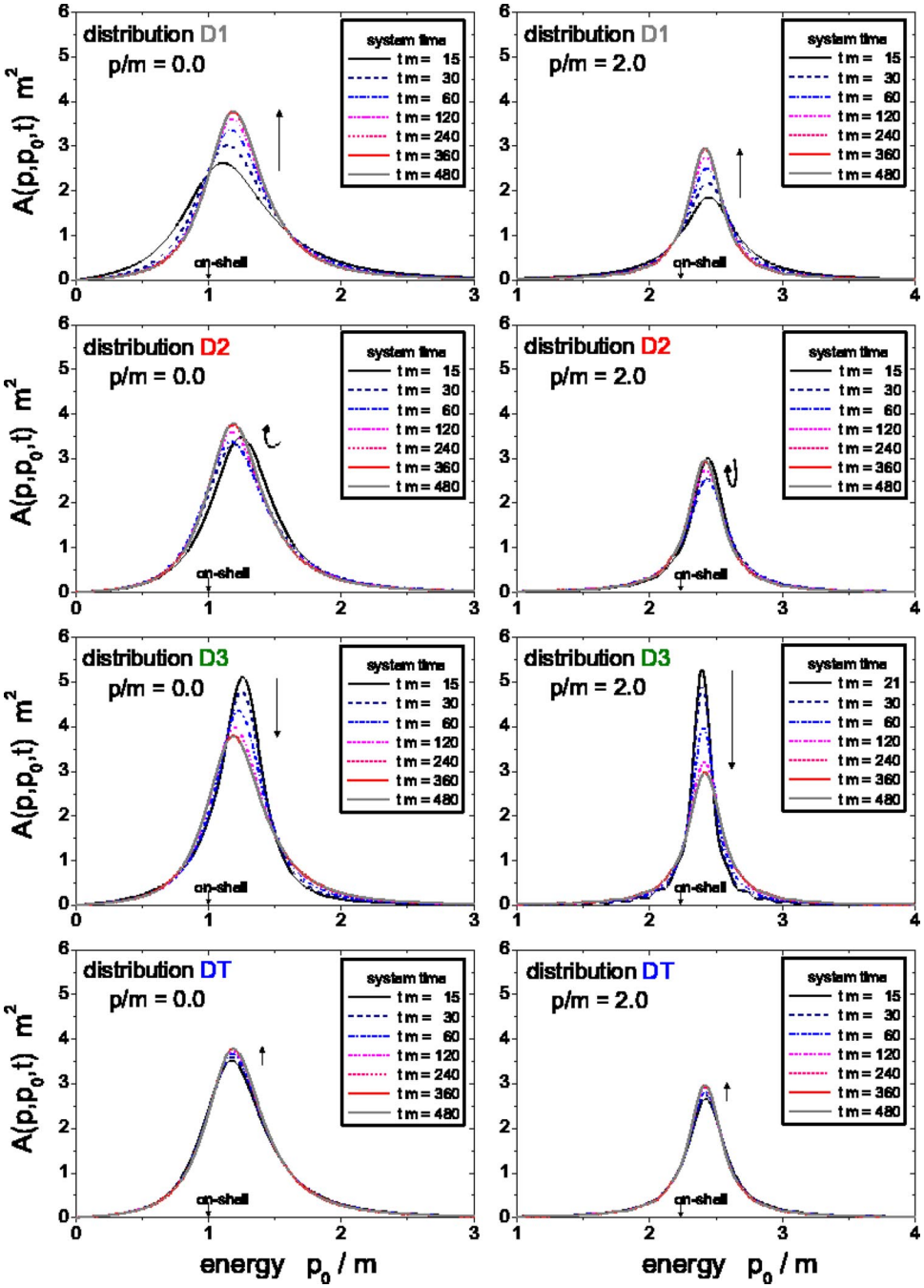

FIG. 7. Time evolution of the spectral function $A(\mathbf{p},p_0,t)$ for the initial distributions D1, D2, D3, and DT (from top to bottom) with coupling constant $\lambda/m=18$ and for the two momenta $|\mathbf{p}|/m=0.0$ (LHS) and $|\mathbf{p}|/m=2.0$ (RHS). The spectral function is shown for several times $tm=15$, 30, 60, 120, 240, 360, 480 as indicated by the different line types.

the spectral widths. In Fig. 8 we display the time dependence of the on-shell energies $\omega(\mathbf{p},t)$—defined by the maximum of the spectral function—of the momentum modes $|\mathbf{p}|/m=0.0$ (LHS) and $|\mathbf{p}|/m=2.0$ (RHS) for the four initial distributions D1, D2, D3, and DT. We see that the on-shell energy for the zero momentum mode increases with time for the initial distribution D1 and to a certain extent for the free thermal distribution DT (as can be also extracted from Fig. 7). The on-shell energy of distribution D3 shows a monotonic decrease during the evolution while it passes through a minimum for distribution D2 before joining the line for the initialization D1. For momentum $|\mathbf{p}|/m=2.0$ a rather opposite behavior is observed. Here the on-shell energy for distribution D1 (and less pronounced for the distribution DT) are reduced in time whereas it is increased in the case of D3. The result for the initialization D2 is monotonous for this mode and already matches the one for D1 for moderate times. Thus we find that the time evolution of the on-shell energies not only depends on the initial conditions, but might also be different for various momentum modes. It turns out—for the initial distributions investigated—that the above described characteristics change around $|\mathbf{p}|/m=1.5$ and are retained for larger momenta (not presented here).

Furthermore, we show in Fig. 9 the time evolution of the on-shell width for the usual momentum modes and different initial distributions. The on-shell width γ_ω is given by the imaginary part of the retarded sunset self-energy at the on-shell energy of each respective momentum mode as

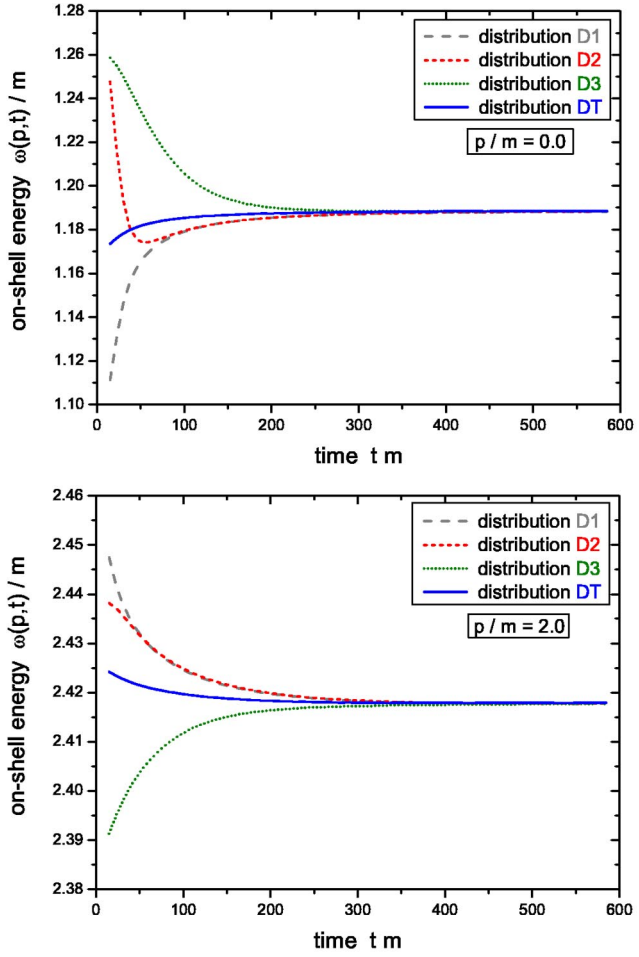

FIG. 8. Time evolution of the on-shell energies $\omega(\mathbf{p},t)$ of the momentum modes $|\mathbf{p}|/m=0.0$ and $|\mathbf{p}|/m=2.0$ for the different initializations D1, D2, D3, and DT with $\lambda/m=18$. The on-shell self-energies are extracted from the maxima of the time-dependent spectral functions.

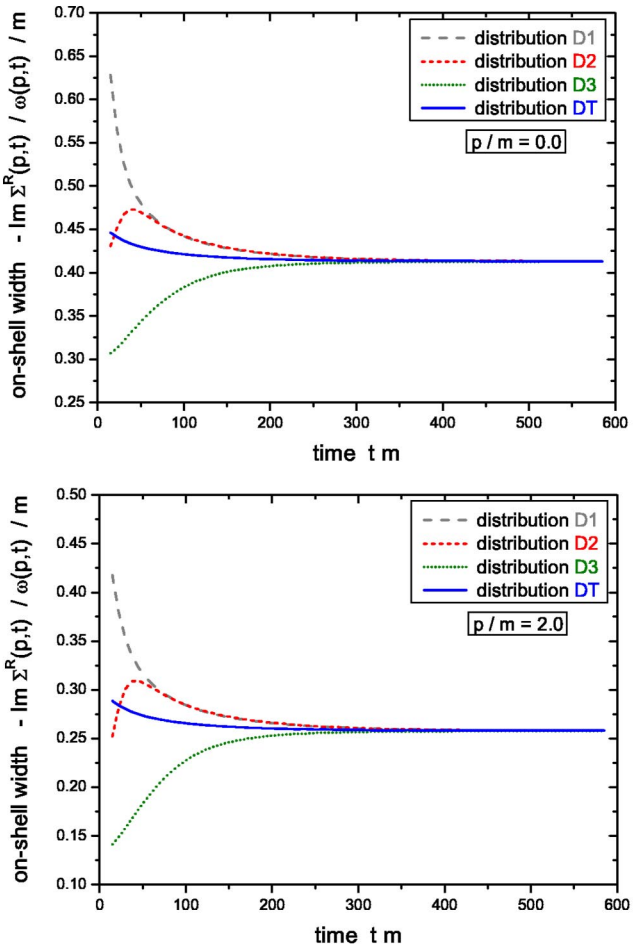

FIG. 9. Time evolution of the on-shell widths $-\mathrm{Im}\,\Sigma^R[\mathbf{p},\omega(\mathbf{p},t),t]/\omega(\mathbf{p},t)$ of the momentum modes $|\mathbf{p}|/m=0.0$ and $|\mathbf{p}|/m=2.0$ for the different initializations D1, D2, D3, and DT with $\lambda/m=18$.

$$\gamma_\omega(\mathbf{p},t)=\frac{-2\,\mathrm{Im}\,\Sigma^R[\mathbf{p},\omega(\mathbf{p},t),t]}{2\,\omega(\mathbf{p},t)}=\frac{\Gamma[\mathbf{p},\omega(\mathbf{p},t),t]}{2\,\omega(\mathbf{p},t)}. \tag{4.7}$$

As already discussed in connection with Fig. 7 we observe for both momentum modes a strong decrease of the on-shell width for the initial distribution D1 (long dashed lines) associated with a narrowing of the spectral function. In contrast, the on-shell widths of distribution D3 (dotted lines) increase with time such that the corresponding spectral functions broaden towards the common stationary shape. For the initialization D2 (short dashed lines) we observe a nonmonotonic evolution of the on-shell widths connected with a broadening of the spectral function at intermediate times. Similar to the case of the on-shell energies we find, that the results for the on-shell widths of the distributions D1 and D2 coincide well above a certain system time. As expected from the lower plots of Fig. 7, the on-shell width for the free thermal distribution DT (solid lines) exhibits only a weak time dependence with a slight decrease in the initial phase of the time evolution.

In summarizing this subsection we point out, that there is no universal time evolution of the spectral functions for the initial distributions considered. Peak positions and widths depend on the initial configuration and evolve differently in time. However, we find only effects in the order of $<10\%$ for the on-shell energies in the initial phase of the system evolution and initial variations of $<50\%$ for the widths of the dominant momentum modes. Thus, depending on the physics problem of interest, one might eventually discard an explicit time dependence of the spectral functions and adopt the equilibrium shape.

C. The equilibrium state

In Sec. III we have seen that arbitrary initial momentum configurations of the same energy density approach a stationary limit for $t\to\infty$, which is the same for all initial distributions. In this subsection we will investigate, whether this stationary state is the proper thermal state for interacting Bose particles.

This question has already been addressed in Ref. [44] for an $O(N)$-invariant scalar field theory with unbroken symmetry. There it was shown that in the next-to-leading order (NLO) approximation the only translational invariant solutions are thermal ones. The importance of using the NLO approximation lies in the fact that—in contrast to the leading order (LO) calculation—scattering processes are included in the propagation which provide thermalization. Furthermore, the correlations induced by scattering lead to a nontrivial spectral function, whereas in the LO approximation one obtains the δ-function quasiparticle shape. Additionally, in the NLO calculation particle number nonconserving processes are allowed that lead to a change of the chemical potential μ, which approaches zero in the equilibrium state in agreement with the expectations for a neutral scalar theory without conserved quantum numbers.

As shown before, in our present calculations within the three-loop approximation of the 2PI effective action we describe kinetic equilibration via the sunset self-energies and also obtain a finite width for the particle spectral function. It is not obvious, however, if the stationary state obtained for $t\to\infty$ corresponds to the proper equilibrium state.

In order to clarify the nature of the asymptotic stationary state of our calculations we first change into Wigner space. The Green function and the spectral function in energy p_0 are obtained by Fourier transformation with respect to the relative time $\Delta t=t_1-t_2$ at every system time $t=(t_1+t_2)/2$ [see Eq. (4.5)]

$$G^{\gtrless}(\mathbf{p},p_0,t)=\int_{-\infty}^{\infty}d\Delta t\,\exp(ip_0\Delta t)\times G^{\gtrless}(\mathbf{p},t_1=t+\Delta t/2,t_2=t-\Delta t/2), \quad (4.8)$$

$$A(\mathbf{p},p_0,t)=\int_{-\infty}^{\infty}d\Delta t\,\exp(ip_0\Delta t)\times A(\mathbf{p},t_1=t+\Delta t/2,t_2=t-\Delta t/2). \quad (4.9)$$

We recall that the spectral function (4.9) can also be obtained directly from the Green functions in Wigner space by Eq. (4.4)

$$A(\mathbf{p},p_0,t)=i[G^{>}(\mathbf{p},p_0,t)-G^{<}(\mathbf{p},p_0,t)]. \quad (4.10)$$

Now we introduce the energy and momentum dependent distribution function $N(\mathbf{p},p_0,t)$ at any system time t by

$$iG^{<}(\mathbf{p},p_0,t)=A(\mathbf{p},p_0,t)N(\mathbf{p},p_0,t),$$

$$iG^{>}(\mathbf{p},p_0,t)=A(\mathbf{p},p_0,t)[N(\mathbf{p},p_0,t)+1]. \quad (4.11)$$

In equilibrium (at temperature T) the Green functions obey the Kubo-Martin-Schwinger (KMS) relation [91,92] for all momenta $\mathbf{p}$

$$G^{>}_{\rm eq}(\mathbf{p},p_0)=\exp(p_0/T)G^{<}_{\rm eq}(\mathbf{p},p_0), \quad \forall\mathbf{p}. \quad (4.12)$$

If there exists a conserved quantum number in the theory we have, furthermore, a contribution of the corresponding chemical potential in the exponential function, which leads to a shift of arguments $p_0/T\to(p_0-\mu)/T$. In the present case, however, there is no conserved quantum number and thus the equilibrium state has to give $\mu=0$.

From the KMS condition of the Green functions (4.12) we obtain the equilibrium form of the distribution function (4.11) at temperature T as

$$N_{\rm eq}(\mathbf{p},p_0)=N_{\rm eq}(p_0)=\frac{1}{\exp(p_0/T)-1}=N_{\rm Bose}(p_0/T), \quad (4.13)$$

which is the well-known Bose distribution. As is obvious from Eq. (4.13) the equilibrium distribution can only be a function of energy p_0 and not of the momentum variable explicitly.

In Fig. 10 (lower part) we present the spectral function $A(\mathbf{p},p_0,t)$ for the initial distribution D2 at late time $t\cdot m=540$ for various momentum modes $|\mathbf{p}|/m=0.0$, 0.8, 1.6, 2.4, 3.2, 4.0 as a function of the energy p_0. We note that for all other initial distributions—with equal energy density—the spectral function looks very similar at this time since the systems proceed to the same stationary state (see Sec. IV C). We recognize that the spectral function is quite broad, especially for the low momentum modes, while for the higher momentum modes its width is slightly lower.

The distribution function $N(p_0)$ as extracted from Eq. (4.11) is displayed in Fig. 10 (upper part) for the same momentum modes as a function of the energy p_0. The comparison is achieved by selecting a certain energy band around the maximum of each momentum mode considering all energies p_0 with $A(|\mathbf{p}|,p_0)m^2\geqslant 0.5$. We find that $N(p_0)$ for all momentum modes can be fitted by a single Bose function with temperature $T/m=1.835$. Thus the distribution function emerging from the Kadanoff-Baym time evolution for $t\to\infty$ approaches a Bose function in the energy p_0 that is independent of the momentum as demanded by the equilibrium form (4.13).

Figure 10 (upper part) demonstrates, furthermore, that the KMS condition is fulfilled not only for on-shell energies, but for all p_0. We, therefore, have obtained the full off-shell equilibrium state by integrating the Kadanoff-Baym equations in time. In addition, the limiting stationary state is the correct equilibrium state for all energies p_0, i.e. also away from the quasiparticle energies.

We note in closing this subsection that the chemical potential μ—used as a second fit parameter—is already close to zero for these late times as expected for the correct equilibrium state of the neutral ϕ^4 theory which is characterized by a vanishing chemical potential μ in equilibrium. This, at first sight, seems rather trivial but we will show in the next subsection that it is a consequence of our exact treatment. In contrast, the Boltzmann equation (see Sec. V

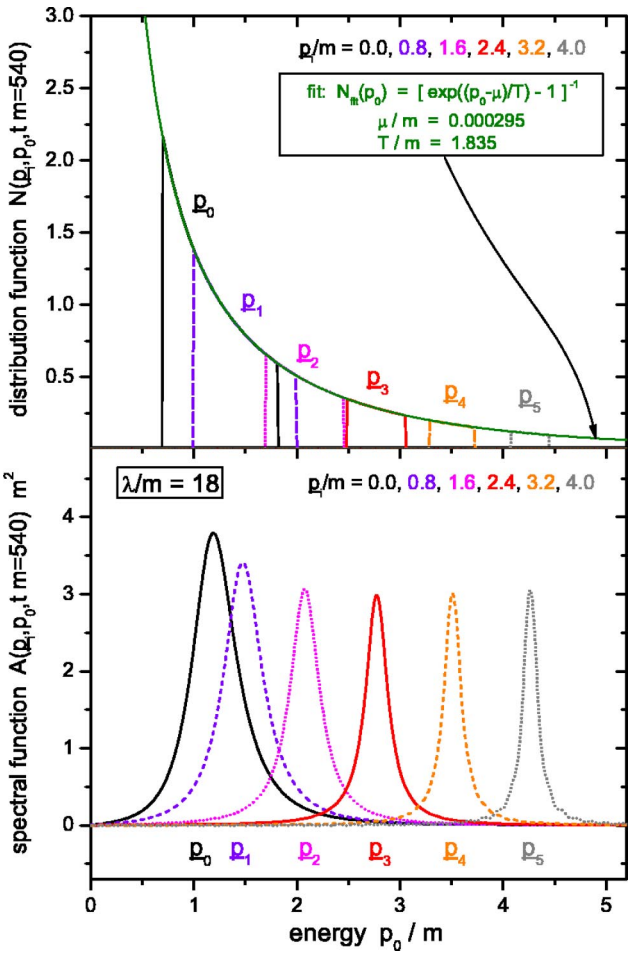

FIG. 10. Spectral function A for various momentum modes $|\mathbf{p}|/m=0.0$, 0.8, 1.6, 2.4, 3.2, 4.0 as a function of energy for late time $t\cdot m=540$ (lower part). As shown is the corresponding distribution function N at the same time for the same momentum modes (upper part). All momentum modes can be fitted with a single Bose function of temperature $T_{\mathrm{eq}}/m=1.835$ and a chemical potential close to zero.

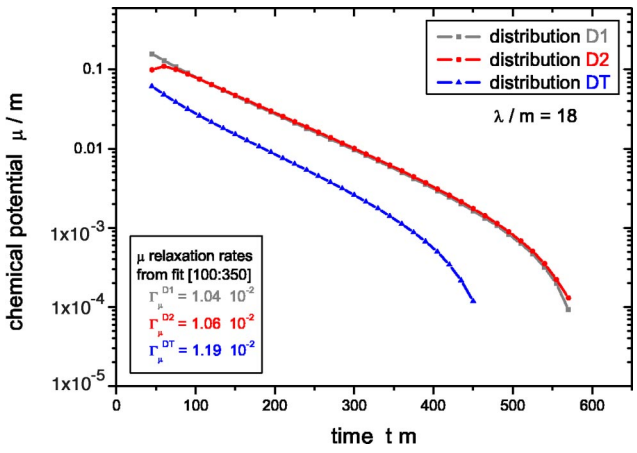

FIG. 11. Logarithmic representation of the time evolution of the chemical potential μ for the initial distributions D1, D2, and DT. The corresponding relaxation rate Γ_{μ}^{-} is determined from the exponential decrease.

and Appendix E) in general leads to a stationary state for $t\rightarrow\infty$ with a finite chemical potential. We will attribute this failure of the Boltzmann approach to the absence of particle number nonconserving processes in the quasiparticle limit (see below).

D. Chemical equilibration and approach to KMS

As we have seen in the previous subsection the chemical potential μ for the stationary state of the propagation at large times is close to zero in agreement with the properties of the neutral ϕ^4 theory. In this subsection we will address the question of chemical equilibration in the late time evolution of the systems calculated before. In particular we are interested in examining how the chemical potential μ vanishes with time for configurations initialized with finite chemical potentials $\mu\neq 0$ at $t=0$.

To this aim we calculate the distribution function $N(p_0,t)$ for various system times t and extract the time-dependent chemical potential $\mu(t)$ by fitting a Bose function with parameters μ and T. The time evolution of the chemical potential μ (as extracted from the zero momentum mode) is displayed in Fig. 11 for various initial configurations and found to decrease almost exponentially with t to zero. For small times t the curves do not show an exponential behavior since here we are still in the regime of kinetic nonequilibrium. Moreover, the chemical potential relaxation rate is nearly the same for all initial configurations with the same energy density.

In order to understand the reason for this observation we calculate an estimate for this relaxation rate along the lines of Calzetta and Hu [44]. For reasons of transparency we first provide a brief derivation for the three-loop approximation of the 2PI effective action.

Since we are interested in the properties of the system close to equilibrium we again change to a Wigner representation for the Kadanoff-Baym equation. A first order gradient expansion of the Wigner transformed equation yields the following real valued transport equation [81–83]:

$$\begin{aligned}
&\diamondsuit\{p^2-m^2-\overline{\Sigma}^{\delta}(t)-\mathrm{Re}\,\Sigma^R(p,t)\}\{iG^<(p,t)\}\\
&\quad-\diamondsuit\{i\Sigma^<(p,t)\}\{ReG^R(p,t)\}\\
&\quad=\frac{1}{2}[G^>(p,t)\Sigma^<(p,t)-G^<(p,t)\Sigma^>(p,t)]\\
&\quad=C(p,t). \qquad (4.14)
\end{aligned}$$

Here the operator $\diamondsuit$ denotes the $(d+1)$-dimensional representation of the general Poisson bracket. For the present case of spatially homogeneous systems all derivatives with respect to the mean spatial coordinates vanish. Thus it contains mean time and energy derivatives, only, and is given for arbitrary functions $F_{1/2}=F_{1/2}(p,t)=F_{1/2}(\mathbf{p},p_0,t)$ as

$$\diamond\{F_1\}\{F_2\}=\frac{1}{2}\left(\frac{\partial F_1}{\partial t}\frac{\partial F_2}{\partial p_0}-\frac{\partial F_1}{\partial p_0}\frac{\partial F_2}{\partial t}\right). \quad (4.15)$$

We first concentrate on the collision term $C(p,t)$—as given by the RHS of Eq. (4.14)—for small deviations from thermal equilibrium. In our representation the correlation self-energies $\Sigma^{\gtrless}$ read in Wigner space

$$\Sigma^{\gtrless}(\mathbf{p},p_0,t)=-\frac{\lambda^2}{6}\int\frac{d^{d+1}q}{(2\pi)^{d+1}}\int\frac{d^{d+1}r}{(2\pi)^{d+1}}\int\frac{d^{d+1}s}{(2\pi)^{d+1}}\times(2\pi)^{d+1}\delta^{(d+1)}(p-q-r-s)\times G^{\gtrless}(\mathbf{q},q_0,t)G^{\gtrless}(\mathbf{r},r_0,t)G^{\gtrless}(\mathbf{s},s_0,t), \quad (4.16)$$

where the energy and momentum integrals extend from $-\infty$ to ∞. In order to simplify the collision term we express the Green functions [similar to Eq. (4.11)] by the spectral function A and a distribution function $\tilde{N}$ via

$$iG^{\gtrless}(\mathbf{p},p_0,t)=\mathrm{sgn}(p_0)A(\mathbf{p},p_0,t)\times[\Theta(\pm p_0)+\tilde{N}(\mathbf{p},p_0,t)]. \quad (4.17)$$

The advantage of this representation is that the spectral function term $\mathrm{sgn}(p_0)A(\mathbf{p},p_0,t)$ as well as the modified distribution function $\tilde{N}(\mathbf{p},p_0,t)$ are symmetric in the energy coordinate p_0 as can be deduced from $G^{>}(\mathbf{p},p_0,t)=G^{<}(-\mathbf{p},-p_0,t)=G^{<}(\mathbf{p},-p_0,t)$ for the momentum symmetric $(\mathbf{p}\to-\mathbf{p})$ configurations considered here. The remaining asymmetric character of the Green functions is contained in the step functions in energy. By this separation we may express the integrations over the full energy space in terms of integrations over the positive energy axis, only. Thus the collision term—additionally integrated over momenta and positive energies—can be written as

$$\int\frac{d^{d+1}p}{(2\pi)^{d+1}}\Theta(p_0)C(p,t)=-\frac{i}{2}\int\frac{d^{d+1}p}{(2\pi)^{d+1}}\Theta(p_0)\,A(p,t)\{[1+\tilde{N}(p,t)]\Sigma^{<}(p,t)-\tilde{N}(p,t)\Sigma^{>}(p,t)\} \quad (4.18)$$

$$=-\frac{i}{2}\int Dp\{[1+\tilde{N}(p,t)]\Sigma^{<}(p,t)-\tilde{N}(p,t)\Sigma^{>}(p,t)\}$$

$$=-\frac{\lambda^2}{6}\int Dp\int Dq\int Dr\int Ds(2\pi)^{d+1}\delta^{(d+1)}(p-q-r-s)\times\{\tilde{N}(p,t)[1+\tilde{N}(q,t)][1+\tilde{N}(r,t)][1+\tilde{N}(s,t)]-[1+\tilde{N}(p,t)]\tilde{N}(q,t)\tilde{N}(r,t)\tilde{N}(s,t)\}.$$

Here we have introduced the short-hand notation

$$\int Dp=\int\frac{d^{d+1}p}{(2\pi)^{d+1}}\Theta(p_0)A(p,t)=\int\frac{dp_0}{(2\pi)}\Theta(p_0)\int\frac{d^dp}{(2\pi)^d}A(\mathbf{p},p_0,t). \quad (4.19)$$

We are interested especially in the very late time evolution, where the system is already close to equilibrium. Thus we can evaluate the integrated collision term with further approximations. First, we use the thermal spectral function $A_{\mathrm{eq}}(\mathbf{p},p_0)$ at the equilibrium temperature T_{eq}. This spectral function is calculated separately within a self-consistent scheme, which is explained in detail in Appendix D. We note in passing, that the self-consistent thermal spectral functions (calculated numerically) are in excellent agreement with the dynamical spectral functions in the long-time limit of the nonequilibrium Kadanoff-Baym dynamics. Second, we adopt an equilibrium Bose function for the symmetrical nonequilibrium distribution function $\tilde{N}$ in energy, but allow for a small deviation in terms of a small chemical potential $\bar{\mu}=\mu/T$. This chemical potential $\bar{\mu}$ depends on the system time t as indicated by its relaxation observed in Fig. 11, but is assumed to be independent of energy and momentum. The near equilibrium distribution function is thus given by

$$\tilde{N}(p)\approx\tilde{N}^{\bar{\mu}}(p_0)=\frac{1}{\exp(|p_0|/T-\bar{\mu})-1}\xrightarrow{\bar{\mu}\to0}\tilde{N}^0(p_0)=N_{\mathrm{Bose}}(|p_0|/T). \quad (4.20)$$

We now expand the integrated collision term with respect to

the small parameter $\bar{\mu}$ around the equilibrium value $\bar{\mu}_{\rm eq}=0$. Since the zero-order contribution vanishes for the collision term in equilibrium, the first nonvanishing order is given by

$$\int \frac{d^{d+1}p}{(2\pi)^{d+1}}\Theta(p_0)C(p,t)\frac{\lambda^2}{6}2\bar{\mu} \times\int Dp_{\rm eq}\int Dq_{\rm eq}\int Dr_{\rm eq}\int Ds_{\rm eq}(2\pi)^{d+1}\delta^{(d+1)} \times(p-q-r-s)[1+\tilde{N}^0(p)]\tilde{N}^0(q)\tilde{N}^0(r)\tilde{N}^0(s) \tag{4.21}$$

with the integration weighted by the thermal spectral function $A_{\rm eq}$ as

$$\int Dp_{\rm eq}=\int\frac{d^{d+1}p}{(2\pi)^{d+1}}\Theta(p_0)A_{\rm eq}(p) =\int\frac{dp_0}{(2\pi)}\Theta(p_0)\int\frac{d^dp}{(2\pi)^d}A_{\rm eq}(\mathbf{p},p_0). \tag{4.22}$$

On the left-hand-side of the transport equation we neglect, furthermore, the time derivative terms of the self-energies as well as the second Poisson bracket. The only contribution then stems from the drift term $p_0\partial_t G^<(\mathbf{p},p_0,t)$, which might be extended by considering the energy derivative of the real part of the retarded self-energy.

The Green function is expressed again in terms of symmetric functions in energy (4.17), where the distribution function $\tilde{N}$ is given by the near equilibrium estimate (4.20) with a small time-dependent deviation $\bar{\mu}(t)$. Since the spectral function is approximated by its equilibrium form, the time derivative of the drift term gives only a contribution from the chemical potential. When integrating the complete drift term over momentum and (positive) energy space—as done above for the right-hand side—we obtain in lowest order of the small chemical potential

$$\int\frac{d^{d+1}p}{(2\pi)^{d+1}}\Theta(p_0)\{-p_0\partial_t iG^<(p,t)\} \approx-\int\frac{d^{d+1}p}{(2\pi)^{d+1}}\Theta(p_0)A_{\rm eq}(p)p_0\partial_t\tilde{N}^{\bar{\mu}}(p,t) \approx-\frac{\partial\bar{\mu}(t)}{\partial t}\int D\,p_{\rm eq}\,p_0\,\tilde{N}^0(p_0)[1+\tilde{N}^0(p_0)]. \tag{4.23}$$

By taking also into account the energy derivative of the retarded self-energy we gain the improved result

$$\int\frac{d^{d+1}p}{(2\pi)^{d+1}}\Theta(p_0)\left\{-\left(p_0-\frac{1}{2}\partial_{p_0}{\rm Re}\,\Sigma^R_{\rm eq}(p)\right)\partial_t iG^<(p,t)\right\} \approx-\frac{\partial\bar{\mu}(t)}{\partial t}\int Dp_{\rm eq}\left(p_0-\frac{1}{2}\partial_{p_0}{\rm Re}\,\Sigma^R_{\rm eq}(p)\right)\tilde{N}^0(p_0) \times[1+\tilde{N}^0(p_0)]. \tag{4.24}$$

Combining now both half-sides of the approximated transport equation we obtain

$$-\frac{\partial\bar{\mu}(t)}{\partial t}K_1([A_{\rm eq}(\lambda,T)];T)=\bar{\mu}(t)K_2([A_{\rm eq}(\lambda,T)];T,\lambda) \tag{4.25}$$

with the temperature and coupling constant dependent functions

$$K_1([A_{\rm eq}(\lambda,T)];T)=\int Dp_{\rm eq}\left(p_0-\frac{1}{2}\partial_{p_0}{\rm Re}\,\Sigma^R_{\rm eq}(p)\right) \times\tilde{N}^0(p_0)[1+\tilde{N}^0(p_0)], \tag{4.26}$$

$$K_2([A_{\rm eq}(\lambda,T)];T,\lambda)=\frac{\lambda^2}{3}\int Dp_{\rm eq}\int Dq_{\rm eq}\int Dr_{\rm eq}\int Ds_{\rm eq}(2\pi)^{d+1}\delta^{(d+1)}(p-q-r-s)[1+\tilde{N}^0(p_0)]\tilde{N}^0(q_0)\tilde{N}^0(r_0)\tilde{N}^0(s_0) =\frac{\lambda^2}{3}\int Dp_{\rm eq}\int Dq_{\rm eq}\int Dr_{\rm eq}\int Ds_{\rm eq}(2\pi)^{d+1}\delta^{(d+1)}(p-q-r-s)\tilde{N}^0(p_0)[1+\tilde{N}^0(q_0)][1+\tilde{N}^0(r_0)] \times[1+\tilde{N}^0(s_0)].$$

Thus the chemical potential decreases exponentially as

$$\bar{\mu}(t)=\exp(-K_2/K_1t)=\exp(-\Gamma_{\bar{\mu}}t) \tag{4.27}$$

with the relaxation rate given by

$$\Gamma_{\bar{\mu}}=K_2/K_1. \tag{4.28}$$

The equations above provide an explanation for the observed behavior of the relaxation of the chemical potential. At first

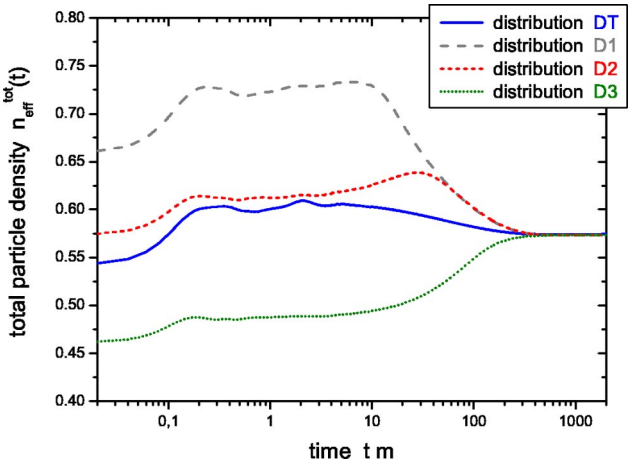

FIG. 12. Total particle number density $n_{\mathrm{eff}}^{\mathrm{tot}}(t)$ for the initializations D1, D2, D3, and DT as a function of time. The particle number is not constant during the evolution, but changes due to nonconserving transitions ($1\leftrightarrow 3$) that are allowed within the full Kadanoff-Baym dynamics.

we recognize the exponential nature (4.27) of the processes seen in Fig. 11. The relaxation of the chemical potential originates—as seen from Eq. (4.26)—from particle number nonconserving $1\leftrightarrow 3$ processes. This is easily recognized when considering the distribution functions $\tilde{N}$ assigned to incoming particles as well as the corresponding Bose enhancement factors $1+\tilde{N}$ for the outgoing ones. Ordinary particle number conserving $2\leftrightarrow 2$ scattering processes do not contribute. Thus it is not surprising, that a relaxation of the chemical potential is not described in the on-shell Boltzmann limit and the correct equilibrium state with vanishing chemical potential is missed (see Appendix E).

The corresponding time evolution of the total particle number density $n_{\mathrm{eff}}^{\mathrm{tot}}$ is shown in Fig. 12. It is obtained as the momentum space integral over the effective distribution function, which is defined for symmetric ($\mathbf{p}\rightarrow -\mathbf{p}$) configurations by the equal-time Green functions as [62]

$$n_{\mathrm{eff}}(\mathbf{p},t)=\sqrt{G_{\phi\phi}^{<}(\mathbf{p},t,t)G_{\pi\pi}^{<}(\mathbf{p},t,t)}-\frac{1}{2}. \qquad (4.29)$$

From Fig. 12 we clearly see that the particle number for the full Kadanoff-Baym equation is not constant in time, but changes due to $1\leftrightarrow 3$ transitions. Finally, the distributions D1, D2, and DT show an excess of particles—related to their positive chemical potential—that is reduced until the common particle number is reached in the stationary limit. In contrast, the distribution D3 (dotted line) with initially well separated maxima in momentum space has too few particles, however, during the time evolution particles are produced such that the system reaches the common equilibrium state as well.

Furthermore, we point out the importance of the spectral function entering the relaxation rate (4.26) via the integral measures. Since $1\leftrightarrow 3$ processes are responsible for the chemical equilibration, especially the shape of the spectral functions for high and low energies, i.e., above and below the three-particle threshold, is of great importance. From the formula above we also find an explanation for the fact, that all equal energy initializations—although starting with different absolute values of the chemical potential—show approximately the same relaxation rate. The spectral functions for the different initializations have already almost converged to the thermal spectral function (for the equilibrium temperature of $T_{\mathrm{eq}}/m=1.835$ and coupling constant $\lambda/m=18$) and are therefore comparable during the late stage of the evolution. The same holds approximately for the respective distribution functions, that approach Bose distribution functions at temperature T_{eq}. Thus we can deduce from Eq. (4.26) that the relaxation rate should be approximately the same for the different initial value problems considered.

Indeed, the estimate for the chemical relaxation (4.28) rate works rather well quantitatively. By calculating the thermal spectral functions independently within a self-consistent scheme at equilibrium temperature T_{eq} for coupling constant $\lambda/m=18$ we find (together with the distribution functions of the same temperature)—by solving the multidimensional integrations—a value of $\Gamma_{\bar{\mu}}/m\approx 1.12\times 10^{-2}$ (for the drift term only) and $\Gamma_{\bar{\mu}}/m\approx 1.17\times 10^{-2}$ (when including additionally the energy dependence of the retarded self-energy) for the relaxation rate. The agreement with the results of the actual calculations in Fig. 11 given by $\Gamma_{\bar{\mu}}^{\mathrm{D1}}/m\approx 1.04\times 10^{-2}$, $\Gamma_{\bar{\mu}}^{\mathrm{D2}}/m\approx 1.06\times 10^{-2}$, and $\Gamma_{\bar{\mu}}^{\mathrm{DT}}/m\approx 1.19\times 10^{-2}$, is sufficiently good.

E. Dynamics close to the thermal state

In this subsection we address the properties of systems close to thermal equilibrium. It is a widely used assumption that there exists a regime close to the thermal state, where the relaxation approximation is valid. Especially interesting are settings, where all momentum modes are in equilibrium, but only a single momentum mode $\mathbf{p}$ is out of equilibrium and deviates from its equilibrium value by a small amount δN. In such a case $\delta N(t)$ should decrease exponentially in time. The corresponding rate can be calculated in the usual quasiparticle approximation (i.e., starting from the standard Boltzmann equation) and is given by the on-shell width of the particle as determined from the imaginary part of the retarded self-energy at the on-shell energy (with respect to the momentum $\mathbf{p}$) as $\gamma_{\omega}(\mathbf{p})=-\mathrm{Im}\,\Sigma^{R}(\mathbf{p},\omega(\mathbf{p}))/\omega(\mathbf{p})$.

In order to study the relaxation behavior within the full Kadanoff-Baym theory we generate a corresponding initial state by the following procedure: We first start with a general nonequilibrium distribution at $t=0$ and let it evolve in time. After a sufficiently long time period all momentum modes of the system get close to equilibrium. We then excite only a single momentum mode at a specific time t_k by multiplying the equal-time Green functions $G_{\phi\phi}^{<}(\mathbf{p},t,t)$ and $G_{\pi\pi}^{<}(\mathbf{p},t,t)$ at $t=t_k$ with a factor close to 1. As a result the corresponding effective occupation number $n_{\mathrm{eff}}(\mathbf{p},t)$ (4.29) differs slightly from its equilibrium value by $\Delta N(t_k)$.

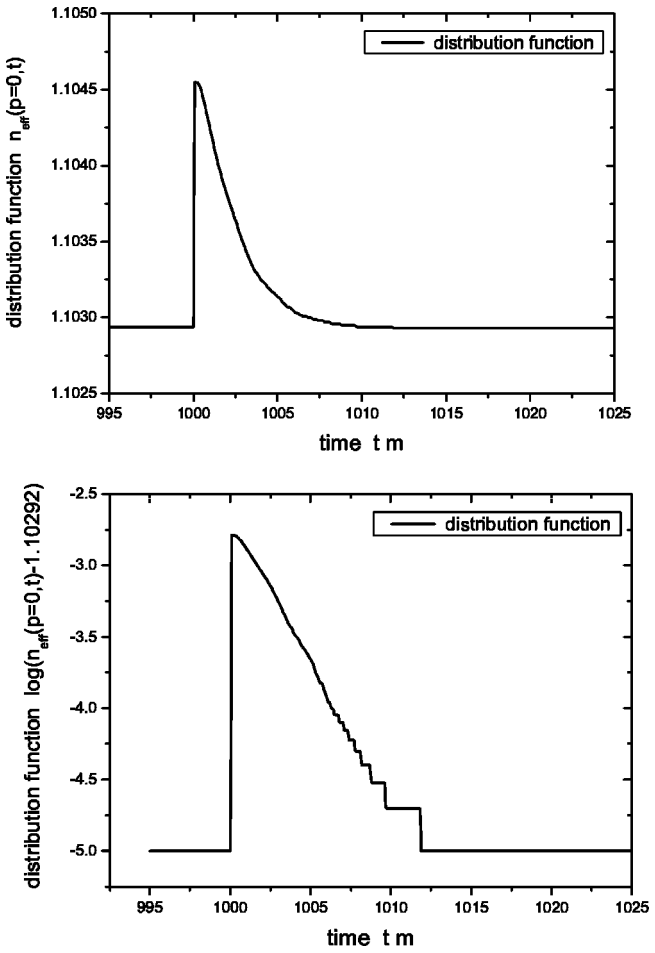

FIG. 13. Time evolution of the zero momentum mode of the distribution function that has been excited at the system time $t_k \cdot m = 1000$ (upper part). From the exponential decrease of the deviation from the equilibrium value (that has been subtracted in the lower plot) the relaxation rate can be extracted.

For $t > t_k$ this deviation $\Delta N(t)$ indeed vanishes exponentially according to the full Kadanoff-Baym equations as shown in Fig. 13 for the zero momentum mode of the distribution function. For the specific case shown in Fig. 13 the equilibrium state has been generated by starting with the initial distribution DT for a coupling constant $\lambda/m = 18$. At the time $t_k \cdot m = 1000$ both Green functions have been changed simultaneously by only 10^{-3} in order to avoid large disturbances of the system. From the exponential decrease of the deviation one can directly extract the relaxation rate.

This extraction has been done for several momentum modes which leads to the numbers displayed in Fig. 14 by the full squares. In this plot, furthermore, the extracted relaxation rates are compared to the on-shell width of the particles as indicated by the line. The latter values have been obtained within an independent finite temperature calculation involving the self-consistent spectral function (and width). The exact method is described in detail in Appendix D. We note, that—apart from the coupling constant—only the equilibrium temperature $T_{eq}/m = 1.835$ enters into the self-consistent scheme as input. It yields the on-shell energies

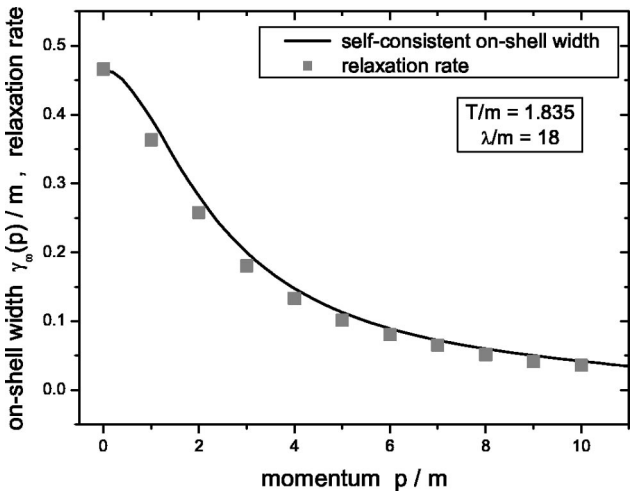

FIG. 14. Comparison of the relaxation rates for single excited momentum modes (full dots) with the on-shell widths calculated at finite temperature for various momentum modes. The equilibrium state is characterized by $\lambda/m = 18$ and a temperature of $T_{eq}/m = 1.835$.

$\omega(\mathbf{p})$ and the self-consistent width for all momenta and energies such that the on-shell width $\gamma_\omega(\mathbf{p})$ can be determined via Eq. (4.7). The comparison in Fig. 14 shows a very good agreement of the results for the relaxation rate obtained from a time-dependent single mode excitation of an equilibrated system with the findings for the on-shell width calculated within the self-consistent thermal approach. Thus the strong relation between both quantities has been shown explicitly for the case of a general off-shell nonequilibrium theory.

V. FULL VERSUS APPROXIMATE DYNAMICS

The Kadanoff-Baym equations studied in the previous sections represent the full quantum field theoretical equations with the chosen topology for the self-consistent dissipative self-energy on the single-particle level. However, its numerical solution is quite involved and it is of interest to investigate, in how far approximate schemes deviate from the full calculation. Nowadays, transport models are widely used in the description of quantum system out of equilibrium (see the Introduction). Most of these models work in the ''quasiparticle'' picture, where all particles obey a fixed energy-momentum relation and the energy is no longer an independent degree of freedom; it is determined by the momentum and the (effective) mass of the particle. Accordingly, these particles are treated with their δ-function spectral shape as infinitely long living, i.e., stable objects. This assumption is rather questionable, e.g., for high-energy heavy-ion reactions, where the particles achieve a large width due to the frequent collisions with other particles in the high density and/or high energy regime. Furthermore, this is doubtful for particles that are unstable even in the vacuum. The question, in how far the quasiparticle approximation influences the dynamics in comparison to the full Kadanoff-Baym calculation, is of general interest [54,57].

We also remark that the recent studies in Refs. [61–63,66,77], where homogeneous systems in 1+1 dimensions have been investigated, are rather special as the on-shell 2-to-2 elastic collisions are strictly forward. Thus an on-shell Boltzmann description will not lead to any kinetic equilibration in momentum space. This is different in 2+1 dimensions as we will see below.

A. Derivation of the Boltzmann approximation

In the following we will give a short derivation of the Boltzmann equation starting directly from the Kadanoff-Baym dynamics in the two-time and momentum-space representation as employed within this work. This derivation is briefly reviewed since we want (i) to emphasize the link of the full Kadanoff-Baym equation with its approximated version and (ii) to clarify the assumptions that enter the Boltzmann equation. The conventionally employed derivation of the (equivalent) Boltzmann equation will be discussed later on.

Since the Boltzmann equation describes the time evolution of distribution functions for quasiparticles we first consider the quasiparticle Green functions in two-time representation for homogeneous systems:

$$
\begin{aligned}
G^{\gtrless}_{\phi\phi,\mathrm{qp}}(\mathbf{p},t_1,t_2) &= \frac{-i}{2\omega_{\mathbf{p}}}\{N_{\mathrm{qp}}(\mp\mathbf{p})\exp[\pm i\omega_{\mathbf{p}}(t_1-t_2)] \\
&\quad +[N_{\mathrm{qp}}(\pm\mathbf{p})+1]\exp[\mp i\omega_{\mathbf{p}}(t_1-t_2)]\},\\
G^{\gtrless}_{\phi\pi,\mathrm{qp}}(\mathbf{p},t_1,t_2) &= \frac{1}{2}\{\mp N_{\mathrm{qp}}(\mp\mathbf{p})\exp[\pm i\omega_{\mathbf{p}}(t_1-t_2)] \\
&\quad \pm[N_{\mathrm{qp}}(\pm\mathbf{p})+1]\exp[\mp i\omega_{\mathbf{p}}(t_1-t_2)]\},\\
G^{\gtrless}_{\pi\phi,\mathrm{qp}}(\mathbf{p},t_1,t_2) &= \frac{1}{2}\{\pm N_{\mathrm{qp}}(\mp\mathbf{p})\exp[\pm i\omega_{\mathbf{p}}(t_1-t_2)] \\
&\quad \mp[N_{\mathrm{qp}}(\pm\mathbf{p})+1]\exp[\mp i\omega_{\mathbf{p}}(t_1-t_2)]\},\\
G^{\gtrless}_{\pi\pi,\mathrm{qp}}(\mathbf{p},t_1,t_2) &= \frac{-i\omega_{\mathbf{p}}}{2}\{N_{\mathrm{qp}}(\mp\mathbf{p})\exp[\pm i\omega_{\mathbf{p}}(t_1-t_2)] \\
&\quad +[N_{\mathrm{qp}}(\pm\mathbf{p})+1]\exp[\mp i\omega_{\mathbf{p}}(t_1-t_2)]\}.
\end{aligned}
\tag{5.1}
$$

For each momentum $\mathbf{p}$ the Green functions are freely oscillating in relative time t_1-t_2 with the on-shell energy $\omega_{\mathbf{p}}$. The time-dependent quasiparticle distribution functions are given with the energy variable fixed to the on-shell energy as $N_{\mathrm{qp}}(\mathbf{p},t)\equiv N(\mathbf{p},p_0=\omega_{\mathbf{p}},t)$, where the on-shell energies $\omega_{\mathbf{p}}$ might depend on time as well. Such a time variation, e.g., might be due to an effective mass as generated by the (renormalized) time-dependent tadpole self-energy. In this case the on-shell energy reads

$$
\omega_{\mathbf{p}}(t)=\sqrt{\mathbf{p}^{\,2}+m^2+\bar{\Sigma}^{\delta}_{\mathrm{ren}}(t)}. \tag{5.2}
$$

Vice versa we can define the quasiparticle distribution function by means of the quasiparticle Green functions at equal times t as [20]

$$
\begin{aligned}
N_{\mathrm{qp}}(\mathbf{p},t) &= \left[\frac{\omega_{\mathbf{p}}(t)}{2}iG^{<}_{\phi\phi,\mathrm{qp}}(\mathbf{p},t,t)+\frac{1}{2\omega_{\mathbf{p}}(t)}iG^{<}_{\pi\pi,\mathrm{qp}}(\mathbf{p},t,t)\right] \\
&\quad -\frac{1}{2}[G^{<}_{\pi\phi,\mathrm{qp}}(\mathbf{p},t,t)-G^{<}_{\phi\pi,\mathrm{qp}}(\mathbf{p},t,t)].
\end{aligned}
\tag{5.3}
$$

Using the equations of motions for the Green functions in diagonal time direction (A2) (exploiting $G^{<}_{\phi\pi}(\mathbf{p},t,t)=-[G^{<}_{\pi\phi}(\mathbf{p},t,t)]^*$) the time evolution of this distribution function is given by

$$
\partial_t N_{\mathrm{qp}}(\mathbf{p},t)=-\mathrm{Re}\{I^{<}_{1;\mathrm{qp}}(\mathbf{p},t,t)\}-\frac{1}{\omega_{\mathbf{p}}(t)}\mathrm{Im}\{I^{<}_{1,2;\mathrm{qp}}(\mathbf{p},t,t)\}. \tag{5.4}
$$

The time derivatives of the on-shell energies cancel out since the quasiparticle Green functions obey

$$
G^{<}_{\pi\pi}(\mathbf{p},t,t)=\omega^2_{\mathbf{p}}(t)G^{<}_{\phi\phi}(\mathbf{p},t,t) \tag{5.5}
$$

as seen from Eq. (5.1). Furthermore, we remark that contributions containing the energy $\omega^2_{\mathbf{p}}$—as present in the equation of motion for the Green functions (A2)—no longer show up. The time evolution of the distribution function is entirely determined by (equal-time) collision integrals containing (time derivatives of the) Green functions and self-energies,

$$
\begin{aligned}
I^{<}_{1;\mathrm{qp}}(\mathbf{p},t,t) &= \int_{t_0}^{t}dt'\,\Sigma^{<}_{\mathrm{qp}}(\mathbf{p},t,t')G^{>}_{\phi\phi,\mathrm{qp}}(\mathbf{p},t',t) \\
&\quad -\Sigma^{>}_{\mathrm{qp}}(\mathbf{p},t,t')G^{<}_{\phi\phi,\mathrm{qp}}(\mathbf{p},t',t),
\end{aligned}
\tag{5.6}
$$

$$
\begin{aligned}
I^{<}_{1,2;\mathrm{qp}}(\mathbf{p},t,t) &= \int_{t_0}^{t}dt'\,\Sigma^{<}_{\mathrm{qp}}(\mathbf{p},t,t')G^{>}_{\phi\pi,\mathrm{qp}}(\mathbf{p},t',t) \\
&\quad -\Sigma^{>}_{\mathrm{qp}}(\mathbf{p},t,t')G^{<}_{\phi\pi,\mathrm{qp}}(\mathbf{p},t',t).
\end{aligned}
$$

Since we are dealing with a system of on-shell quasiparticles within the Boltzmann approximation, the Green functions in the collision integrals (5.6) are given by the respective quasiparticle quantities of Eq. (5.1). This holds for the collisional self-energies as well and is indicated by the index "qp."

The actual Boltzmann approximation is defined in the limit, that the distribution functions have to be taken always at the latest time argument of the two-time Green function [55,57]. Accordingly, for the general nonequilibrium case we introduce the ansatz for the Green functions in the collision term

$$G^{\gtrless}_{\phi\phi,\mathrm{qp}}(\mathbf{p},t_1,t_2)=\frac{-i}{2\omega_{\mathbf{p}}}\{N_{\mathrm{qp}}(\mp\mathbf{p},t_{\max})\exp[\pm i\omega_{\mathbf{p}}(t_1-t_2)]+[N_{\mathrm{qp}}(\pm\mathbf{p},t_{\max})+1]\times\exp[\mp i\omega_{\mathbf{p}}(t_1-t_2)]\},$$

$$G^{\gtrless}_{\phi\pi,\mathrm{qp}}(\mathbf{p},t_1,t_2)=\frac{1}{2}\{\mp N_{\mathrm{qp}}(\mp\mathbf{p},t_{\max})\exp[\pm i\omega_{\mathbf{p}}(t_1-t_2)]\pm[N_{\mathrm{qp}}(\pm\mathbf{p},t_{\max})+1]\times\exp[\mp i\omega_{\mathbf{p}}(t_1-t_2)]\}, \tag{5.7}$$

with the maximum time $t_{\max}=\max(t_1,t_2)$. The same ansatz is employed for the time-dependent on-shell energies which enter the representation of the quasiparticle two-time Green functions (5.7) with their value at $t_{\max}$, i.e., $\omega_{\mathbf{p}}=\omega_{\mathbf{p}}(t_{\max}=\max(t_1,t_2))$.

The collision term contains a time integration which extends from an initial time t_0 to the current time t. All two-time Green functions and self-energies depend on the current time t as well as on the integration time $t'\leqslant t$. Thus only distribution functions at the current time, i.e., the maximum time of all appearing two-time functions, enter the collision integrals and the evolution equation for the distribution function becomes local in time. Since the distribution functions are given at fixed time t, they can be taken out of the time integral. When inserting the expressions for the self-energies and the Green functions in the collision integrals the evolution equation for the quasiparticle distribution function reads

$$\begin{aligned}\partial_t N_{\mathrm{qp}}(\mathbf{p},t)=\frac{\lambda^2}{3}\int\frac{d^dq}{(2\pi)^d}\int\frac{d^dr}{(2\pi)^d}\int\frac{d^ds}{(2\pi)^d}(2\pi)^d\delta^{(d)}(\mathbf{p}-\mathbf{q}-\mathbf{r}-\mathbf{s})\frac{1}{2\omega_{\mathbf{p}}2\omega_{\mathbf{q}}2\omega_{\mathbf{r}}2\omega_{\mathbf{s}}}\\
\times\Big\{[\overline{N}_{\mathbf{p},t}\overline{N}_{-\mathbf{q},t}\overline{N}_{-\mathbf{r},t}\overline{N}_{-\mathbf{s},t}-N_{\mathbf{p},t}N_{-\mathbf{q},t}N_{-\mathbf{r},t}N_{-\mathbf{s},t}]\int_{t_0}^{t}dt'\cos([t-t'][\omega_{\mathbf{p}}+\omega_{\mathbf{q}}+\omega_{\mathbf{r}}+\omega_{\mathbf{s}}])\\
+3[\overline{N}_{\mathbf{p},t}\overline{N}_{-\mathbf{q},t}\overline{N}_{-\mathbf{r},t}N_{\mathbf{s},t}-N_{\mathbf{p},t}N_{-\mathbf{q},t}N_{-\mathbf{r},t}\overline{N}_{\mathbf{s},t}]\int_{t_0}^{t}dt'\cos([t-t'][\omega_{\mathbf{p}}+\omega_{\mathbf{q}}+\omega_{\mathbf{r}}-\omega_{\mathbf{s}}])\\
+3[\overline{N}_{\mathbf{p},t}\overline{N}_{-\mathbf{q},t}N_{\mathbf{r},t}N_{\mathbf{s},t}-N_{\mathbf{p},t}N_{-\mathbf{q},t}\overline{N}_{\mathbf{r},t}\overline{N}_{\mathbf{s},t}]\int_{t_0}^{t}dt'\cos([t-t'][\omega_{\mathbf{p}}+\omega_{\mathbf{q}}-\omega_{\mathbf{r}}-\omega_{\mathbf{s}}])\\
+[\overline{N}_{\mathbf{p},t}N_{\mathbf{q},t}N_{\mathbf{r},t}N_{\mathbf{s},t}-N_{\mathbf{p},t}\overline{N}_{\mathbf{q},t}\overline{N}_{\mathbf{r},t}\overline{N}_{\mathbf{s},t}]\int_{t_0}^{t}dt'\cos([t-t'][\omega_{\mathbf{p}}-\omega_{\mathbf{q}}-\omega_{\mathbf{r}}-\omega_{\mathbf{s}}])\Big\},\end{aligned} \tag{5.8}$$

where we have introduced the abbreviation $N_{\mathbf{p},t}=N_{\mathrm{qp}}(\mathbf{p},t)$ for the quasiparticle distribution function at current time t and $\overline{N}_{\mathbf{p},t}=N_{\mathrm{qp}}(\mathbf{p},t)+1$ for the according Bose factor. Furthermore, a possible time dependence of the on-shell energies is suppressed in the above notation.

The time evolution of the quasiparticle distribution is given as an initial value problem for the function $N_{\mathrm{qp}}(\mathbf{p})$ prepared at initial time t_0. For large system times t (compared to the initial time) the time integration over the trigonometric function results in an energy conserving δ-function:

$$\lim_{t-t_0\to\infty}\int_{t_0}^{t}dt'\cos([t-t']\hat{\omega})=\lim_{t-t_0\to\infty}\frac{1}{\hat{\omega}}\sin[(t-t_0)\hat{\omega}]=\pi\delta(\hat{\omega}). \tag{5.9}$$

Here $\hat{\omega}=\omega_{\mathbf{p}}\pm\omega_{\mathbf{q}}\pm\omega_{\mathbf{r}}\pm\omega_{\mathbf{s}}$ represents the energy sum which is conserved in the limit $t-t_0\to\infty$ where the initial time t_0 is considered as fixed. In the energy conserving long-time limit (5.9) only the $2\leftrightarrow 2$ scattering processes [third line in Eq. (5.8)] are contributing. All other terms vanish since the corresponding energy δ-functions cannot be fulfilled for on-shell quasiparticles. In the following we will solve the energy conserving Boltzmann equation for on-shell particles:

$$\begin{aligned}\partial_t N_{\mathrm{qp}}(\mathbf{p},t)=\frac{\lambda^2}{2}\int\frac{d^dq}{(2\pi)^d}\int\frac{d^dr}{(2\pi)^d}\int\frac{d^ds}{(2\pi)^d}\\
\times(2\pi)^{d+1}\frac{1}{2\omega_{\mathbf{p}}2\omega_{\mathbf{q}}2\omega_{\mathbf{r}}2\omega_{\mathbf{s}}}\\
\times[\overline{N}_{\mathbf{p},t}\overline{N}_{\mathbf{q},t}N_{\mathbf{r},t}N_{\mathbf{s},t}-N_{\mathbf{p},t}N_{\mathbf{q},t}\overline{N}_{\mathbf{r},t}\overline{N}_{\mathbf{s},t}]\\
\times\delta^{(d)}(\mathbf{p}+\mathbf{q}-\mathbf{r}-\mathbf{s})\,\delta(\omega_{\mathbf{p}}+\omega_{\mathbf{q}}-\omega_{\mathbf{r}}-\omega_{\mathbf{s}}).\end{aligned} \tag{5.10}$$

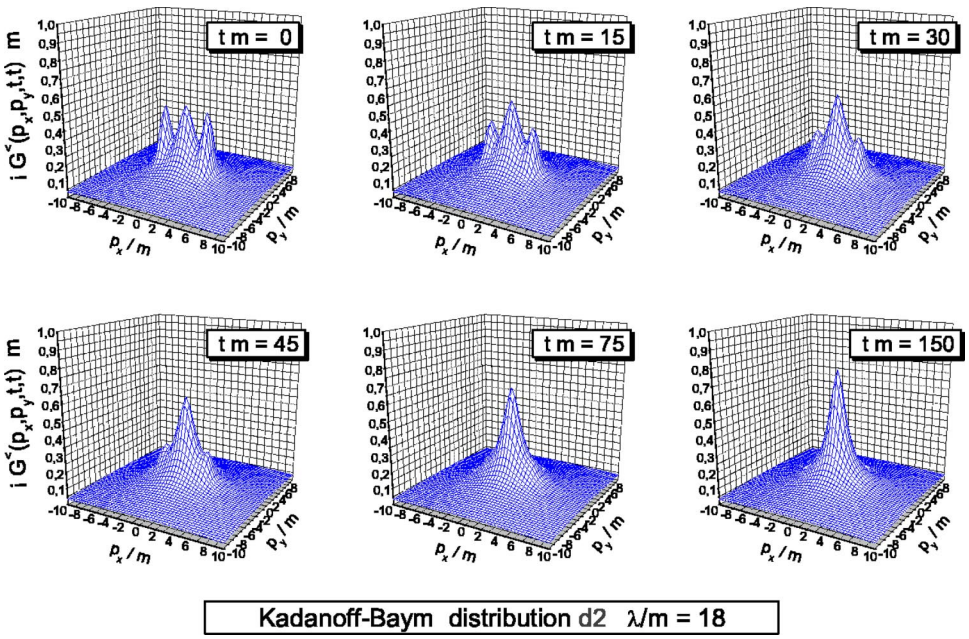

FIG. 15. Evolution of the Green function in momentum space within the full Kadanoff-Baym dynamics. The equal-time Green function is displayed for various times $tm=0$, 15, 30, 45, 75, 150. Starting from an initially nonisotropic shape it develops towards a rotational symmetric distribution in momentum space.

The system evolution given by Eq. (5.10) is explicitly local in time since it depends only on the current configuration; there are no memory effects from the integration over past times as present in the full Kadanoff-Baym equation.

We point out that the numerical algorithm for the time integration of Eq. (5.10) is basically the same as the one employed for the solution of the Kadanoff-Baym equation (see Appendix A). Energy conservation can be assured by a precalculation including a shift of the lower boundary t_0 to earlier times. Even small time shifts suffice to keep the kinetic energy conserved. We note, that in contrast to the Kadanoff-Baym equation no correlation energy is generated in the Boltzmann limit.

In addition to the procedure presented above, we calculate the actual momentum-dependent on-shell energy for every momentum mode by a solution of the dispersion relation including contributions from the tadpole and the real part of the (retarded) sunset self-energy. In this way one can guarantee that at every time t the particles are treated as quasiparticles with the correct energy-momentum relation.

Before presenting the actual numerical results we will comment on the derivation of the Boltzmann equation within the conventional scheme that is different from ours. Here, at first the Kadanoff-Baym equation (in coordinate space) is transformed to the Wigner representation by Fourier transformation with respect to the relative coordinates in space and time (for ϕ^4 theory see Refs. [20,27]). The problem then is formulated in terms of energy and momentum variables together with a single system time. For nonhomogeneous systems a mean spatial coordinate is necessary as well. As a next step the ''semiclassical approximation'' is introduced, which consists of a gradient expansion of the convolution integrals in coordinate space within the Wigner transformation. For the time evolution only contributions up to first order in the gradients are kept [see Eq. (4.14)]. Finally, the quasiparticle assumption is introduced as follows: The Green functions appearing in the transport equation—explicitly or implicitly via the self-energies—are written in Wigner representation as a product of a distribution function N and the spectral function A (see Sec. IV D). The quasiparticle assumption is then realized by employing a δ-like form for the spectral function which connects the energy variable to the momentum. By integrating the first order transport equation over all (positive) energies, furthermore, the Boltzmann equation for the time evolution of the on-shell distribution function (5.10) is obtained.

Inspite of the fact, that the Boltzmann equation (5.10) can be obtained in different subsequent approximation schemes, it is of basic interest, how its actual solutions compare to those from the full Kadanoff-Baym dynamics.

B. Boltzmann vs Kadanoff-Baym dynamics

In the following we will compare the solutions of the Boltzmann equation with the solution of the Kadanoff-Baym theory. We start with a presentation of the nonequilibrium time evolution of two colliding particle accumulations (tsunamis) [39] within the full Kadanoff-Baym calculation (see Fig. 15). Such configurations are also used for simulations in the heavy-ion physics context [39,54–57].

During the time evolution the bumps at finite momenta (in p_x direction) gradually disappear, while the one close to zero momentum—which initially stems from the vacuum contribution to the Green function—is increased as seen for different snapshots at times $tm=0$, 15, 30, 45, 75, 150 in Fig. 15. The system with initially apparent collision axis slowly merges—as expected—into an isotropic final distribution in momentum space.

For the comparison between the full Kadanoff-Baym dynamics and the Boltzmann approximation we concentrate on equilibration times. To this aim we define a quadrupole moment for a given momentum distribution $N(\mathbf{p})$ at time t as

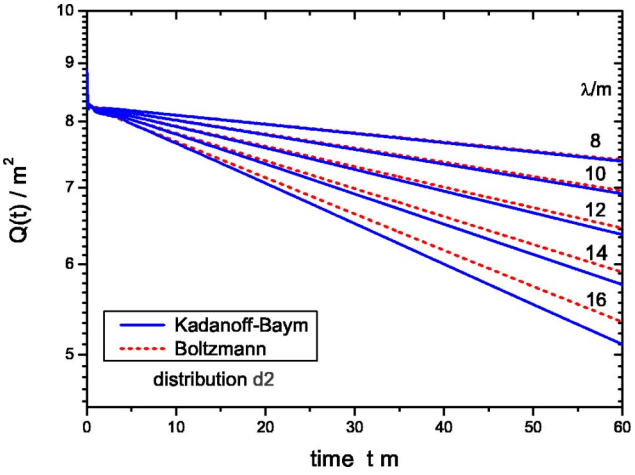

FIG. 16. Decrease of the quadrupole moment in time for different coupling constants $\lambda/m=8\rightarrow16$ in steps of 2 for the full Kadanoff-Baym calculation (solid lines) and the Boltzmann approximation (dashed lines).

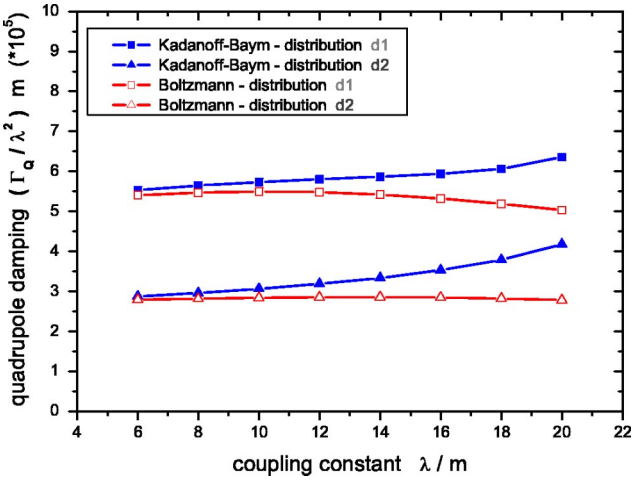

FIG. 17. Relaxation rate (divided by the coupling λ squared) for Kadanoff-Baym and Boltzmann calculations as a function of the interaction strength. For the two different initial configurations the full Kadanoff-Baym evolution leads to a faster equilibration.

$$Q(t)=\frac{\int \frac{d^2p}{(2\pi)^2}[p_x^2-p_y^2]N(\mathbf{p},t)}{\int \frac{d^2p}{(2\pi)^2}N(\mathbf{p},t)}, \tag{5.11}$$

which vanishes for the equilibrium state. For the Kadanoff-Baym case we use in Eq. (5.11) the effective distribution function $n_{\mathrm{eff}}(\mathbf{p},t)$, which is determined by the equal-time Green functions (4.29). When constructing the distribution function by means of equal-time Green functions the energy variable has been effectively integrated out. This has the advantage that the distribution function is given independently of the actual on-shell energies. We note that a calculation with the on-shell energies basically leads to the same results.

The relaxation of the quadrupole moment (5.11) has been studied for two different initial distributions: The evolution of distribution d2 is displayed in Fig. 15 while for distribution d1 the position and the width of the two particle bumps have been modified. The calculated quadrupole moment (5.11) shows a nearly exponential decrease with time (see Fig. 16) and we can extract a relaxation rate Γ_Q via the relation

$$Q(t)\propto\exp(-\Gamma_Q t). \tag{5.12}$$

Figure 17 shows for both initializations that the relaxation in the full quantum calculation occurs faster for large coupling constants λ than in the quasiclassical approximation, whereas for small couplings the equilibration times of the full and the approximate evolutions are comparable. We find that the scaled relaxation rate Γ_Q/λ^2 is nearly constant in the Boltzmann case, but increases with the coupling strength in the Kadanoff-Baym calculation (especially for the initial distribution d2).

These findings are explained as follows: Since the free Green function—as used in the Boltzmann calculation—has only support on the mass-shell, only $(2\leftrightarrow2)$ scattering processes are described in the Boltzmann limit. All other processes with a different number of incoming and outgoing particles vanish (as noted before). Within the full Kadanoff-Baym calculation this is different, since here the spectral function—determined from the self-consistent Green function (see Sec. IV C)—acquires a finite width. Thus the Green function has support at all energies although it drops fast far off the mass-shell. Especially for large coupling constants, where the spectral function is sufficiently broad, the three particle production process gives a significant contribution to the collision integral. Since the width of the spectral function increases with the interaction strength, such processes become more important in the high coupling regime. As a consequence the difference between both approaches is larger for stronger interactions as observed in Fig. 17. For small couplings λ/m in both approaches basically the usual $2\leftrightarrow2$ scattering contributes and the results for the rate Γ_Q are quite similar.

In summarizing this section we point out that the full solution of the Kadanoff-Baym equations does include $0\leftrightarrow4$, $1\leftrightarrow3$, and $2\leftrightarrow2$ off-shell collision processes which—in comparison to the Boltzmann on-shell $2\leftrightarrow2$ collision limit—become important when the spectral width of the particles reaches $\sim1/3$ of the particle mass. On the other hand, the simple Boltzmann limit works surprisingly well for smaller couplings and those cases, where the spectral function is sufficiently narrow.

C. Estimate for the quadrupole relaxation

In this subsection we concentrate on the quadrupole relaxation rates observed for the full Kadanoff-Baym and the Boltzmann approximation in order to provide a simple and intuitive explanation for the actual values extracted in the last subsection. To this aim we study an idealized initial state

given by two δ-functions in momentum space. For symmetry reasons they are placed on the positive and negative p_x axis at $p_y=0$. Thus the initial distribution function reads

$$N^{\delta}(\mathbf{p},t=0)=N_0^{\delta}\delta(p_y)[\delta(p_x-p_{\rm ini})+\delta(p_x+p_{\rm ini})], \tag{5.13}$$

where N_0^{δ} is a normalization constant. We are now interested in the time evolution of this distribution function in particular in view of the relaxation rate of the quadrupole moment. For simplicity we will explore this question employing the Boltzmann equation, since the differences between the full and the quasiparticle calculation are rather moderate.

The special form of the initial distribution N^{δ} (5.13) has the particular advantage, that the collision term of the Boltzmann equation can be calculated analytically at the beginning of the evolution. We find for the time evolution of momentum moments within the Boltzmann approximation in $2+1$ space-time dimensions:

$$\begin{aligned}\frac{d}{dt}\langle\mathcal{O}\rangle(t)&=\frac{d}{dt}\int\frac{d^2p}{(2\pi)^2}\mathcal{O}N(\mathbf{p},t)=\int\frac{d^2p}{(2\pi)^2}\mathcal{O}\frac{d}{dt}N(\mathbf{p},t)\\&=\frac{\lambda^2}{2}\int\frac{d^2p}{(2\pi)^2}\int\frac{d^2q}{(2\pi)^2}\int\frac{d^2r}{(2\pi)^2}\int\frac{d^2s}{(2\pi)^2}\mathcal{O}\frac{1}{2\omega_{\mathbf{p}}2\omega_{\mathbf{q}}2\omega_{\mathbf{r}}2\omega_{\mathbf{s}}}(2\pi)^{2+1}\delta^{(2+1)}(p+q-r-s)\\&\quad\times\{[1+N(\mathbf{p},t)][1+N(\mathbf{q},t)]N(\mathbf{r},t)N(\mathbf{s},t)-N(\mathbf{p},t)N(\mathbf{q},t)[1+N(\mathbf{r},t)][1+N(\mathbf{s},t)]\}.\end{aligned} \tag{5.14}$$

Here $\mathcal{O}$ can be a function of the momentum coordinates, but is assumed to be independent of time, e.g., $\mathcal{O}\in\{1,p_x^2,p_y^2\}$. Furthermore, the energy is fixed in this quasiparticle calculation by the momentum as $p_0=\omega_{\mathbf{p}}=\sqrt{m^2+\mathbf{p}^2}$. For our special initial state N^{δ} and for the chosen operators $\mathcal{O}$ all contributions of products of more than two distribution functions cancel out. Thus the derivative of the mean value is given by

$$\begin{aligned}\frac{d}{dt}\langle\mathcal{O}\rangle(t)&=\frac{\lambda^2}{32}\int\frac{d^2p}{(2\pi)^2}\int\frac{d^2q}{(2\pi)^2}\int\frac{d^2r}{(2\pi)^2}\int\frac{d^2s}{(2\pi)^2}\\&\quad\times\mathcal{O}\frac{1}{\omega_{\mathbf{p}}\omega_{\mathbf{q}}\omega_{\mathbf{r}}\omega_{\mathbf{s}}}(2\pi)^{2+1}\delta^{(2+1)}(p+q-r-s)\\&\quad\times\{N^{\delta}(\mathbf{r},t)N^{\delta}(\mathbf{s},t)-N^{\delta}(\mathbf{p},t)N^{\delta}(\mathbf{q},t)\}.\end{aligned} \tag{5.15}$$

By inserting the explicit form of the initial conditions and performing the integrations over the momentum δ-functions we obtain for the gain term

$$\begin{aligned}\frac{d}{dt}\left\langle\begin{Bmatrix}p_x^2\\p_y^2\\1\end{Bmatrix}\right\rangle_{\rm gain}&=N_0^{\delta\,2}\frac{\lambda^2}{32}\int\frac{d^2p}{(2\pi)^5}\begin{Bmatrix}p_x^2\\p_y^2\\1\end{Bmatrix}\\&\quad\times\left[2\frac{1}{\omega_{\mathbf{p}}^2\omega_{\rm ini}^2}\delta(2\omega_{\mathbf{p}}-2\omega_{\rm ini})\right.\\&\quad+\frac{1}{\omega_{\mathbf{p}}\omega_{\rm ini}^2\omega_{\mathbf{p}+}}\delta(\omega_{\mathbf{p}}+\omega_{\mathbf{p}+}-2\omega_{\rm ini})\\&\quad\left.+\frac{1}{\omega_{\mathbf{p}}\omega_{\rm ini}^2\omega_{\mathbf{p}-}}\delta(\omega_{\mathbf{p}}+\omega_{\mathbf{p}-}-2\omega_{\rm ini})\right],\end{aligned} \tag{5.16}$$

where we take into account explicitly the different choices for the operator $\mathcal{O}\in\{1,p_x^2,p_y^2\}$. In Eq. (5.16) we have introduced the on-shell energy of the initial particle localization in momentum space $\omega_{\rm ini}=\sqrt{m^2+p_{\rm ini}^2}$ as well as the energies $\omega_{\mathbf{p}\pm}=\sqrt{m^2+(p_x\pm 2p_{\rm ini})^2+p_y^2}$. Since the integration over the last two δ-functions in energy yields zero, the only contribution to the integral stems from the first term, which can be evaluated as

$$\frac{d}{dt}\left\langle\begin{Bmatrix}p_x^2\\p_y^2\\1\end{Bmatrix}\right\rangle_{\rm gain}=N_0^{\delta\,2}\frac{\lambda^2}{64(2\pi)^4}\frac{1}{\omega_{\rm ini}^3}\begin{Bmatrix}p_{\rm ini}^2\\p_{\rm ini}^2\\2\end{Bmatrix}. \tag{5.17}$$

For the loss term we find (after carrying out the momentum space integrals)

$$\begin{aligned}\frac{d}{dt}\left\langle\begin{Bmatrix}p_x^2\\p_y^2\\1\end{Bmatrix}\right\rangle_{\rm loss}&=N_0^{\delta\,2}\frac{\lambda^2}{32}\int\frac{d^2r}{(2\pi)^5}\begin{Bmatrix}p_{\rm ini}^2\\0\\1\end{Bmatrix}\\&\quad\times\left[2\frac{1}{\omega_{\mathbf{r}}^2\omega_{\rm ini}^2}\delta(2\omega_{\mathbf{r}}-2\omega_{\rm ini})\right.\\&\quad+\frac{1}{\omega_{\mathbf{r}}\omega_{\rm ini}^2\omega_{\mathbf{r}+}}\delta(\omega_{\mathbf{r}}+\omega_{\mathbf{r}+}-2\omega_{\rm ini})\\&\quad\left.+\frac{1}{\omega_{\mathbf{r}}\omega_{\rm ini}^2\omega_{\mathbf{r}-}}\delta(\omega_{\mathbf{r}}+\omega_{\mathbf{r}-}-2\omega_{\rm ini})\right]\end{aligned} \tag{5.18}$$

with the energy functions $\omega_{\mathbf{r}\pm}$ given as above. Due to the appearance of $N^{\delta}(\mathbf{p})$ in the loss term the integration over the momentum $\mathbf{p}$ is performed directly such that the values of the operator are fixed. Again only the first term of the integral gives a nonzero result and we get for the loss term in the early time evolution

$$\frac{d}{dt}\left\langle \begin{Bmatrix} p_x^2 \\ p_y^2 \\ 1 \end{Bmatrix} \right\rangle_{\text{loss}} = N_0^{\delta\,2} \frac{\lambda^2}{64(2\pi)^4} \frac{1}{\omega_{\text{ini}}^3} \begin{Bmatrix} 2p_{\text{ini}}^2 \\ 0 \\ 2 \end{Bmatrix}. \tag{5.19}$$

From Eqs. (5.17) and (5.19) we find—in agreement with the general properties of the Boltzmann equation—that the total particle number is conserved for our particular initial state

$$\frac{d}{dt}N_{\text{tot}}(t) = \int \frac{d^2p}{(2\pi)^2} \frac{d}{dt}N(\mathbf{p})\bigg|_{t=0} = 0. \tag{5.20}$$

Thus the total particle number is given by $N_{\text{tot}}(t) = 2N_0^{\delta}/(2\pi)^2$ for all times t. Furthermore, for the reduction of the quadrupole moment (calculated with the initial distribution N^{δ}) we obtain

$$\begin{aligned} \frac{d}{dt}Q(t)\bigg|_{t=0} &= \frac{1}{N_{\text{tot}}}\int \frac{d^2p}{(2\pi)^2}[p_x^2 - p_y^2]\frac{d}{dt}N(\mathbf{p})\bigg|_{t=0} \\ &= -N_0^{\delta}\frac{\lambda^2}{64(2\pi)^2}\frac{p_{\text{ini}}^2}{\omega_{\text{ini}}^3}, \end{aligned} \tag{5.21}$$

where the gain term does not give a contribution due to the symmetry in the momentum coordinates p_x and p_y.

As indicated by the numerical studies shown in the last subsection the quadrupole moment decreases nearly exponentially in time. Thus assuming a decrease of the quadrupole moment of the form $Q(t) = Q_0 \exp(-\Gamma_Q t)$ we can determine the relaxation rate as

$$\Gamma_Q = -\frac{\dot{Q}(t=0)}{Q(t=0)} = N_0^{\delta}\frac{\lambda^2}{64(2\pi)^2}\frac{1}{\sqrt{m^2+p_{\text{ini}}^2}^3} \tag{5.22}$$

with the initial value $Q(t=0) = p_{\text{ini}}^2$. In order to connect this result to the initial distributions employed in our calculations

$$n(\mathbf{p}, t=0) = n_0 \exp[-(|p_x| - p_{\text{ini}})^2/2\sigma_x^2] \exp(-p_y^2/2\sigma_y^2) \tag{5.23}$$

we avail the corresponding representation of the δ-function and identify $N_0^{\delta} = 2\pi n_0 \sigma_x \sigma_y$. Thus we can estimate the relaxation rate for the distribution d1 ($n_0 = 1$, $\sigma_x = 0.75$, $\mathrm{d}_y = 0.75$, $p_{\text{ini}} = 2.5$) as $\Gamma_Q^{\text{d1}} \approx 7.16 \times 10^{-5} \cdot \lambda^2$ and for distribution d2 ($n_0 = 1$, $\sigma_x = 0.5$, $\sigma_y = 1.0$, $p_{\text{ini}} = 3.0$) as $\Gamma_Q^{\text{d2}} \approx 3.93 \times 10^{-5} \cdot \lambda^2$, respectively. In both cases an initial mass $m = 1$ has been used. A comparison of this rather rough estimate with the results from the actual calculations shows a remarkably good agreement. When taking into account, that the effective mass slightly increases with the coupling λ/m in the full calculations, the agreement is even better.

Thus momentum relaxation in the full Kadanoff-Baym equations as well as in the Boltzmann limit can be understood in rather simple terms. Turning the argument around, we can conclude that relaxation phenomena—as described by the Kadanoff-Baym equations—do not differ very much in comparison to semiclassical limits though the full quantum off-shell propagation is invoked.

In addition, we note that the relaxation time for the quadrupole moment is one order of magnitude larger than the typical inverse damping width, which dictates the relaxation of a single mode out of equilibrium (see Sec. IV E). Going from Eq. (5.14) to Eq. (5.15) one notices that the Bose enhancement factors have dropped out for the further estimate of the quadrupole relaxation rate. On the other hand these factors enter crucially in the total width. For a (2+1)-dimensional system these Bose factors are of special importance and increase significantly the damping width. This explains the obvious difference between the quadrupole relaxation—characterizing kinetic equilibration of a far-from-equilibrium system—and the relaxation of a single mode out of equilibrium.

VI. SUMMARY AND OUTLOOK

In this work we have studied the quantum time evolution of ϕ^4-field theory for homogeneous systems in 2+1 space-time dimensions for far-from-equilibrium initial conditions on the basis of the Kadanoff-Baym equations. We have included the tadpole and sunset self-energies, where the tadpole contribution corresponds to a dynamical mass term and the sunset self-energy is responsible for dissipation and an equilibration of the system. Since both self-energies are ultraviolet divergent we have renormalized the theory by including proper counterterms (see Appendix B). The numerical solutions for different initial configurations out of equilibrium (with the same energy density) show, that the asymptotic state achieved for $t \to \infty$ is the same for all initial conditions. In fact, we have shown that this asymptotic state corresponds to the exact off-shell thermal state of the system obeying the equilibrium Kubo-Martin-Schwinger (KMS) relations among the various two-point functions. Hence within these approximations the Kadanoff-Baym equations manifest irreversibility as expected from its coarse graining nature expressing the dynamics in terms solely of two-point functions.

During the equilibration we have identified three different stages which are related to (i) the initial build up of correlations, (ii) a kinetic thermalization, and finally (iii) a chemical equilibration. We find that the correlations are formed at very short times scales practically independent from the coupling strength involved. This result is in agreement with earlier studies of the nonrelativistic Kadanoff-Baym theory in the nuclear physics context [58]. We have, furthermore, observed that during the second phase of kinetic equilibration the time evolution of the occupation numbers of states (momentum modes) may be nonmonotonic; here a memory to the initial configuration is kept in the full off-shell dynamics. This is not observed in the pure kinetic Boltzmann descrip-

tion. In the final state, which is achieved due to chemical equilibration, we have demonstrated that the distribution functions can adequately be described by thermal Bose functions employing a temperature T and chemical potential μ as Lagrange parameters. Since the ϕ^4 theory does not include an explicitly conserved quantum number, the chemical potential μ has to vanish in thermal equilibrium. This limit is achieved dynamically within the Kadanoff-Baym scheme by off-shell $1\leftrightarrow 3$ transitions that violate particle number conservation as recently conjectured in Ref. [44]. Such processes are inhibited in the Boltzmann limit due to number-conserving $2\leftrightarrow 2$ on-shell scattering processes. The approach to chemical equilibrium, moreover, is found to be well described in an approximate scheme that only involves small deviations from the equilibrium state.

The spectral (''off-shell'') distributions of the excited quantum modes have been evaluated by a Fourier transformation with respect to the time difference $t-t'$ from the retarded Green functions. For the systems investigated we have found no universal time evolution for these spectral functions, however, they differ only in the phase of kinetic nonequilibrium and rather fast approach the thermal equilibrium shapes. The width of the spectral functions increases with the coupling strength λ employed in the interacting theory.

Furthermore, a detailed comparison of the full quantum dynamics to approximate schemes similar to that of a standard kinetic (on-shell) Boltzmann equation has been performed. Our analysis shows that the consistent inclusion of the dynamical spectral function has a significant impact on relaxation phenomena. We find that far off-shell $1\leftrightarrow 3$ processes are also responsible for a shortening of the quadrupole relaxation rate in case of larger couplings λ relative to the Boltzmann limit, which is attributed again to the fact that the latter transitions are missed in the Boltzmann approximation. Nevertheless, the relaxation is rather adequately described in the Boltzmann limit for small and moderate couplings, such that the full off-shell dynamics has only a small effect on the relaxation processes in momentum space. We have shown additionally, that the relaxation rates can also approximately be determined by a simple relaxation ansatz with satisfying results.

Moreover, we have demonstrated, that the monotonous evolution within the number conserving Boltzmann limit does not approach the correct equilibrium state, but shows a finite chemical potential in the stationary limit (Appendix E). This, of course, must be considered as a shortcoming of the semiclassical on-shell approximation, which in principle could be cured by inclusion of higher order processes. Another important task in this context will be the investigation of more involved approximation schemes in terms of generalized transport equations [35,80–84] in order to prove whether these gradient expansion schemes including off-shell particles yield a reliable description of the dynamics. In particular, the range of validity has to be explored depending of the actual nonequilibrium conditions. Due to the off-shell nature it is expected that the correct final state (with vanishing chemical potential) will be assumed, too.

As discussed in Appendix D, we have briefly considered the case of massless fields [$m\to 0$ in the original Lagrangian (2.1)] as well. In principle, we find no qualitative difference in the dynamics of massless fields compared to the one with finite mass for moderate couplings due to the generation of an effective thermal mass by the leading tadpole diagram. However, close to a critical coupling $\lambda/T\approx 4.266$ we obtain a substantial decrease of the pole mass for the zero momentum mode, which is accompanied by a large increase of the width (see Fig. 23). Simultaneously the occupation number of the lowest mode changes drastically while the occupation of the higher momentum modes remain about the same. We address this effect as due to the onset of Bose condensation, where our successive iteration scheme breaks down. We note that in the present approach the system has to stay in a symmetric phase which dynamically might no longer be preferred. Thus a future investigation including nonvanishing field expectation values [49] will be necessary to clarify the properties of this phase transition.

ACKNOWLEDGMENTS

The authors thank S. Leupold for various discussions throughout our investigations. This work was supported by GSI Darmstadt and DFG.

APPENDIX A: NUMERICAL IMPLEMENTATION

For the solution of the Kadanoff-Baym equations we have developed a computer program which differs in several points from the approach presented in Refs. [61,77]. Instead of solving the second order differential equation (2.16) we generate a set of first order differential equations for the Green functions in the Heisenberg picture

$$
\begin{aligned}
iG^<_{\phi\phi}(x_1,x_2) &= \langle \phi(x_2)\phi(x_1)\rangle = iG^<(x_1,x_2),\\
iG^<_{\pi\phi}(x_1,x_2) &= \langle \phi(x_2)\pi(x_1)\rangle = \partial_{t_1} iG^<_{\phi\phi}(x_1,x_2),\\
iG^<_{\phi\pi}(x_1,x_2) &= \langle \pi(x_2)\phi(x_1)\rangle = \partial_{t_2} iG^<_{\phi\phi}(x_1,x_2),\\
iG^<_{\pi\pi}(x_1,x_2) &= \langle \pi(x_2)\pi(x_1)\rangle = \partial_{t_1}\partial_{t_2} iG^<_{\phi\phi}(x_1,x_2),
\end{aligned}
\tag{A1}
$$

with the canonical field momentum $\pi(x)=\partial_{x_0}\phi(x)$. The first index π or ϕ is always related to the first space-time argument. Exploiting the time-reflection symmetry of the Green functions some of the differential equations are redundant. The required equations of motion are given as

$$
\begin{aligned}
\partial_{t_1} G^<_{\phi\phi}(\mathbf{p},t_1,t_2) &= G^<_{\pi\phi}(\mathbf{p},t_1,t_2),\\
\partial_t G^<_{\phi\phi}(\mathbf{p},t,t) &= 2i\,\mathrm{Im}\{G^<_{\pi\phi}(\mathbf{p},t,t)\},\\
\partial_{t_1} G^<_{\pi\phi}(\mathbf{p},t_1,t_2) &= -\Omega^2(t_1) G^<_{\phi\phi}(\mathbf{p},t_1,t_2) + I^<_1(\mathbf{p},t_1,t_2),\\
\partial_{t_2} G^<_{\pi\phi}(\mathbf{p},t_1,t_2) &= G^<_{\pi\pi}(\mathbf{p},t_1,t_2),
\end{aligned}
$$

$$\partial_t G^<_{\pi\phi}(\mathbf{p},t,t) = -\Omega^2(t) G^<_{\phi\phi}(\mathbf{p},t,t) + G^<_{\pi\pi}(\mathbf{p},t,t) + I^<_1(\mathbf{p},t,t),$$

$$\partial_{t_1} G^<_{\pi\pi}(\mathbf{p},t_1,t_2) = -\Omega^2(t_1) G^<_{\phi\pi}(\mathbf{p},t_1,t_2) + I^<_{1,2}(\mathbf{p},t_1,t_2),$$

$$\partial_t G^<_{\pi\pi}(\mathbf{p},t,t) = -\Omega^2(t) 2i\,\mathrm{Im}\{G^<_{\pi\phi}(\mathbf{p},t,t)\} + 2i\,\mathrm{Im}\{I^<_{1,2}(\mathbf{p},t,t)\}, \tag{A2}$$

where $t=(t_1+t_2)/2$ is the mean time variable. Thus we explicitly consider the propagation in the time diagonal direction as in Ref. [57]. In the equations of motion (A2) the current (renormalized) effective energy including the time dependent tadpole contribution enters

$$\Omega^2(t) = \mathbf{p}^{\,2} + m^2 + \delta m^2_{\mathrm{tad}} + \delta m^2_{\mathrm{sun}} + \overline{\Sigma}^{\delta}(t). \tag{A3}$$

The evolution in the t_2 direction has not be taken into account for $G^<_{\phi\phi}$ and $G^<_{\pi\pi}$ since the Green functions beyond the time diagonal ($t_2>t_1$) are determined via the time reflection symmetry $G^<_{\phi\phi/\pi\pi}(\mathbf{p},t_1,t_2) = -[G^<_{\phi\phi/\pi\pi}(\mathbf{p},t_2,t_1)]^*$ from the known values for the lower time triangle in both cases. Since there is no time reflection symmetry for the $G_{\pi\phi}$ functions, they have to be calculated (and stored) in the whole t_1, t_2 range. However, we can ignore the evolution of $G_{\phi\pi}$ since it is obtained by the relation $G^<_{\phi\pi}(\mathbf{p},t_1,t_2) = -[G^<_{\pi\phi}(\mathbf{p},t_2,t_1)]^*$. The correlation integrals in Eq. (A2) are given by

$$I^<_1(\mathbf{p},t_1,t_2) = -\int_0^{t_1} dt' [\Sigma^>(\mathbf{p},t_1,t') - \Sigma^<(\mathbf{p},t_1,t')] \times G^<_{\phi\phi}(\mathbf{p},t',t_2) + \int_0^{t_2} dt' \Sigma^<(\mathbf{p},t_1,t') \times [G^<_{\phi\phi}(-\mathbf{p},t_2,t') - G^<_{\phi\phi}(\mathbf{p},t',t_2)], \tag{A4}$$

$$I^<_{1,2}(\mathbf{p},t_1,t_2) \equiv \partial_{t_2} I^<_1(\mathbf{p},t_1,t_2) = -\int_0^{t_1} dt' [\Sigma^>(\mathbf{p},t_1,t') - \Sigma^<(\mathbf{p},t_1,t')] \times G^<_{\phi\pi}(\mathbf{p},t',t_2) + \int_0^{t_2} dt' \Sigma^<(\mathbf{p},t_1,t') \times [G^<_{\pi\phi}(-\mathbf{p},t_2,t') - G^<_{\phi\pi}(\mathbf{p},t',t_2)]. \tag{A5}$$

In Eqs. (A2) and (A5) one can replace $G^<_{\phi\pi}(\mathbf{p},t_1,t_2) = -[G^<_{\pi\phi}(\mathbf{p},t_2,t_1)]^*$ such that the set of equations is closed in the Green functions $G^<_{\phi\phi}$, $G^<_{\pi\phi}$, and $G^<_{\pi\pi}$.

The disadvantage, to integrate more Green functions in time in this first-order scheme, is compensated by its good accuracy. As mentioned before, we especially take into account the propagation along the time diagonal which leads to an improved numerical precision. The set of differential equations (A2) is solved by means of a fourth-order Runge-Kutta algorithm. For the calculation of the self-energies we apply a Fourier-method similar to that used in Refs. [54,57]. The self-energies (2.18), furthermore, are calculated in coordinate space where they are products of coordinate-space Green functions (that are available by Fourier transformation) and finally transformed to momentum space.

APPENDIX B: RENORMALIZATION OF ϕ^4 THEORY IN 2+1 DIMENSIONS

In 2+1 space-time dimensions both self-energies (see Fig. 2) incorporated in the present case are ultraviolet divergent. Since we consider particles with a finite mass no problems arise from the infrared momentum regime. The ultraviolet regime, however, has to be treated explicitly.

For the renormalization of the divergences we only assume that the time-dependent nonequilibrium distribution functions are decreasing for large momenta comparable to the equilibrium distribution functions, i.e., exponentially. Thus we can apply the conventional finite temperature renormalization scheme. By separating the real-time (equilibrium) Green functions into vacuum ($T=0$) and thermal parts it becomes apparent, that only the pure vacuum contributions of the self-energies are divergent. For the linear divergent tadpole diagram we introduce a mass counterterm (at the renormalized mass m) as

$$\delta m^2_{\mathrm{tad}} = \int \frac{d^2p}{(2\pi)^2} \frac{1}{2\omega_{\mathbf{p}}}, \quad \omega_{\mathbf{p}} = \sqrt{\mathbf{p}^2+m^2}, \tag{B1}$$

that cancels the contribution from the momentum integration of the vacuum part of the Green function.

In the case of a sunset diagram only the logarithmically divergent pure vacuum part requires a renormalization, while it remains finite as long as at least one temperature line is involved. Contrary to the case of 3+1 dimensions it is not necessary to employ the involved techniques developed for the renormalization of self-consistent theories (in equilibrium) in Refs. [93,94]. Since the divergence only appears (in energy-momentum space) in the real part of the Feynman self-energy Σ^c at $T=0$ (and equivalently in the real part of the retarded/advanced self-energies $\Sigma^{R/A}$), it can be absorbed by another mass counterterm

$$\delta m^2_{\mathrm{sun}} = -\,\mathrm{Re}\,\Sigma^c_{T=0}(p^2) = -\,\mathrm{Re}\,\Sigma^{\mathrm{R/A}}_{T=0}(p^2) = \frac{\lambda^2}{6}\int \frac{d^2q}{(2\pi)^2}\int \frac{d^2r}{(2\pi)^2} \times \frac{1}{4\omega_{\mathbf{q}}\omega_{\mathbf{r}}\omega_{\mathbf{q}+\mathbf{r}-\mathbf{p}}} \frac{\omega_{\mathbf{q}}+\omega_{\mathbf{r}}+\omega_{\mathbf{q}+\mathbf{r}-\mathbf{p}}}{[\omega_{\mathbf{q}}+\omega_{\mathbf{r}}+\omega_{\mathbf{q}+\mathbf{r}-\mathbf{p}}]^2 - p_0^2} \tag{B2}$$

at given 4-momentum $p=(p_0,\mathbf{p})$ and renormalized mass m.

In summary, we replace the nonrenormalized mass m contained in the original Lagrangian (2.1) by $m_B^2 = m^2 + \delta m^2_{\mathrm{tad}} + \delta m^2_{\mathrm{sun}}$ with the mass counterterms given by Eqs. (B1) and (B2). Thus the divergent part of both diagrams is

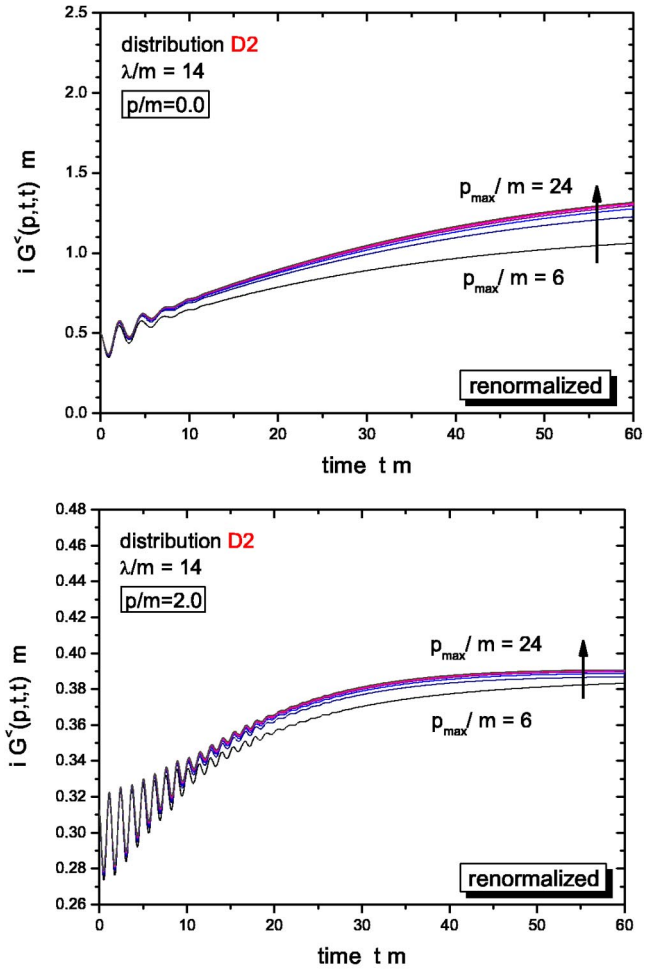

FIG. 18. Time evolution of two momentum modes $|\mathbf{p}|/m = 0.0$, $|\mathbf{p}|/m = 2.0$ of the equal-time Green function starting from the initial distribution D2 (as specified in Sec. III A) with coupling constant $\lambda/m = 14$. With the renormalization of the sunset diagram a proper limit is obtained when increasing the momentum cutoff $p_{\max}/m = 6$, 8, 10, 12, 14, 16, 18, 20, 22, 24.

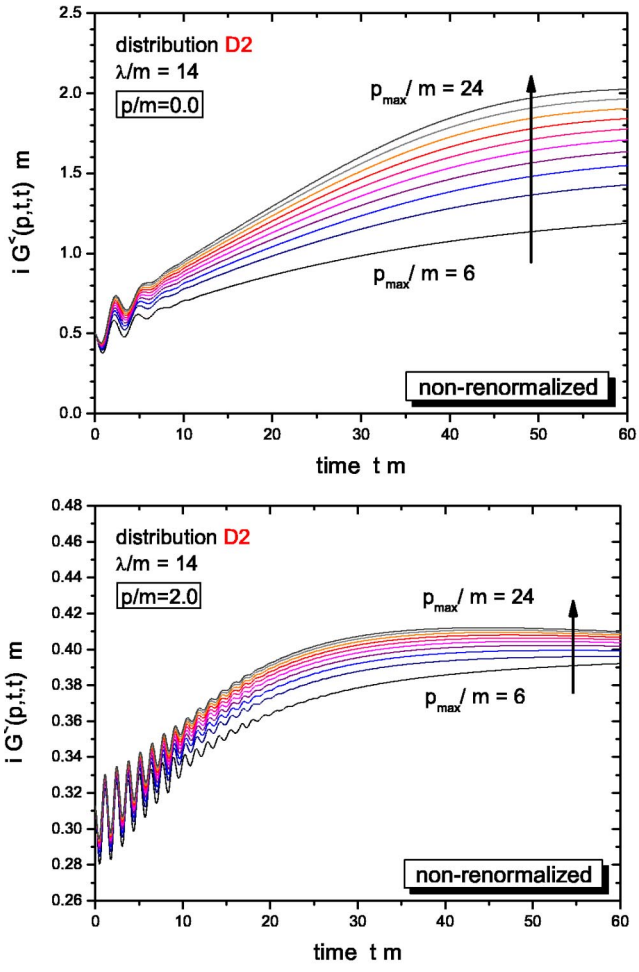

FIG. 19. Time evolution of two momentum modes $|\mathbf{p}|/m = 0.0$, $|\mathbf{p}|/m = 2.0$ of the equal-time Green function starting from the initial distribution D2 with coupling constant $\lambda/m = 14$. Without the renormalization of the sunset diagram the curves tend to infinity when enlarging the ultraviolet cutoff.

subtracted. The finite part is fixed such that for the vacuum case $[n(\mathbf{p}) \equiv 0]$ both renormalized self-energies vanish at the renormalized mass m.

In Figs. 18 and 19 we demonstrate the applicability of the renormalization prescription. To this aim we display two momentum modes $|\mathbf{p}|/m = 0.0$ (upper plots) and $|\mathbf{p}|/m = 2.0$ (lower plots) of the equal-time Green function $iG^<(|\mathbf{p}|,t,t)$ for various momentum cutoffs $p_{\max}/m =$ 6, 8, 10, 12, 14, 16, 18, 20, 22, 24 with (see Fig. 18) and without (see Fig. 19) renormalization of the sunset self-energy. For both cases the renormalization of the tadpole diagram has been used. We mention, that a nonrenormalization of the tadpole self-energy has even more drastic consequences in accordance with the linear degree of divergence. For the nonrenormalized calculations—with respect to the sunset diagram—we observe that both momentum modes do not converge with increasing momentum space cutoff. In fact, all lines tend to infinity when the maximum momentum is enlarged (since the grid size of the momentum grid is kept constant). Although the divergence (as a function of the momentum cutoff) is rather weak—in accordance with the logarithmic divergence of the sunset self-energy in 2+1 space-time dimensions—a proper ultraviolet limit is not obtained.

This problem is cured by the sunset mass counterterm (B2) as seen from Fig. 18. For the momentum mode $|\mathbf{p}|/m = 2.0$ the calculations converge to a limiting curve with increasing momentum cutoff. Even for the more selective case of the $|\mathbf{p}|/m = 0.0$ mode of the equal-time Green function the convergence is established. We point out that this limit is obtained for the unequal-time Green functions as well (not shown here explicitly). In fact, it turns out that the equal-time functions provide the most crucial test for the applicability of the renormalization prescription, since the divergent behavior appears to be less pronounced for the propagation along a single time direction t_1 or t_2. Thus we can conclude, that the renormalization scheme introduced above, i.e., including mass counterterms for the divergent tadpole and sunset self-energies, leads to ultraviolet stable results.

APPENDIX C: GENERAL INITIAL CONDITIONS

In Sec. III we briefly have described our choice for the initial conditions for the full dynamical equations; i.e., we have taken some particular initial momentum distribution of interest $n(\mathbf{p},t=0)$ which is then inserted in the standard quasiparticle expressions [compare Eq. (5.1)]:

$$G^{\gtrless}_{\phi\phi,\mathrm{qp}}(\mathbf{p},t=0,t'=0)=\frac{-i}{2\omega_{\mathbf{p}}}\{n(\mp\mathbf{p})+[n(\pm\mathbf{p})+1]\},$$

$$G^{\gtrless}_{\phi\pi,\mathrm{qp}}(\mathbf{p},t=0,t'=0)=\frac{1}{2}\{\mp n(\mp\mathbf{p})\pm[n(\pm\mathbf{p})+1]\},$$

$$G^{\gtrless}_{\pi\phi,\mathrm{qp}}(\mathbf{p},t=0,t'=0)=\frac{1}{2}\{\pm n(\mp\mathbf{p})\mp[n(\pm\mathbf{p})+1]\},$$

$$G^{\gtrless}_{\pi\pi,\mathrm{qp}}(\mathbf{p},t=0,t'=0)=\frac{-i\omega_{\mathbf{p}}}{2}\{n(\mp\mathbf{p})+[n(\pm\mathbf{p})+1]\}. \tag{C1}$$

We note that for the energy $\omega_{\mathbf{p}}$ in the above expression we have taken the on-shell energy with the bare mass. This straightforward procedure, though, is not the most general form for initial conditions within the standard Kadanoff-Baym scheme. In principle, there exist *four* independent real valued numbers for characterizing the most general initial condition instead of the two distributions $n(\mathbf{p},t=0)$ and $n(-\mathbf{p},t=0)$ in Eq. (C1).To this aim we first remark that the formal solution of the Kadanoff-Baym equations (2.9), including all boundary conditions at the initial time t_0, can be cast in the form [20]

$$\begin{aligned}
G^{<}_{\phi\phi}(\mathbf{x_1},t_1;\mathbf{x_2},t_2)=&\int_{t_0=0}^{\infty}dt'\,dt''\int d^3x'\,d^3x''\,G^{\mathrm{R}}(\mathbf{x_1},t_1;\mathbf{x}',t')\,\Sigma^{<}(\mathbf{x}',t';\mathbf{x}'',t'')\,G^{\mathrm{A}}(\mathbf{x}'',t'';\mathbf{x_2},t_2)\\
&+\int d^3x'\,d^3x''\Big[G^{\mathrm{R}}(\mathbf{x_1},t_1;\mathbf{x}',t_0=0)\,G^{<}_{\pi\pi}(\mathbf{x}',t_0;\mathbf{x}'',t_0)\,G^{\mathrm{A}}(\mathbf{x}'',t_0;\mathbf{x_2},t_2)\\
&-G^{\mathrm{R}}(\mathbf{x_1},t_1;\mathbf{x}',t_0=0)\,G^{<}_{\pi\phi}(\mathbf{x}',t_0;\mathbf{x}'',t_0)\,\frac{\partial}{\partial t_0''}G^{\mathrm{A}}(\mathbf{x}'',t_0'';\mathbf{x_2},t_2)\\
&-\frac{\partial}{\partial t_0'}G^{\mathrm{R}}(\mathbf{x_1},t_1;\mathbf{x}',t_0')\,G^{<}_{\phi\pi}(\mathbf{x}',t_0;\mathbf{x}'',t_0)\,G^{\mathrm{A}}(\mathbf{x}'',t_0;\mathbf{x_2},t_2)\\
&+\frac{\partial}{\partial t_0'}G^{\mathrm{R}}(\mathbf{x_1},t_1;\mathbf{x}',t_0')\,G^{<}_{\phi\phi}(\mathbf{x}',t_0;\mathbf{x}'',t_0)\,\frac{\partial}{\partial t_0''}G^{\mathrm{A}}(\mathbf{x}'',t_0'';\mathbf{x_2},t_2)\Big]_{t_0=t_0'=t_0''=0}.
\end{aligned} \tag{C2}$$

This relation is sometimes denoted as a generalized fluctuation-dissipation theorem in the literature [15,16,20,24]. G^{R} and G^{A} represent the self-consistently dressed retarded and advanced propagator, respectively, within the real-time formalism (2.13), (2.14). Since the Kadanoff-Baym equations are second order differential equations in time for both time arguments in case of a relativistic bosonic theory, Eq. (C2) obviously has to contain four independent initial real valued quantities. It is straightforward to show that $iG^{<}_{\phi\phi}(\mathbf{p},t,t)$ and $iG^{<}_{\pi\pi}(\mathbf{p},t,t)$ are real valued, whereas $iG^{<}_{\phi\pi}(\mathbf{p},t,t)$ and $iG^{<}_{\pi\phi}(\mathbf{p},t,t)$ are related to each other by complex conjugation; hence we get two further real quantities for the initial conditions. Furthermore, due to the equal-time commutation relations, one first notes that (i) $G^{<}_{\phi\phi}(\mathbf{p},t,t)=G^{<}_{\phi\phi}(-\mathbf{p},t,t)$, $G^{<}_{\pi\pi}(\mathbf{p},t,t)=G^{<}_{\pi\pi}(-\mathbf{p},t,t)$, and (ii) $G^{<}_{\phi\pi}(\mathbf{p},t,t)=G^{<}_{\pi\phi}(-\mathbf{p},t,t)-1$. Hence, for a real relativistic field theory for scalar bosons all the various Green functions for equal times at momentum $-\mathbf{p}$ are directly related to those at momentum $\mathbf{p}$. In total, this proves that apart from the two distributions $n(\mathbf{p})$ and $n(-\mathbf{p})$ there exist two further independent quantities for the initial Green functions (C1). One is allowed, for example, to freely choose the real and imaginary part of $G^{<}_{\phi\pi}(\mathbf{p},t,t)$ instead of those stated in Eq. (C1). In more physical terms, the four initial conditions correspond to the amplitudes and the phases of the two momentum modes $\mathbf{p}$ and $-\mathbf{p}$. The ansatz in Eq. (C1) represents a statistically averaged distribution for the phases.

Inspecting further the formal solution (C2), one notices that all the various terms containing the four initial conditions and contributing to $G^{<}_{\phi\phi}$ are damped by the retarded and advanced propagator for times $t_1,t_2>t_0=0$ and thus will die out on a time scale of the inverse damping width (4.7). Correspondingly, this is also the time scale of dephasing and decoherence of the initial modes if particular phases would have been chosen initially. As an example, some moderate initial oscillations in the equal-time Green function can be seen in Figs. 4 and 18. The modes need some time to acquire their characteristic spectral dressing and collective

phase correlations, before the further (and rather smooth) dynamics proceeds. This time is indeed roughly the inverse damping width for the various modes. The destruction of initial (phase) correlations resembles the old conjecture of Bogolyubov [95] that the initial conditions do vanish after some finite time and do not show up any further in the subsequent dynamics of the system.

As a final remark we note that one can principally also take care of higher order initial correlations within the dynamical prescription, which are *not* incorporated in Eq. (C2) and in the standard Kadanoff-Baym equations [15,96–98]. We recall that the standard real-time prescription stems from a perturbative Wick-type expansion, which is valid for a special initial density operator of single-particle (Gaussian) type. The Kadanoff-Baym equations then correspond to self-consistent and resummed Dyson-Schwinger equations in real-time for a given set of skeleton-type diagrams. On the other hand, initial correlations might (or should) exist *beyond* the single-particle mean-field (or Gaussian) level. As we have discussed in Sec. IV A, some particular higher order correlations—in this case due to the quantal collisions—will be generated dynamically during the course of the evolution. Hence, in principle, such correlations should also be taken care of in the beginning of the evolution. This is not a simple task, though: These nontrivial correlations lead to nonzero expectation values of normal-ordered operators, which can be taken care of by defining new types of contractions, which couple the time evolution of the system also to those higher order correlations. For details of such a procedure we refer the interested reader to Refs. [15,96–98].

APPENDIX D: SELF-CONSISTENT SPECTRAL FUNCTIONS AT FINITE TEMPERATURE

Whenever dealing with strongly interacting systems the single-particle spectral function is of great importance. In particular for systems at high temperature and/or high densities the spectral functions may exhibit a large width connected to a possibly complicated structure rather than showing a δ-function shape as in the case of on-shell quasiparticles.

For systems in equilibrium there are two standard approaches for calculating the spectral function: (i) within the imaginary-time formalism (ITF) by summation over discrete Matsubara frequencies, (ii) within the real-time formalism (RTF), where the energy is considered as a real and continuous variable [92]. One great advantage of the approach (ii) lies in the fact that it can be easily connected to the nonequilibrium situation. Therefore, we will use for our further developments the real-time formalism as familiar from nonequilibrium calculations. We recall that the perturbative calculation of the sunset graph has been given in various works [99–102]. Very recently a first self-consistent treatment of the ϕ^4 theory in 3+1 dimensions up to this order has been presented in Ref. [94].

In this appendix we present a method for the calculation of self-consistent spectral functions, which (i) treats different order contributions in the number of loops of the self-energy on the same footing and (ii) incorporates the finite width due to the imaginary part of the self-energy. Thus the actual spectral function reenters the calculation and is iterated until self-consistency is reached.

Our iteration scheme is divided into the following steps.

(1) The Green functions $G^<$, $G^>$ are specified in energy-momentum space $(\mathbf{p},p_0)$. In the initial step this can be done by assuming free Green functions (i.e., with δ-function like spectral functions) at the desired equilibrium temperature T.

(2) We change to the mixed representation by Fourier transformation with respect to p_0 and calculate the Green functions $G^<$, $G^>$ as a function of momentum $\mathbf{p}$ and relative time Δt. Since we are interested in a (static) equilibrium situation, there is no dependence on a mean time variable. In case of the initial on-shell Green functions the mixed representation $(\mathbf{p},\Delta t)$ is obtained analytically (5.1).

(3) The collisional self-energies $\Sigma^{\gtrless}(\mathbf{p},\Delta t)$ are calculated in the mixed representation with the Green functions $G^{\gtrless}(\mathbf{p},\Delta t)$ via Eq. (2.18).

Step 3 can be performed in several ways depending on the explicit structure of the self-energy diagrams. For the case of the sunset diagram in ϕ^4 theory we utilize another Fourier method. Here the self-energies are first evaluated as a function of relative spatial (and time) coordinates, since the sunset self-energy is (in coordinate space) simply a product of coordinate space Green functions that are available by Fourier transformation with respect to the momentum. In the final step these self-energies are transformed by a spatial Fourier transformation back into the desired mixed representation.

(4) From the collisional self-energies $\Sigma^{\gtrless}(\mathbf{p},\Delta t)$ we determine the retarded self-energy as

$$\Sigma^R(\mathbf{p},\Delta t)=\Theta(\Delta t)[\Sigma^>(\mathbf{p},\Delta t)-\Sigma^<(\mathbf{p},\Delta t)]. \quad \text{(D1)}$$

Thus the retarded self-energy is calculated in the mixed representation by explicit introduction of a step-function in relative time. As we will discuss below this is the main advantage of our scheme because it guarantees analyticity and thus the normalization of the self-consistent spectral function.

(5) The retarded self-energy is Fourier transformed back into energy-momentum space $(\mathbf{p},p_0)$ and separated into its real part $\mathrm{Re}\,\Sigma^R(\mathbf{p},p_0)$ and its imaginary part, which is related to the width as $\Gamma(\mathbf{p},p_0)=-2\,\mathrm{Im}\,\Sigma^R(\mathbf{p},p_0)$.

(6) Calculating, furthermore, the purely real tadpole self-energy $\overline{\Sigma}^{\delta}$ the spectral function is given as

$$A(\mathbf{p},p_0)=\frac{\Gamma(\mathbf{p},p_0)}{[p_0^2-\mathbf{p}^2-m^2-\delta m^2-\overline{\Sigma}^{\delta}-\mathrm{Re}\,\Sigma^R(\mathbf{p},p_0)]^2+\Gamma^2(\mathbf{p},p_0)/4}. \quad \text{(D2)}$$

Here, in addition to the initial physical mass m the mass counterterms $\delta m^2 = \delta m^2_{\rm tad} + \delta m^2_{\rm sun}$ enter and have to be calculated independently (see Appendix B). The expression (D2) for the spectral function is valid in general within a first order gradient expansion of the transport equation and is exact in equilibrium [81]. It is obtained as $A(\mathbf{p},p_0) = -2\,\mathrm{Im}\,G^R(\mathbf{p},p_0)$ from the Green function that solves the retarded Dyson-Schwinger equation (2.15).

(7) Now we can determine the Wightman functions $G^<$, $G^>$ in the next iteration step in energy-momentum space by the relations

$$iG^<(\mathbf{p},p_0) = N_{\rm eq}(p_0,T)\,A(\mathbf{p},p_0),$$

$$iG^>(\mathbf{p},p_0) = [1+N_{\rm eq}(p_0,T)]\,A(\mathbf{p},p_0). \qquad \text{(D3)}$$

The separation of the Wightman functions into distribution functions N and spectral function A is always possible and well-known from the derivation of transport equations [81]. We recall that in thermal equilibrium the distribution function N only depends on the energy variable p_0 and is independent of the momenta $\mathbf{p}$. It is given—for the scalar theory—by the Bose distribution

$$N_{\rm eq}(p_0,T) = \frac{1}{\exp(p_0/T)-1} \qquad \text{(D4)}$$

at equilibrium temperature T. The method is not restricted to finite temperature, but can be easily extended to finite densities. The presence of conserved quantities, as given for a charged complex scalar theory in the most simple case, can be accounted for by inclusion of a corresponding chemical potential μ in the Bose distribution function. In thermal equilibrium the Wightman functions are connected by the Kubo-Martin-Schwinger (KMS) periodicity condition

$$G^>(\mathbf{p},p_0) = \exp(p_0/T)\,G^<(\mathbf{p},p_0) \qquad \text{(D5)}$$

as inherent in the relations (D3). The same holds for the collisional self-energies at finite temperature. Thus the calculations take slightly less effort than implied above.

By calculating the new Green functions in step (7) we have closed the iteration loop. The iteration procedure is reentered at step (2), where the new Green functions are transformed to relative time space in order to calculate the corresponding new collisional self-energies. The alternating calculation of the Green function $G^<$ and of the spectral function A is performed until self-consistency is reached.

The scheme proposed above has one central advantage in comparison to the related approach given in Ref. [103]. In that case an iteration loop between the Green function and the spectral function or—to be more precise—the width is used as well. The width is determined from the imaginary part of the collisional self-energies directly in energy-momentum space and inserted into the equation for the spectral function. The real part, however, is either neglected or calculated by a dispersion relation in energy. The improvement of our method lies in using the mixed representation: Since the retarded self-energy is calculated in $(\mathbf{p},\Delta t)$ space with an explicit Θ-function in relative time, analyticity is imposed automatically, i.e., the real part $\mathrm{Re}\,\Sigma^R(\mathbf{p},p_0)$ and the imaginary part $\mathrm{Im}\,\Sigma^R(\mathbf{p},p_0)$ of the retarded self-energy in energy-momentum space are connected by a dispersion relation. Furthermore, the spectral function A is normalized accordingly. This is not the case for some schemes that obtain the real part and the imaginary part of the retarded self-energy by different methods. Here problems with the normalization of the spectral function and analyticity may arise. Later on we will illustrate this point in detail.

A further advantage lies in the fact that our method, especially in combination with the Fourier prescription for the momentum integrals, is computationally fast in comparison to standard procedures of calculating multidimensional momentum integrals. Furthermore, due to the spherical symmetry of the equilibrium state it can be performed very efficiently. Moreover, it is easily applied to all temperatures and chemical potentials, i.e., as long as the distribution function $N_{\rm eq}(p_0,T,\mu)$ is specified.

Our scheme is appropriate for simple self-energies, as for example the sunset diagram. Basically it is applicable also for more complex diagrams since it always reduces the number of necessary integrations. The whole procedure profits from the fact that the appearing convolution integrals in momentum and energy correspond to ordinary products of coordinate-space functions. Thus the required integrations to obtain the self-energy can be reduced considerably. In case of the sunset diagram, that has only two external points (given by the coordinates of the self-energy) but no internal points, integrations can be avoided completely besides the Fourier transformation itself. For more complicated diagrams one has to integrate over the space-time coordinates of all internal points. Nevertheless, at least the contributions from the external points can be handled in a multiplicative manner rather than performing time consuming energy-momentum integrations.

When discussing the range of applicability of our method one should note as well, that it is mainly suited for field theories that are void of complicated renormalization prescriptions. In our case of ϕ^4 theory in $2+1$ space-time dimensions the renormalization can be done by simple mass counterterms since only the pure vacuum contributions of both self-energies diverge. This mass renormalization scheme can be easily included in the iteration procedure as seen by the representation for the spectral function (D2). In cases of diverging diagrams, that contain temperature dependent parts, the renormalization procedure is much more involved [93,94]. In such situations our method might be complicated significantly.

In the following we show the actual results calculated within the self-consistent scheme described above. The tadpole self-energy as well as the retarded sunset self-energy are included self-consistently using the renormalization prescription of Appendix B. In Fig. 20 the width Γ is displayed as a function of the energy p_0 for four different momentum modes $|\mathbf{p}|/m = 0,\ 2,\ 4,\ 6$ for a temperature of $T/m = 1.835$ and a coupling constant of $\lambda/m = 18$. This configuration corresponds to the thermalized state obtained by the time evolution of the polar symmetric initial momentum distributions

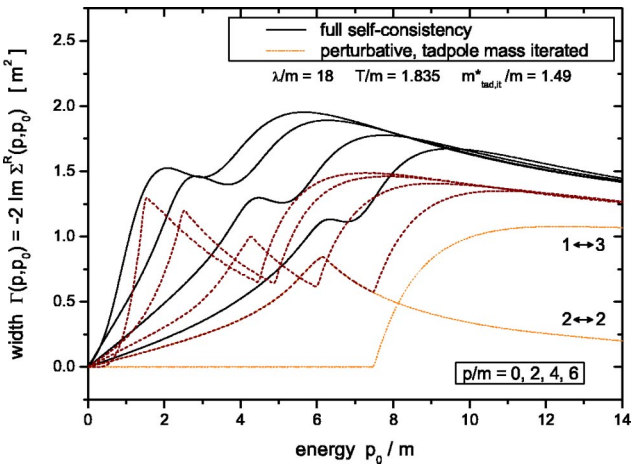

FIG. 20. Self-consistent width (solid lines) and perturbative width (dashed lines) as a function of the energy p_0/m for various momentum modes $|\mathbf{p}|/m=0$, 2, 4, 6 for a thermal system at temperature $T/m=1.835$ with coupling constant $\lambda/m=18$. For the highest momentum mode $|\mathbf{p}|/m=6$ of the perturbative calculation, the collision contribution ($2\leftrightarrow 2$) and the decay contribution ($1\leftrightarrow 3$) to the width are explicitly displayed.

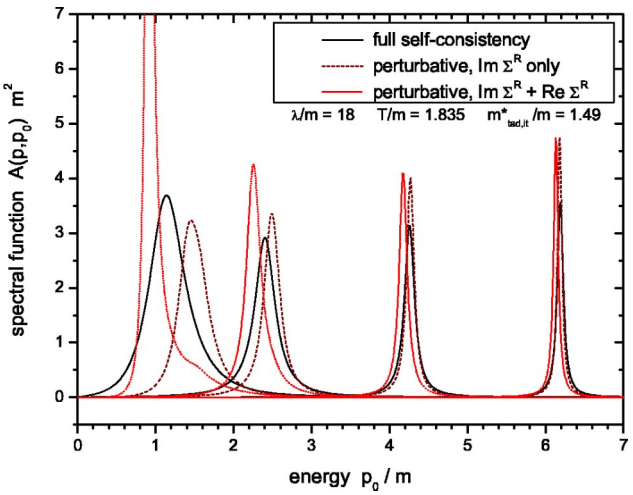

FIG. 21. Self-consistent spectral function as a function of the energy p_0/m for various momentum modes $|\mathbf{p}|/m=0$, 2, 4, 6 for a thermal system at temperature $T/m=1.835$ with coupling constant $\lambda/m=18$ (solid lines). Furthermore, spectral functions as obtained in a perturbative calculation with (dotted lines) and without (dashed lines) inclusion of the real part of the retarded self-energy are shown in comparison.

D1, D2, D3, and DT in Sec. III. For comparison we present, furthermore, the width as obtained by a perturbative calculation (as indicated by the dashed lines) for the same momentum modes, and with the same external parameters T and λ. The results have been obtained with the (self-consistent) effective mass $m^*_{\mathrm{tad,it}}/m=1.490$ on the tadpole level, i.e., by the iterative solution of the tadpole gap equation. This is in the spirit of Wang and Heinz [101] who firstly determined the effective mass in lowest order (also in a self-consistent way) and inserted this mass in the following into the expressions for the width calculated within the next order. We see from Fig. 20 that the perturbative width shows a similar (two maxima) shape for all momentum modes (for the given case of $m^*<T_{\mathrm{eq}}$). It is characterized by an increase towards a maximum around the on-shell energy $\omega^*_{\mathbf{p}}=\sqrt{\mathbf{p}^2+m^{*\,2}}$ and falling off beyond. This behavior stems from the $2\leftrightarrow 2$ processes in the self-energies as indicated for the highest momentum mode $|\mathbf{p}|/m=6$ by the thin line. Particles can be scattered by other particles—present in the system at finite temperature—such that they achieve the shown (collisional) damping width. This collision contribution vanishes for a system at temperature $T=0$. Furthermore, particles with sufficient energy can decay into three other particles. Above the threshold of $p_{0,\mathrm{th}}(\mathbf{p})=\sqrt{\mathbf{p}^2+(3m^*)^2}$ these $1\leftrightarrow 3$ processes lead to an increase of the width (as marked for the highest momentum mode by the second thin line). Finally, the width Γ decreases for larger energies and assumes a momentum independent constant value in the high energy limit. This behavior is in contrast to the case of $3+1$ dimensions, where the width shows a monotonous increase for very high energies.

In comparison, the width calculated within the self-consistent scheme shows a similar two maximum shape. Here, both processes are incorporated although they cannot be separated easily due to the self-consistent iteration. Apparently, the sharp structures present in the perturbative calculation have been washed out considerably. The kink structures resulting from threshold effects slightly disappear since the (broad) spectral function reenters the evaluation in this iteration scheme. Furthermore, also the position of the first maximum can be moved, as seen especially for the low momentum modes. This is an effect of the self-consistent spectral function that accounts also for mass shifts caused by the tadpole self-energy and the real part of the retarded sunset self-energy. Overall, Fig. 20 shows that the width in the self-consistent calculation can be significantly larger than in the corresponding perturbative estimate. However, the differences are reduced for smaller coupling constants in agreement with results obtained within the classical approximation [104].

In Fig. 21 we present the corresponding spectral functions for the system at temperature $T/m=1.835$ and coupling constant $\lambda/m=18$. The spectral functions are displayed as a function of the energy for the same four momentum modes of $|\mathbf{p}|/m=0$, 2, 4, 6. We observe that the larger width of the full self-consistent calculation (solid lines) in comparison to the perturbative result (dashed lines in Fig. 21) reflects itself in a slightly broader spectral function. Furthermore, the perturbative spectral function is located at higher energies compared to the full result, in particular for the low momentum modes. This is due to the fact that in the perturbative calculation the effective mass of the particles is fixed before evaluating the width by a solution of the tadpole gap equation. Mass modifications due to the interactions of higher order are neglected within this approximation in line with Ref. [101], where the spectral function is determined solely by the imaginary part of the retarded self-energy. On the other hand, the reduction of the effective mass due to the real part of the retarded sunset self-energy is included in the self-consistent approach leading to a shift of the spectral function maxima to lower on-shell energies. Moreover, the tadpole

mass shift is not fixed in that calculation but modified during the iteration process as well. In the present case the momentum and energy independent tadpole mass shift within the self-consistent second order calculation is given as $\Delta m^2_{\mathrm{tad}}/m^2 = 1.094$ in comparison to the value obtained for the first order calculation by the tadpole gap equation of $\Delta m^2_{\mathrm{tad}}/m^2 = 1.220$. This indicates already a shift of the spectral function to lower on-shell energies although the size is small compared to the effect coming from the second order self-energy. Thus both spectral functions are getting closer again for higher momenta where the sunset mass shift is smaller.

At this point we emphasize that the spectral function obtained by the self-consistent scheme obeys the normalization condition to high accuracy (4.6). This is not the case for a perturbative calculation where only the imaginary part of the retarded self-energy is taken into account as in Ref. [101]. When inserting only the expression for the width into the equilibrium form of the spectral function but neglecting the real part of the retarded self-energy, the normalization condition may be violated strongly. In the present perturbative calculation the correct normalization is underestimated by $\approx 20\%$ for the small momentum modes. Thus these kinds of spectral functions, furthermore, strongly violate the desired analyticity properties. In order to show the importance of the real part of the retarded self-energy even on the shape of the spectral function we present in Fig. 21 a calculation which takes this contribution explicitly into account. Calculating the complete retarded self-energy perturbatively with an effective mass of $m^*_{\mathrm{tad,it}}/m = 1.490$ yields the spectral function displayed for the same momentum modes with dotted lines. We see that the shape of the spectral function is strongly affected in particular for the small momentum modes. The inclusion of the real part causes a significant shift of the spectral function downwards to lower energies. Since the width is smaller in that region (see Fig. 20), the spectral function assumes—especially for the low momentum modes—a much narrower shape. Nevertheless, the inclusion of the real part of the retarded self-energy leads to a proper normalization of the corresponding spectral functions. Still there is a significant disagreement between the improved perturbative (dotted line) and the self-consistent solution (solid line).

As the final part of this appendix we consider the case of massless scalar fields in the Lagrangian (2.1). The dynamics of massless quantum field theory has been extensively discussed over the last years especially for the dynamics of the soft, infrared modes which might be described by classical wave dynamics. In particular the diffusion rate of the topological charge in electroweak theory has been calculated within classical simulations [105]. The connection between classical and quantal correlation functions has then been worked out in a variety of papers [106]. Also it was shown recently within ϕ^4 theory that the classical wave dynamics is equivalent to a standard Boltzmann description for the soft modes when including the correct Bose statistics and staying in the weak coupling regime [107].

From our (numerical) studies we find no qualitative difference in the dynamics of massless fields compared to the one with finite masses for moderate couplings. This is the case due to the generation of an effective thermal mass by the leading tadpole diagram as suggested in Ref. [108]. We note that there is a logarithmic divergence in the infrared sector for the sunset self-energy in vacuum for $2+1$ dimensions [see Eq. (B2)] and thus a subtlety, which we have cured by evaluating the vacuum counterterm in our renormalization description at a very small but finite mass.

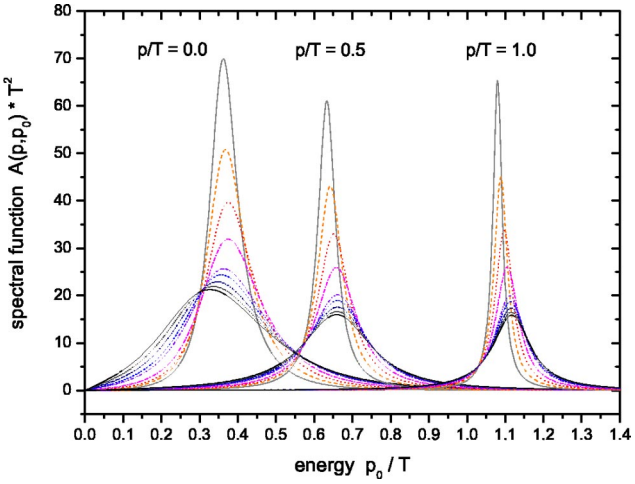

FIG. 22. Spectral functions of three momentum modes $|\mathbf{p}|/T = 0.0,\ 0.5,\ 1.0$ for different coupling constants $\lambda/T = 2,\ 2.5,\ 3,\ 3.5,\ 4,\ 4.1,\ 4.2,\ 4.25,\ 4.265$ as a function of energy for the massless case $m = 0$. With increasing coupling λ/T the spectral function of the zero momentum mode becomes broader and moves to lower energies.

In the following we concentrate on the structure of the spectral function with respect to the coupling strength λ/T. In Fig. 22 the spectral function of three low momentum modes $|\mathbf{p}|/T = 0.0,\ 0.5,\ 1.0$ for various coupling constants $\lambda/T = 2,\ 2.5,\ 3,\ 3.5,\ 4,\ 4.1,\ 4.2,\ 4.25,\ 4.265$ as a function of energy p_0/T is displayed. Since the temperature represents the scale for the massless case, we give all quantities in units of T. We find that the spectral function is shifted to larger energies with increasing and still moderate coupling strength ($\lambda/T \leqslant 3.5$). However, in the strong coupling regime ($\lambda/T > 3.5$) especially the spectral function of the zero momentum mode moves downward again, leading to a major reduction of the effective mass. Simultaneously, the spectral width grows with the coupling constant λ/T. Thus for large couplings the on-shell width becomes comparable to the effective mass (as given by the maximum position of the zero mode spectral function).

To summarize our findings we show in Fig. 23 (upper part) the evolution of the on-shell energy of the zero momentum mode as a function of the coupling constant λ/T. The effective mass—as given by the maximum of the spectral function—increases with λ/T up to moderate couplings $\lambda/T \approx 3.5$ which is—as already discussed for the nonzero mass case—essentially an effect of the mass generation by the tadpole self-energy. For larger couplings $\lambda/T > 3.5$ the contribution from the retarded self-energy plays a more important role and results in a decrease of the effective mass. The reduction of the effective mass becomes rather strong

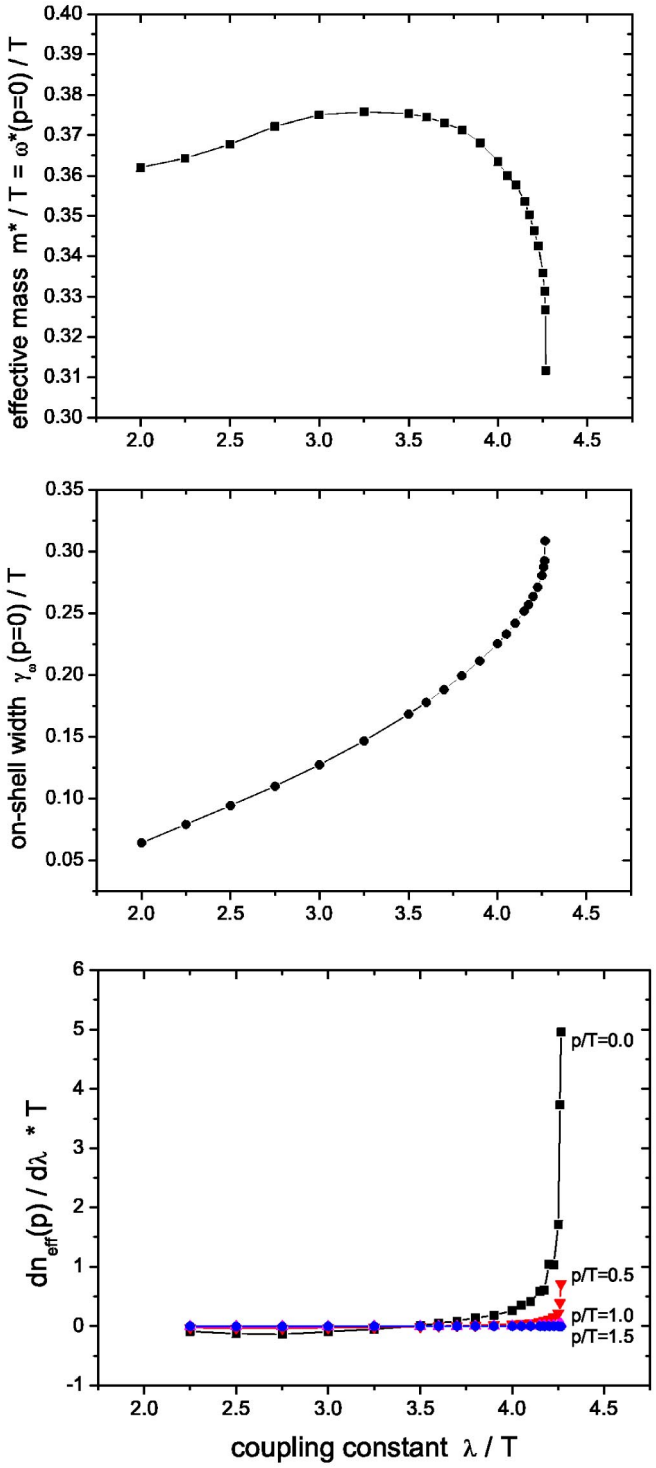

FIG. 23. Effective mass (upper plot) and on-shell width of the zero momentum mode (middle plot) as a function of the coupling constant λ/T for a massless theory. With increasing coupling λ/T the occupation number of the zero momentum mode grows considerably in contrast to higher momentum modes (lower plot) indicating the onset of Bose condensation for $\lambda/T>4.26$.

for couplings $\lambda/T\geqslant 4.25$ indicating a significant shift of the corresponding self-consistent spectral function to smaller energies. This behavior is accompanied by a strong increase of the on-shell width $\gamma_\omega(|\mathbf{p}|=0)$ of the zero momentum mode as seen from Fig. 23 (middle part). While the width grows smoothly with the coupling constant for moderate couplings, we find a strong steepening in the high coupling regime as well. Thus the zero mode spectral function for high coupling constants becomes extremely broad with an on-shell width comparable to or even larger than its effective mass.

As seen from Fig. 23 the evolution of the self-consistent spectral function in the strong coupling regime becomes singular and critical, such that the iteration processes do not lead to a convergent result for $\lambda/m\approx 4.266$. We address this effect to the onset of Bose condensation. In order to illustrate this interpretation we show in Fig. 23 (lower part) the change of the effective occupation number [as obtained from the equal-time Green functions (4.29)] with the coupling λ/T for four different momentum modes $|\mathbf{p}|/T=0.0,\ 0.5,\ 1.0,\ 1.5$. Whereas the effective particle number of the higher momentum modes remain approximately constant, the occupation number of the zero momentum mode changes rapidly for $\lambda/T>4.26$ indicating a preferential occupation of the condensate mode for higher couplings.

We recall that such an onset of a Bose condensation is possible for the massless relativistic theory in $2+1$ space-time dimensions. Although the effective mass is not identical to zero we observe significant spectral support at low energies due to the broad spectral functions for the strongly interacting system. We note that in the present description the system has to stay in the symmetric phase, where no coherent field can develop. However, when including additionally a nonvanishing field expectation value [49], the symmetry will be broken and the system might enter a new phase. A detailed investigation of the issue we delay to a future study.

APPENDIX E: STATIONARY STATE OF THE BOLTZMANN EVOLUTION

In Secs. III and IV we have described the characteristics of equilibration within the full Kadanoff-Baym theory. In this appendix we additionally show the nonequilibrium evolution in the Boltzmann limit and in particular work out the differences in both approaches.

In Fig. 24 we present the time evolution of various momentum modes for the initial momentum space distributions D1, D2, D3 within the Boltzmann equation. In these calculations the effective on-shell energies are determined by including the time-dependent renormalized tadpole self-energy. The distributions D1, D2, D3 have been modified relative to our study of the Kadanoff-Baym dynamics in Sec. III such that they (i) have the same energy density with respect to the modified total energy (where all sunset contributions are absent) and (ii) are self-consistent with respect to the effective tadpole mass in order to avoid strong initial oscillations induced by a sudden change of the on-shell energies at very early times. For completeness we note, that the initial effective masses are determined by the solution of a gap equation taking into account the energy- and momentum-independent tadpole self-energy for the given initial momentum distribution.

We see from Fig. 24 that the time evolution given by the on-shell Boltzmann approximation deviates in several as-

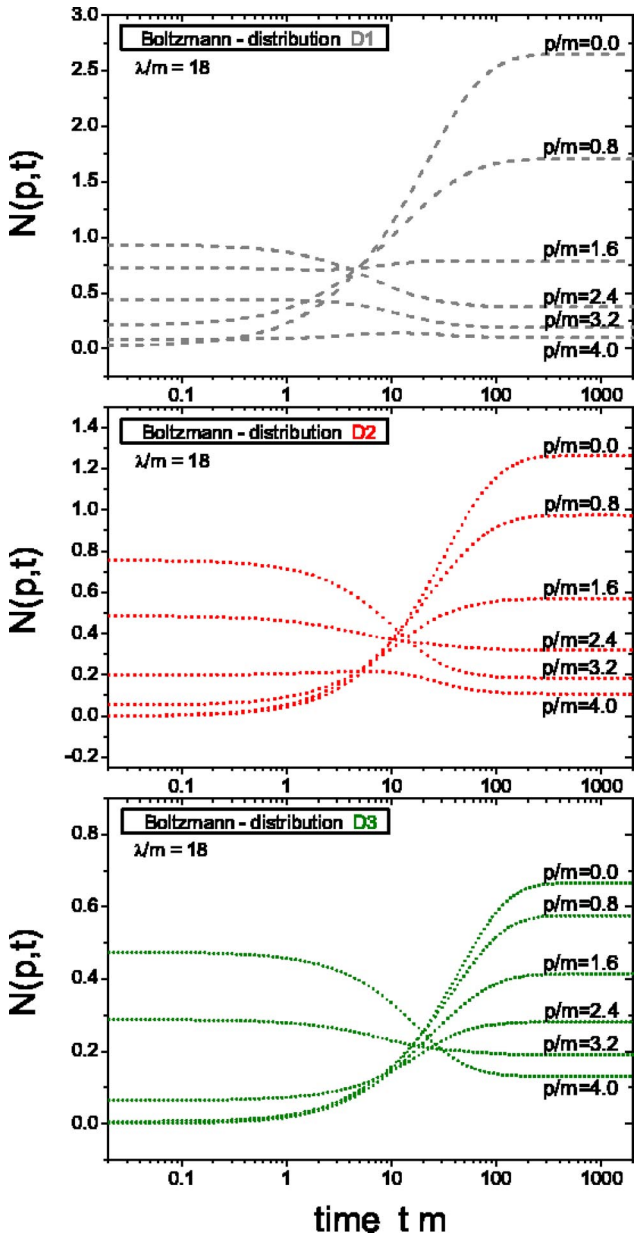

FIG. 24. Time evolution of momentum modes $|\mathbf{p}|/m=0.0$, 0.8, 1.6, 2.4, 3.2, 4.0 of the distribution function N for initializations D1 (upper plot), D2 (middle plot), and D3 (lower plot) in the Boltzmann approximation for $\lambda/m=18$. All initial configurations (of the same energy) equilibrate, but lead to different stationary states (note the different scales).

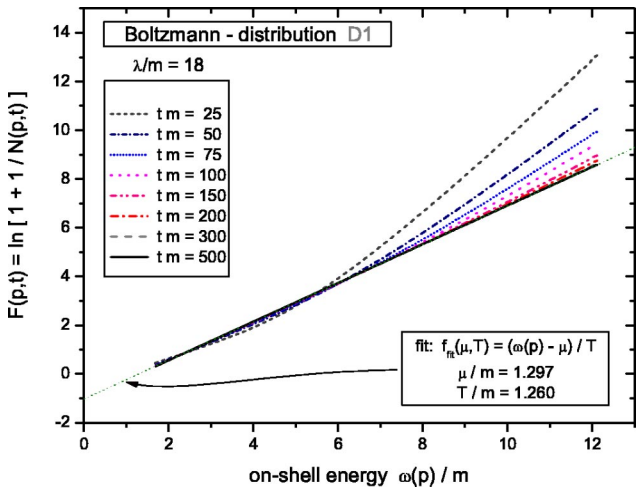

FIG. 25. Distribution function F as a function of the time-dependent on-shell energy $\omega_{\mathbf{p}}(t)$ for various times $t\cdot m=25$, 50, 75, 100, 150, 200, 300, 500 starting from an initial configuration D1 with coupling constant $\lambda/m=18$. For large times a thermal state—characterized by a straight line in this representation—is reached with temperature $T/m=1.260$ and finite chemical potential $\mu/m=1.297$ as indicated by the fitting function (dotted lines).

pects from the Kadanoff-Baym dynamics. At first we find that in case of the Boltzmann equation the equal-energy initial distributions D1, D2, and D3 equilibrate towards different stationary states for $t\rightarrow\infty$. This can directly been read off from Fig. 24 when comparing the final occupation numbers of the various momentum modes. This behavior is in contrast to the Kadanoff-Baym evolution where all initial distributions with the same energy reach a common stationary state (see Fig. 4). As pointed out in Sec. IV D this is an effect of the chemical equilibration mediated by particle number nonconserving processes, which are included in the Kadanoff-Baym dynamics since the full spectral function is taken into account. For the on-shell Boltzmann approximation, however, the particle number is strictly conserved and thus the initializations D1, D2, D3, that contain different number of particles, cannot approach the same final state. Accordingly, the stationary state of the nonthermal initializations D1, D2, D3 exhibits a finite chemical potential (see below). Without explicit representation we note that the self-consistent initial configuration DT is already the thermal state of the Boltzmann equation and all momentum modes remain constant in time, whereas within the Kadanoff-Baym dynamics the ''free'' thermal initialization DT evolves in time due to the generation of correlations (see Sec. IV A).

In order to demonstrate, that the time evolution on the basis of the Boltzmann equation leads to a thermal state of quasiparticle excitations, we show in Fig. 25 the on-shell distribution $N(\mathbf{p},t)$ as a function of the time-dependent on-shell energy $\omega_{\mathbf{p}}(t)$ for various times $t\cdot m=25$, 50, 75, 100, 150, 200, 300, 500 for the initialization D1 and coupling strength $\lambda/m=18$. We have displayed the quantity

$$F(\mathbf{p},t)=\ln[1+1/N(\mathbf{p},t)] \tag{E1}$$

in order to obtain a straight line with slope $1/T$ and intersection point $-\mu/T$ in case of a Bose distribution $N=1/\{\exp[(\omega_{\mathbf{p}}-\mu)/T]-1\}$ with temperature T and chemical potential μ. We see from Fig. 25 that the distribution at early times ($t\cdot m=25$) is small for very low and very high momenta as reflected by the high values of the quantity F in the low and high energy regime. The particle accumulation at finite momentum for initialization D1 [see Fig. 3 (lower part)] shows up as a small dip in the curve. In course of the time evolution these structures slowly vanish such that finally a straight line is reached (see lines for $t\cdot m=300$, 500)

indicating that the stationary limit is indeed a thermal distribution (at temperature $T/m=1.260$). However, the chemical potential of the stationary distribution is nonvanishing—as recognized by the nonzero intersect of the dotted fit function—as $\mu/m=1.297$. The initializations D2, D3 achieve different asymptotic temperatures which are given by $T/m=1.562$ for D2 and $T/m=2.218$ for D3. The chemical potential of the stationary state for these distributions is nonzero as well and has the values $\mu/m=0.658$ for D2 and $\mu/m=-0.521$ for D3. We recall, that systems with large chemical potential distribute the total energy on many particles such that the final temperature is considerably lower. Thus, in general, the Boltzmann approximation does not drive the system to the proper equilibrium state of the neutral ϕ^4 theory, which is characterized by a vanishing chemical potential.

Furthermore, we see from Fig. 24 that in the Boltzmann limit the momentum modes evolve monotonically in time; there is no overshooting of the stationary limit as observed in the Kadanoff-Baym picture (see Fig. 4). Thus the nonmonotonic behavior shows up as a quantum phenomenon that is missing in the semiclassical treatment.

[1] D.H. Lyth and A. Riotto, Phys. Rep. **314**, 1 (1999); A. Riotto and M. Trodden, Annu. Rev. Nucl. Part. Sci. **49**, 35 (1999); M. Trodden, Rev. Mod. Phys. **71**, 1463 (1999).

[2] D. Boyanovsky, H.J. de Vega, R. Holman, and J.F.J. Salgado, Phys. Rev. D **54**, 7570 (1996).

[3] L. Kofman, A. Linde, and A.A. Starobinsky, Phys. Rev. D **56**, 3258 (1997).

[4] M. Gell-Mann and J.B. Hartle, Phys. Rev. D **47**, 3345 (1993).

[5] B. Müller, *The Physics of the Quark-Gluon Plasma*, Lecture Notes in Physics No. 225 (Springer, Berlin, 1985); *Quark-Gluon Plasma*, edited by R. Hwa, *Advanced Series on Directions in High Energy Physics* (World Scientific, Singapore, 1990); *Quark-Gluon Plasma II*, edited by R. Hwa, *Advanced Series on Directions in High Energy Physics* (World Scientific, Singapore, 1995).

[6] For a review see the contribution of K. Rajagopal in *Quark-Gluon Plasma II* [5].

[7] D. Boyanovsky, H.J. de Vega, and R. Holman, Phys. Rev. D **51**, 734 (1995); F. Cooper, Y. Kluger, E. Mottola, and J.P. Paz, *ibid.* **51**, 2377 (1995).

[8] T.S. Biro and C. Greiner, Phys. Rev. Lett. **79**, 3138 (1997); Z. Xu and C. Greiner, Phys. Rev. D **62**, 036012 (2000).

[9] J. Schwinger, J. Math. Phys. **2**, 407 (1961).

[10] P.M. Bakshi and K.T. Mahanthappa, J. Math. Phys. **4**, 1 (1963); **4**, 12 (1963).

[11] L.V. Keldysh, Zh. Éksp. Teor. Fiz. **47**, 1515 (1964) [Sov. Phys. JETP **20**, 1018 (1965)].

[12] R.A. Craig, J. Math. Phys. **9**, 605 (1968).

[13] L.P. Kadanoff and G. Baym, *Quantum Statistical Mechanics* (Benjamin, New York, 1962).

[14] D.F. DuBois, in *Lectures in Theoretical Physics*, edited by W.E. Brittin (Gordon and Breach, New York, 1967), pp. 469–619.

[15] P. Danielewicz, Ann. Phys. (N.Y.) **152**, 239 (1984).

[16] K. Chou, Z. Su, B. Hao, and L. Yu, Phys. Rep. **118**, 1 (1985).

[17] J. Rammer and H. Smith, Rev. Mod. Phys. **58**, 323 (1986).

[18] E. Calzetta and B.L. Hu, Phys. Rev. D **37**, 2878 (1988).

[19] H. Haug and A.P. Jauho, *Quantum Kinetics in Transport and Optics of Semiconductors* (Springer, New York, 1999).

[20] C. Greiner and S. Leupold, Ann. Phys. (N.Y.) **270**, 328 (1998).

[21] W. Cassing, Z. Phys. A **327**, 447 (1987).

[22] W. Cassing, K. Niita, and S.J. Wang, Z. Phys. A **331**, 439 (1988).

[23] W. Cassing, V. Metag, U. Mosel, and K. Niita, Phys. Rep. **188**, 363 (1990).

[24] B. Bezzerides and D.F. DuBois, Ann. Phys. (N.Y.) **70**, 10 (1972).

[25] P. Lipavský, V. Špička, and B. Velický, Phys. Rev. B **34**, 6933 (1986).

[26] W. Botermans and R. Malfliet, Phys. Rep. **198**, 115 (1990).

[27] S. Mrówczyński and P. Danielewicz, Nucl. Phys. **B342**, 345 (1990).

[28] V. Špička and P. Lipavský, Phys. Rev. Lett. **73**, 3439 (1994); Phys. Rev. B **52**, 14 615 (1995).

[29] A. Makhlin, Phys. Rev. C **52**, 995 (1995); A. Makhlin and E. Surdutovich, *ibid.* **58**, 389 (1998).

[30] K. Geiger, Phys. Rev. D **54**, 949 (1996); **56**, 2665 (1997).

[31] D.A. Brown and P. Danielewicz, Phys. Rev. D **58**, 094003 (1998).

[32] J.P. Blaizot and E. Iancu, Nucl. Phys. **B557**, 183 (1999).

[33] M. Imamovic-Tomasovic and A. Griffin, Phys. Rev. A **60**, 494 (1999).

[34] Y.B. Ivanov, J. Knoll, and D.N. Voskresensky, Nucl. Phys. **A657**, 413 (1999).

[35] J. Knoll, Y.B. Ivanov, and D.N. Voskresensky, Ann. Phys. (N.Y.) **293**, 126 (2001).

[36] F. Cooper, S. Habib, Y. Kluger, E. Mottola, J.P. Paz, and P.R. Anderson, Phys. Rev. D **50**, 2848 (1994).

[37] D. Boyanovsky, H.J. de Vega, R. Holman, D.-S. Lee, and A. Singh, Phys. Rev. D **51**, 4419 (1995).

[38] D. Boyanovsky, M. D'Attanasio, H.J. de Vega, R. Holman, and D.-S. Lee, Phys. Rev. D **52**, 6805 (1995).

[39] D. Boyanovsky, H.J. de Vega, R. Holman, S.P. Kumar, and R. Pisarski, Phys. Rev. D **57**, 3653 (1998).

[40] J.W. Negele, Rev. Mod. Phys. **54**, 913 (1982).

[41] D. Boyanovsky, I.D. Lawrie, and D.-S. Lee, Phys. Rev. D **54**, 4013 (1996).

[42] D. Boyanovsky, H.J. de Vega, R. Holman, S.P. Kumar, R.D. Pisarski, and J. Salgado, Phys. Rev. D **58**, 125009 (1998).

[43] D. Boyanovsky, H.J. de Vega, R. Holman, and M. Simionato, Phys. Rev. D **60**, 065003 (1999).

[44] E.A. Calzetta and B.L. Hu, hep-ph/0205271.

[45] S. Sengupta, F.C. Khanna, and S.P. Kim, Phys. Rev. D **68**, 105014 (2003).

[46] A. Peter, W. Cassing, J.M. Häuser, and A. Pfitzner, Nucl. Phys. **A573**, 93 (1994).

[47] S.J. Wang, W. Zuo, and W. Cassing, Nucl. Phys. **A573**, 245 (1994).

[48] J.M. Häuser, W. Cassing, A. Peter, and M.H. Thoma, Z. Phys. A **353**, 301 (1995).

[49] A. Peter, W. Cassing, J.M. Häuser, and M.H. Thoma, Z. Phys. C **71**, 515 (1996).
[50] A. Peter, W. Cassing, J.M. Häuser, and M.H. Thoma, Z. Phys. A **358**, 91 (1997).
[51] J.M. Häuser, W. Cassing, S. Leupold, and M.H. Thoma, Ann. Phys. (N.Y.) **265**, 155 (1998).
[52] T. Altherr and D. Seibert, Phys. Lett. B **333**, 149 (1994).
[53] C. Greiner and S. Leupold, Eur. Phys. J. C **8**, 517 (1999).
[54] P. Danielewicz, Ann. Phys. (N.Y.) **152**, 305 (1984).
[55] C. Greiner, K. Wagner, and P.-G. Reinhard, Phys. Rev. C **49**, 1693 (1994).
[56] C. Greiner, K. Wagner, and P.-G. Reinhard, in *Proceedings of the NATO Advanced Study Institute on "Hot and Dense Matter,"* Bodrum, Turkey, 1993, edited by W. Greiner, H. Stöcker, and A. Gallmann, Vol. 335 of *NATO ASI Series B: Physics* (Plenum, New York, 1994).
[57] H.S. Köhler, Phys. Rev. C **51**, 3232 (1995).
[58] H.S. Köhler and K. Morawetz, Eur. Phys. J. A **4**, 291 (1999); Phys. Rev. C **64**, 024613 (2001).
[59] L. Banyai, D.B. Tran Thoai, E. Reitsamer, H. Haug, D. Steinbach, M.U. Wehner, M. Wegener, T. Marschner, and W. Stoltz, Phys. Rev. Lett. **75**, 2188 (1995); L. Banyai, Q.T. Vu, B. Mieck, and H. Haug, *ibid.* **81**, 882 (1998); Q.T. Vu, H. Haug, W.A. Hügel, S. Chatterjee, and M. Wegener, *ibid.* **85**, 3508 (2000).
[60] A. Wackert, A. Jauho, S. Rott, A. Markus, P. Binder, and G. Döhler, Phys. Rev. Lett. **83**, 836 (1999).
[61] J. Berges and J. Cox, Phys. Lett. B **517**, 369 (2001).
[62] J. Berges, Nucl. Phys. **A699**, 847 (2002).
[63] K.B. Blagoev, F. Cooper, J.F. Dawson, and B. Mihaila, Phys. Rev. D **64**, 125003 (2001).
[64] A.V. Ryzhov and L.G. Yaffe, Phys. Rev. D **62**, 125003 (2000).
[65] G. Aarts, D. Ahrensmeier, R. Baier, J. Berges, and J. Serreau, Phys. Rev. D **66**, 045008 (2002).
[66] F. Cooper, J.F. Dawson, and B. Mihaila, Phys. Rev. D **67**, 056003 (2003).
[67] B. Mihaila, Phys. Rev. D **68**, 036002 (2003).
[68] J. Berges and J. Serreau, Phys. Rev. Lett. **91**, 111601 (2003).
[69] J. Berges, S. Borsanyi, and J. Serreau, Nucl. Phys. **B660**, 51 (2003).
[70] L.M.A. Bettencourt, K. Pao, and J.G. Sanderson, Phys. Rev. D **65**, 025015 (2002).
[71] M. Salle, J. Smit, and J.C. Vink, Phys. Rev. D **64**, 025016 (2001).
[72] M. Salle and J. Smit, Phys. Rev. D **67**, 116006 (2003).
[73] M. Salle, J. Smit, and J.C. Vink, Nucl. Phys. **B625**, 495 (2002).
[74] F.L. Braghin, Phys. Rev. D **64**, 125001 (2001); L.M.A. Bettencourt, F. Cooper, and K. Pao, Phys. Rev. Lett. **89**, 112301 (2002).
[75] Y. Bergner and L.M.A. Bettencourt, hep-th/0305190; L.M.A. Bettencourt, F. Cooper, and K. Pao, Phys. Rev. Lett. **89**, 112301 (2002); M. Salle, Phys. Rev. D (to be published), hep-ph/0307080.
[76] Y. Bergner and L.M.A. Bettencourt, Phys. Rev. D **68**, 025014 (2003); and Phys. Rev. D (to be published), hep-ph/0308107.
[77] G. Aarts and J. Berges, Phys. Rev. D **64**, 105010 (2001).
[78] P.A. Henning, Phys. Rep. **253**, 235 (1995).
[79] M. Effenberger, E.L. Bratkovskaya, and U. Mosel, Phys. Rev. C **60**, 044614 (1999); M. Effenberger and U. Mosel, *ibid.* **60**, 051901 (1999).
[80] Y.B. Ivanov, J. Knoll, and D.N. Voskresensky, Nucl. Phys. **A672**, 313 (2000).
[81] W. Cassing and S. Juchem, Nucl. Phys. **A665**, 377 (2000).
[82] W. Cassing and S. Juchem, Nucl. Phys. **A672**, 417 (2000).
[83] W. Cassing and S. Juchem, Nucl. Phys. **A677**, 445 (2000).
[84] S. Leupold, Nucl. Phys. **A672**, 475 (2000); **A695**, 377 (2001).
[85] W. Cassing and E.L. Bratkovskaya, Phys. Rep. **308**, 65 (1999).
[86] R. Rapp and J. Wambach, Adv. Nucl. Phys. **25**, 1 (2000).
[87] G. Agakichiev *et al.*, Phys. Rev. Lett. **75**, 1272 (1995).
[88] W. Cassing, L. Tolos, E.L. Bratkovskaya, and A. Ramos, Nucl. Phys. **A727**, 59 (2003).
[89] E. Fick and G. Sauermann, *The Quantum Statistics of Dynamic Processes*, Vol. 86 of *Springer Series in Solid-State Sciences* (Springer, Berlin, 1990).
[90] J. Rau and B. Müller, Phys. Rep. **272**, 1 (1996).
[91] R. Kubo, J. Phys. Soc. Jpn. **12**, 570 (1957); C. Martin and J. Schwinger, Phys. Rev. **115**, 1342 (1959).
[92] N.P. Landsman and C.G. van Weert, Phys. Rep. **145**, 141 (1987).
[93] H. van Hees and J. Knoll, Phys. Rev. D **65**, 025010 (2002).
[94] H. van Hees and J. Knoll, Phys. Rev. D **65**, 105005 (2002).
[95] N. Bogolyubov, J. Phys. (USSR) **10**, 257 (1946); **10**, 265 (1946).
[96] S. Fujita, Phys. Rev. A **4**, 1114 (1971).
[97] A.G. Hall, J. Phys. A **8**, 214 (1975).
[98] P.A. Henning, Nucl. Phys. **B337**, 547 (1990).
[99] R.P. Parwani, Phys. Rev. D **45**, 4695 (1992).
[100] S. Jeon, Phys. Rev. D **52**, 3591 (1995).
[101] E. Wang and U. Heinz, Phys. Rev. D **53**, 899 (1996).
[102] T. Nishikawa, O. Morimatsu, and Y. Hidaka, Phys. Rev. D **68**, 076002 (2003).
[103] J. Lehr, M. Effenberger, H. Lenske, and U. Mosel, Phys. Lett. B **483**, 324 (2000); J. Lehr, H. Lenske, S. Leupold, and U. Mosel, Nucl. Phys. **A703**, 393 (2002).
[104] G. Aarts, Phys. Lett. B **518**, 315 (2001).
[105] D.Yu. Grigoriev and V.A. Rubakov, Nucl. Phys. **B299**, 6719 (1988); D.Yu. Grigoriev, V.A. Rubakov, and M.E. Shaposhnikov, *ibid.* **B326**, 737 (1989).
[106] G. Aarts and J. Smit, Phys. Lett. B **393**, 395 (1997); W. Buchmüller and A. Jakovac, *ibid.* **407**, 39 (1997).
[107] A.H. Mueller and D.T. Son, hep-ph/0212198.
[108] S. Mrówczyński, Phys. Rev. D **56**, 2265 (1997).